S-CUBED

A Division of Maxwell Laboratories, Inc.

(10)

SSS-R-84-6684

# DEVELOPMENT OF ADVANCED CONSTITUTIVE MODEL FOR REINFORCED CONCRETE

G. A. Hegemier
H. E. Read
H. Murakami

FINAL REPORT

Submitted to:

AIR FORCE OFFICE OF SCIENTIFIC RESEARCH
BOLLING AIR FORCE BASE
WASHINGTON, D.C. 20332

April 1984



Approved for public release;
distribution unlimited.

*P. O. Box 1620, La Jolla, California 92038-1620*
*(619) 453-0060*

S-CUBED
A Division of Maxwell Laboratories, Inc.

SSS-R-84-6684

# DEVELOPMENT OF ADVANCED CONSTITUTIVE MODEL FOR REINFORCED CONCRETE

G. A. Hegemier
H. E. Read
H. Murakami

FINAL REPORT

Submitted to:

AIR FORCE OFFICE OF SCIENTIFIC RESEARCH
BOLLING AIR FORCE BASE
WASHINGTON, D.C. 20332

April 1984



*P. O. Box 1620, La Jolla, California 92038-1620*
*(619) 453-0060*

Unclassified

SECURITY CLASSIFICATION OF THIS PAGE

## REPORT DOCUMENTATION PAGE

| | |
|---|---|
| 1a. REPORT SECURITY CLASSIFICATION: Unclassified | 1b. RESTRICTIVE MARKINGS: None |
| 2a. SECURITY CLASSIFICATION AUTHORITY: N/A | 3. DISTRIBUTION/AVAILABILITY OF REPORT: Approved for public release; distribution unlimited. |
| 2b. DECLASSIFICATION/DOWNGRADING SCHEDULE: N/A | |
| 4. PERFORMING ORGANIZATION REPORT NUMBER(S): SSS-R-84-6684 | 5. MONITORING ORGANIZATION REPORT NUMBER(S): AFOSR-TR- 84-0427 |
| 6a. NAME OF PERFORMING ORGANIZATION: S-CUBED; 6b. OFFICE SYMBOL (If applicable): | 7a. NAME OF MONITORING ORGANIZATION: AFOSR/NA |
| 6c. ADDRESS (City, State and ZIP Code): P.O. Box 1620, La Jolla, CA 92038-1620 | 7b. ADDRESS (City, State and ZIP Code): Bolling AFB, DC 20332 |
| 8a. NAME OF FUNDING/SPONSORING ORGANIZATION: AFOSR; 8b. OFFICE SYMBOL (If applicable): AFOSR/NA | 9. PROCUREMENT INSTRUMENT IDENTIFICATION NUMBER: Contract F49620-81-C-0033 |
| 8c. ADDRESS (City, State and ZIP Code): Bolling Air Force Base, Washington, D.C. 20332 | 10. SOURCE OF FUNDING NOS. — PROGRAM ELEMENT NO.: 61102F; PROJECT NO.: 2307; TASK NO.: C2; WORK UNIT NO.: |
| 11. TITLE (Include Security Classification): DEVELOPMENT OF ADVANCED CONSTITUTIVE MODEL FOR REINFORCED CONCRETE(U) (UNCLASSIFIED) | |
| 12. PERSONAL AUTHOR(S): G. A. Hegemier, H. E. Read, H. Murakami | |
| 13a. TYPE OF REPORT: Final; 13b. TIME COVERED: FROM 3/81 TO 2/84 | 14. DATE OF REPORT (Yr., Mo., Day): April 30, 1984; 15. PAGE COUNT: 173 |
| 16. SUPPLEMENTARY NOTATION | |

| 17. COSATI CODES | | | 18. SUBJECT TERMS (Continue on reverse if necessary and identify by block number) |
|---|---|---|---|
| FIELD | GROUP | SUB. GR. | REINFORCED CONCRETE; MIXTURE THEORY; CONSTITUTIVE MODELS; COMPOSITE MATERIALS |
| | | | |
| | | | |

19. ABSTRACT (Continue on reverse if necessary and identify by block number)

The objective of this research was to develop an advanced, nonlinear, multiaxial constitutive theory for reinforced concrete which provides a modeling capability that is superior to existing models, especially in the nonlinear response regime. The problem of constructing such a theory is partitioned into two major tasks, which have been pursued concurrently. One task consists of formulating a procedure (mixture theory) for analytically mixing reinforcing steel and plain concrete, so that the interaction between the two, which plays a key role in the overall behavior of reinforced concrete, is properly modeled. The other task consists of developing a model of plain concrete, which accurately portrays its nonlinear, multiaxial behavior and which is computationally feasible for use in conjunction with the mixture theory. The mixture theory is designed to synthesize the global constitutive properties of reinforced concrete from the properties of plain concrete, steel, interfaces and reinforcing geometry.

The progress made during the course of the program toward achieving the above research

| | |
|---|---|
| 20. DISTRIBUTION/AVAILABILITY OF ABSTRACT: UNCLASSIFIED/UNLIMITED ☒ SAME AS RPT. ☐ DTIC USERS ☐ | 21. ABSTRACT SECURITY CLASSIFICATION: UNCLASSIFIED |
| 22a. NAME OF RESPONSIBLE INDIVIDUAL: Lt Col Lawrence D Hokanson | 22b. TELEPHONE NUMBER (Include Area Code): 202/767-4935; 22c. OFFICE SYMBOL: AFOSR/NA |

DD FORM 1473, 83 APR EDITION OF 1 JAN 73 IS OBSOLETE.

Unclassified

SECURITY CLASSIFICATION OF THIS PAGE

Block 19.

objectives is summarized. A detailed account of the accomplishments made during the third year of the program are given, since these are not available elsewhere. Finally, a list of the publications and technical interactions which resulted from this research is given.

A-1

TABLE OF CONTENTS

TABLE OF CONTENTS (continued)

LIST OF FIGURES

LIST OF FIGURES (Cont'd)

LIST OF FIGURES (Cont'd)

LIST OF FIGURES (Cont'd)

# FOREWORD

This final report summarizes the research performed by S-CUBED under AFOSR Contract F49620-81-C-0033 during the period from March 1, 1981 to February 29, 1984. Partial support for that portion of the research conducted to explore the basic concept of strain softening in concrete, rock and soil was provided by the Defense Nuclear Agency under Contract DNA001-84-C-0127. The Co-Principal Investigators for the project were Dr. G. A. Hegemier and Dr. H. E. Read.

The authors express their appreciation to Dr. J. A. Trangenstein, who contributed to the first year's effort, and to Mr. R. G. Herrmann, who provided excellent computer support throughout the study. In addition, thanks are due to Dr. Laura J. Hageman, who performed the numerical simulations and theoretical-experimental comparisons associated with the steel-concrete bond problem.

This Page Left Blank

# I. INTRODUCTION

## 1.1 BACKGROUND AND PRESENT NEEDS

The cost-effective and reliable design of protective structures for the land-based MX system requires that the dynamic behavior of concrete, under the severe loading conditions produced by design attack scenarios, be understood and appropriately described by mathematical models. Economic considerations dictate that the design of modern protective structures include the considerable strength and ductility associated with the post-yield behavior of reinforced concrete. The design environments of protective structures require that a multiplicity of stress states reached through different stress paths, including reversals, be considered. Thus, a rational design and analysis of a protective structure requires a knowledge of nonlinear material behavior under multiaxial, hysteretic stress states and paths. Further, the environment is dynamic. Hence, the influence of loading or deformation rate must be understood and included in any theoretical model intended for use in such applications.

In the past, the design of protective shelters for land-based strategic weapons systems has generally relied on either linear elastic models of concrete behavior or, at best, on relatively simple elasto-plastic models developed on the basis of quasi-static, low-pressure laboratory data on concrete. Generally speaking, the present state-of-the-art in modeling even the quasi-static low pressure behavior of concrete is unsophisticated and approximate, compared with the present capability to model many other materials, such as metals, plastics, composites, etc. This is clearly due to the fact that concrete is the most complex structural material presently used.

The inability of the currently operational constitutive models to adequately describe the nonlinear behavior of plain and/or reinforced concrete appears to be the primary cause of the poor

correlation observed between experimental data and theoretical predictions, and the main reason for the lack of confidence in numerical simulations of structural response. The inaccuracies associated with the currently operation models of reinforced concrete stem from two main sources: (1) the mathematical description(s) of plain concrete and (2) the method(s) by which steel and concrete are mixed or overlayed to form a composite material. In both cases, the nature of the problem requires research at a fundamental level. The reason: although considerable research has been conducted on both plain and reinforced concrete members over the past fifty years, the emphasis was not on the highly nonlinear, highly dynamic material response regime. Such problems consequently necessitate the development of improved modeling techniques and corresponding experiments to validate such techniques.

The need for more sophisticated modeling of concrete came into focus as the MPS basing concept was being considered for the MX system.[1,2] The original plan to construct a large number (4,600) of reinforced concrete protective structures signaled the need for an improved generation of design tools which could produce more reliable and cost-effective shelter designs. In response to this need, the Air Force and the Defense Nuclear Agency initiated research programs to advance the present state-of-the-art in modeling concrete behavior.[3-5] But, because the stress levels and strain rates of interest in the MPS basing concept were relatively low, the major emphasis on these research programs was directed toward the low pressure low strain rate behavior of concrete.

During the past several years, emphasis has shifted from the MPS mode of basing to several alternative modes, including Deep Basing, Close Spaced Basing and Advanced Silo Hardening (ASH). In the ASH Program, many issues pertaining to the survivability of the superhardened shelters are being explored. For the ASH concept to be successful, the protective shelters must be capable of surviving

stress levels as high as 75,000 psi and strain rates in the range 1 to 100 $sec^{-1}$. Such severe dynamic loading conditions drive the concrete into regions of response that are well outside the range where our present knowledge of response has been obtained. There is sufficient evidence, however, from both laboratory and field tests, to indicate that concrete rapidly loaded to high stress levels behaves much differently than when loaded qausi-statically under low confining pressures. This is not surprising, however, since there is a critical confining pressure -- called the brittle/ductile transition pressure -- which separates the two different types of constitutive behavior that concrete exhibits. Below the brittle/ ductile transition pressure, concrete behaves as a rate-dependent brittle material, with the rate-dependence arising from the micro-cracking processes. Above the transition pressure, concrete behaves in a rate-dependent ductile manner, with the rate-dependence arising from the time-dependence of the mortar as it flows around the embedded aggregate.

Despite the importance of concrete as a structural material in the design of strategic weapons systems, relatively little effort has been devoted over the years by the defense community to develop an understanding of its dynamic properties. Even now, the models used for protective structure design are crude and unable to represent many aspects of the response of concrete to static, low pressure loading. If present issues related to the ASH concept are to be resolved, the present knowledge of concrete behavior must be extended into the high pressure, high strain rate region of particular interest to ASH. This will require not only the development of more sophisticated reinforced concrete models, but also the development of new experimental technology, since existing testing devices are not designed to operate in this response region.

## 1.2 OBJECTIVE

The primary objective of the research described here is to construct an advanced, nonlinear, multiaxial, nonphenomenological constitutive model of reinforced concrete that will provide simulation accuracy that is superior to existing models in the nonlinear response regime. The term 'advanced nonlinear multiaxial' implies a model that will provide accuracy superior to existing models in the inelastic, nonlinear response regime and for arbitrary paths in multiaxial stress or strain space. The term 'nonphenomenological' implies a model that is capable of synthesizing the global properties of reinforced concrete from a knowledge of the plain concret and steel properties, the concrete-steel interface properties, and the geometry of the steel reinforcement.

## 1.3 SCOPE AND APPROACH

The nonlinear response of reinforced concrete is largely dominated by complex interactions between the steel and the concrete. Consequently, an accurate model of reinforced concrete must be capable of accounting for such interactions. Further, in an effort to minimize the number and type of tests necessary to define the parameters of a given model, it is highly desirable that it be nonphenomenological, i.e., that the global properties of reinforced concrete be synthesized from the properties of the steel and concrete, the steel-concrete interface physics, and the steel geometry.

A candidate that satisfies the above objectives is the "mixture theory with microstructure." As was noted previously, this modeling concept is a result of previous successful attempts to describe the nonlinear behavior of fibrous composites.[6-10]

According to the mixture concept, the composite constituents (steel and plain concrete) are modeled at each instant of time as superposed continua in space. Each continuum is allowed to undergo

individual deformations. The microstructure of an actual composite of steel and concrete is then simulated by specifying the nature of the interactions between the continua. With respect to reinforced concrete, previous "smearing" or "homogenizing" techniques may be viewed as a mixture theory in which each component is constrained to have the same deformation gradient at the same spatial point. Relaxation of this constraint through an improved mixture framework obtained by micromechanical considerations regarding the interactions of the components leads to a marked improvement in the simulation of real material behavior.

The key to the development of mixture models for reinforced concrete is an asymptotic procedure called "multivariable asymptotic expansions." This mathematical technique, together with a "smoothing" operation, leads to the desired mixture forms. The methodology is applicable to both dense and sparse steel layouts.

This Page Left Blank

# II. PROGRESS SUMMARY AND CURRENT STATUS OF RESEARCH

The progress made during the course of this contract toward achieving the research objectives described earlier is summarized in this section. First, the progress toward developing an advanced mixture theory with microstructure for reinforced concrete is described. Next, the effort to develop a realistic constitutive model of plain concrete for use in conjunction with the mixture theory is summarized. Finally, a list of the publications and technical interactions which resulted from the research performed under this contract is given.

## 2.1 MIXTURE THEORY FOR REINFORCED CONCRETE

The nonlinear response of reinforced concrete is largely dominated by complex interactions between the steel and the concrete. Consequently, an accurate model of reinforced concrete must be capable of accounting for such interactions. Further, in an effort to minimize the number and type of tests necessary to define the parameters of a given model, it is highly desirable that it be nonphenomenological, i.e., that the global properties of reinforced concrete be synthesized from the properties of the steel and concrete, and steel-concrete interface physics, and the steel geometry.

As was noted in Section I, a model that satisfies the above objectives falls into the category of a "mixture theory with microstructure." Using this approach, the problem of formulating a procedure for analytically mixing steel and concrete to furnish an accurate model of reinforced concrete can be partitioned into two basic problems: (a) dense steel layout and (b) sparse steel layout. Within each of these, there are four fundamental sub-problems that must be considered: (1) the steel-concrete bond problem, (2) the steel-concrete dowel problem, (3) the concrete aggregate interlock problem, and (4) the steel buckling-concrete spallation problem. Problem (1) plays a dominant role in the bending and the

nonlinear stretching of reinforced concrete beams, plates and shells. Problem (2) plays a major role in the transverse shear deformation of reinforced concrete beams, and the transverse and in-plane shear deformation of reinforced concrete plates and shells. Problem (3) plays an important role in those cases where relative motion occurs across existing cracks. Problem (4) concerns containment of the concrete by the rebar mesh, spallation of the concrete, and subsequent buckling of the rebar; this problem plays an important role in cases where reinforced concrete structural elements experience significant direct compression.

The following progress has been made during the course of this study with respect to the aforementioned problem areas.

Dense Steel Layout:

A general nonlinear mixture theory has been formulated for a dense unidirectional steel layout. The latter can be curvilinear. The theory accommodates a class of nonlinear material and interfacial constitutive behavior as well as nonlinear geometrical effects. The theory was developed in invariant notation and thus is applicable to any coordinate system. This work is presented in Section 3.1.

Sparse Steel Layout:

A general nonlinear mixture theory has been formulated for a sparse steel layout. As in the case of the dense steel development, the theory accommodates nonlinear material and interfacial constitutive behavior as well as nonlinear geometrical effects. The configuration of the rebar in the initial, unstressed state is arbitrary. This work is presented in Section 3.2.

Variational Principles:

Variational principles have been developed for both of the above mixture theories. Such principles are needed for proper

boundary condition formulations. They also serve as the basis for the development of a finite element method. This effort is discussed in Sections 3.1 and 3.2.

The Steel-Concrete Bond Problem:

The simulation capability and accuracy of the mixture formulations for both dense and sparse steel layouts have been assessed in considerable depth and detail for the special case of the steel-concrete bond problem. As part of this work, a steel-concrete interface model was developed based upon available experimental data. The mixture relations were transformed to numerical form and a computer subroutine was developed to allow test simulations. Using this subroutine, a number of problems involving both monotonic and hysteretic loading of reinforced concrete specimens were investigated. Initial simulations with available experimental data revealed good agreement and simulation capability. In particular, items such as strain hardening, strain softening, stiffness degradation, hysteresis, and the degree of cracking were satisfactorily modeled. This work is reviewed in Section 3.3.

The Dowel and Aggregate Interlock Problem:

A substantial effort has been made to solve the dowel and the aggregate interlock problems. Both problems concern the manner in which shear is transferred across a crack that may be oblique to the principal steel directions. Both problems involve considerable difficulty. However, we have succeeded in formulating a mixture framework that accounts for both dowel action and aggregate interlock. This was accomplished by incorporating surfaces of discontinuity into a general multi-axial mixture formulation.

The simulation capability of the mixture formulation has been addressed for a special dowel problem. The mixture relations were transformed to numerical form and a computer subroutine was developed to allow test simulations. Using this subroutine, both

monotonic and hysteretic loading of reinforced concrete dowel specimens were investigated. These simulations reveal that the model reflects the basic features of the experimental data. The above effort is discussed in Section 3.4.

Based on the validation studies conducted thus far, it appears that the mixture theory framework furnishes a means of incorporating the complex interactions between the steel and concrete. Given an adequate concrete model, the result is a theory which is capable of accurate simulations of reinforced concrete nonlinear response.

## 2.2 PLAIN CONCRETE MODELING

In the first year's work under this contract, the advanced constitutive models of plain concrete available in the literature were reviewed, and from this it was concluded[4] that the plastic fracturing model[11] was the best of the existing models for the present purposes. A detailed examination of this model was conducted, and, as a result, a number of difficulties and inconsistencies were uncovered, which were discussed in Reference 4. Despite these problems, it was felt that the plastic-fracturing approach had considerable merit, and we decided to attempt to reconstruct the model in a consistent manner.

At the start of the second year's work,* we began an effort to reconstruct the plastic-fracturing framework. Our attention was initially focused on a feature of the model that had only received cursory consideration earlier; this feature, called "jump-kinematic" hardening, had been introduced into the plastic-fracturing framework to make the description of unloading-reloading behavior more realistic. On close examination, we found "jump-kinematic" hardening to be objectional on fundamental grounds because it violated Prager's Continuity Condition[12] for multi-axial elastic-plastic behavior.** In view of these difficulties, as well as those reported

---

* A complete description of the progress made during the second year's effort is given in Reference 5.

** See also a recent discussion of jump-kinematic hardening given in Reference 13.

earlier in Reference 4, we removed the plastic-fracturing model of plain concrete from further consideration, and turned attention toward developing a new constitutive theory of plain concrete, using the new endochronic theory, that we had recently developed,[14,15] as a starting point.

Considerable progress was made toward developing a constitutive model of plain concrete, based upon the new endochronic theory.[15] As part of this effort, we focused on obtaining a realistic representation of failure for use with this model, and from this emerged a new failure criterion which provides, in a simple and elegant manner, an excellent description of the failure of plain concrete over a wide range of confining pressures.[16]

Toward the end of the second year's effort, Schreyer[17] proposed a new and novel elasto-plastic constitutive framework for describing materials, such as concrete, soils and rock, whose inelastic response depends upon the first and third invariants of stress. The particular attraction of this new model lay in its apparent ability to describe many of the salient response features of these materials with a relatively simple mathematical formalism. The model employs a non-associated flow rule, describes both dilatancy and compaction, as well as hardening and softening, and because of its incrementally linear form is computationally attractive. As shown in Reference 17, the model provides an excellent representation of the failure of plain concrete, rock and soils under a variety of loading conditions, as well as the response of these materials to triaxial compression. Inasmuch as this model appeared to have most of the capabilities we were looking for and, moreover, was conceptually quite simple, work on the endochronic concrete model was temporarily suspended, and we turned our attention to examining this elasto-plastic model in further detail.

Our investigation of the Schreyer model focused mainly on the yield and failure surfaces, although a numerical scheme and corresponding computer program were developed for the complete model. We performed an extensive check of the failure model against a wide

variety of plain concrete failure data, including that obtained under uniaxial, biaxial, triaxial, proportional loading, pure torsion and torsion-compression loading conditions.* Except for the torsion data, the failure model provided an impressive description of all the other types of failure data, which encompassed a range of confining pressures from 0 to nearly 75,000 psi. The torsion data, on the other hand, are more closely correlated by another failure surface, which appears to be a possible failure surface permitted within the model's mathematical framework. Thus, the mathematical structure of the model allows for the possibility of two different failure surfaces and, from an examination of a variety of concrete failure data, we found that some types of data are best correlated with one failure surface while another type of data (torsion) is best correlated by the other failure surface; such a nonuniqueness is troubling and requires further attention. In addition to the problem of nonuniqueness, the yield and failure surfaces behave in a physically unacceptable manner for negative pressures, indicating that the model is probably unable to realistically describe tensile states. Because of these undesirable features, as well as the uncertainty in the effort that might be required to revise the basic model to eliminate them, we felt that it was not worthwhile pursuing this model any further for the purposes of the present study.

At the beginning of this past year's work, we set out to complete the development of the new endochronic theory for plain concrete, which had been started during the latter part of the previous year's effort. There were several aspects of this theory that needed further development, and attention was first turned to the representation of shear-volumetric coupling. Before the work had progressed very far, however, we received a copy of a letter that Weidlinger Associates had prepared for the Defense Nuclear Agency;[18] this letter focused on the concept of strain softening and raised a number of important theoretical questions regarding

*Details are given in Reference 5.

the acceptability of incorporating strain softening in rate-independent constitutive models intended for use in wave propagation studies. Subsequently, Weidlinger Associates conducted a one-dimensional numerical study of wave propagation in a simple strain softening material to further explore these issues,[19] and the results obtained clearly showed that strain softening caused an unacceptably large sensitivity of the numerical solutions to very small changes in the initial conditions. This was felt to be an important result, with widespread implications for the constitutive modeling community. In essence, it implies that meaningful wave propagation studies cannot be conducted with constitutive models that exhibit strain softening. On the other hand, extensive laboratory testing by numerous experimentalists have established the fact that concrete, rock and dense soils exhibit pronounced strain softening, especially under uniaxial and triaxial compression. This raises the following question: Do the results from the Weidlinger Associates' study therefore mean that one cannot obtain meaningful wave propagation solutions for such materials? Because of the importance of this question to the modeling of plain concrete, it was necessary to suspend further model development and turn attention to this question. In effect, the basic question which lays at the root of this issue is whether or not strain softening is a true material property, or simply a by-product of the manner in which the data from the uniaxial and/or triaxial compression tests are interpreted.

The major portion of the plain concrete modeling effort during the past year was focused on addressing the fundamental questions surrounding the strain softening issue. In the sequel, the experimental and theoretical evidence that were assembled for this purpose, as well as results from the numerical studies that we conducted independently, are presented and discussed in Section IV. On the basis of this evidence, a conclusion is drawn regarding the nature of strain softening and the question of whether or not it should be rightfully included in constitutive models of plain concrete, rock and soils.

## 2.3 PUBLICATIONS AND TECHNICAL INTERACTIONS

The following is a list of publications that have resulted from the present research program:

- Trangenstein, J. A., and H. E. Read, "A Potential Difficulty with Endochronic Plasticity Theories in Implicit Numerical Schemes," accepted for publication by the Journal of Applied Mechanics, pending revision.

- Read, H. E., Discussion of "Hysteretic Endochronic Theory for Sand" by Z. P. Bazant, R. J. Krizek and C.-L Shieh, Journal of Engrg. Mechanics, ASCE, August 1983, to appear in same journal.

- Read, H. E., and G. A. Hegemier, "Strain Softening in Soils, Rocks and concrete" (in preparation). To be submitted to Mechanics of Materials for possible publication.

- Hegemier, G. A., H. Murakami and L. J. Hageman, "On Bond-Slip Analyses of Cracked Reinforced Concrete," to be submitted to Mechanics of Materials for possible publication.

- Murakami, H., and G. A. Hegemier, "A Mixture Theory for Cracked Reinforced Concrete Elements," to be submitted to Mechanics of Materials for possible publication.

- Hageman, L. J., H. Murakami and G. A. Hegemier, "The Simulation of Monotonic and Cyclic R/C Tests by a Mixture Bond-Slip Model," to be submitted to Mechanics of Materials for possible publication.

The following is a list of presentations made at technical meetings and seminars which reported on work done under the present program:

- Hegemier, G. A., and H. E. Read, "Some Comments on Strain Softening," Proceedings of Workshop on the Theoretical Foundation of Large-Scale computations of Nonlinear Material Behavior, Northwestern University, Evanston, Illinois, October 24 - 26, 1983.

- Read, H. E., "Strain Softening of Concrete, Rock and Soil," presented at DNA Concrete Material Properties Meeting, Terra Tek, Salt Lake City, Utah, March 7, 1984.

- Hegemier, G. A., "An Advanced Mixture Theory for Reinforced Concrete," presented at DNA Concrete Material Properties Meeting, Terra Tek, Salt Lake City, Utah, March 7, 1984.

- Hegemier, G. A., "A Mixture Theory with Microstructure for Reinforced Concrete," seminar presented at University of California, Berkeley; Berkeley, California, February 22, 1984.

This Page Left Blank

# III. REINFORCED CONCRETE MIXTURE THEORY

Two models for reinforced concrete are developed in this section. The first, which is treated in subsection 3.1, applies for a dense steel layout; for this case the reinforced concrete composite is mathematically replaced by an equivalent homogenized two-phase material. The second, which is treated in subsection 3.2, applies for a sparse steel layout; here the steel and a certain volume of concrete cover are mathematically replaced by an equivalent homogenized two-phase element; the latter is intended as a new FEM rebar element.

In addition to model development, model validation studies are documented in this section. Information on this topic is presented in subsection 3.4.

The works presented in subsections 3.1 and 3.2 represent generalizations of the theories for dense and sparse steel layouts, respectively, that were developed during the first two years of this research contract, and which are documented in Reference 5. These generalizations, which represent formidable tasks and major portions of the third year's research effort, have taken place along three lines. The first consists of an extension of the previous theories, which are limited to small strains and rotations, to include finite strains and rotations. The second involves an extension of the previous models, which are limited to rectilinear steel layouts and rectangular Cartesian coordinates, to include curvilinear steel layouts and general curvilinear reference coordinate systems. The third concerns a generalization of the variational principle that is used in the model construction process. Generalization of the mixture models to include finite deformations and curvilinear steel layouts was necessary in order to provide simulation capability for an important class of practical structural problems.

Inclusion of finite deformation simulation capability necessitated a selection of a reference configuration. Two such configurations are discussed in subsection 3.3. In one, the current configuration is selected as the reference. This choice is optimum from the standpoint of theoretical developments and "updated Lagrangian" numerical schemes. In the other, the original configuration is selected as the reference. The latter choice, which constitutes a total Lagrangian description, is useful for problems involving moderate deformations.

The model validation studies presented in subsection 3.4 are devoted to the Steel-Concrete Bond Problem and the Dowel Problem (see Section II). For the former, which concerns material nonlinearities but not geometrical nonlinearities, the new theories reduce to the previous[5]. Theoretical versus experimental comparisons, a number of which were extracted from Reference 5 and included herein for completeness, reveal excellent modeling capability for this mode of response. In the case of the Dowel Problem, all previous validation studies[5] were limited to linear interaction terms and small deformations. These studies, conducted during the second year's effort, revealed the necessity of including nonlinear geometrical and constitutive effects. This was accomplished, from the standpoint of both theoretical modeling and simulation exercises, during the third year's work. As part of this effort, a numerical subroutine designed to provide hysteretic simulation capability for the Dowel Problem was constructed. A subset of the nonlinear comparisons conducted between numerical simulations and experimental results are provided in subsection 3.4. These comparisons reveal that the mixture model is capable of simulating complex nonlinear features associated with dowel action. These studies also demonstrate the need for additional high quality test data.

## 3.1 MIXTURE RELATIONS FOR DENSE STEEL

In this section, a mixture theory is formulated for the case of a dense, uniaxial steel layout. This effort represents an extension of our previous theory.[4,5] The new formulation incorporates finite deformations, and provides closure of the mixture theory without the necessity of solving complex nonlinear micro-boundary value problems. This is accomplished by combining the multivariable asymptotic technique with a variational principle.

### Basic Relations

Consider a uniaxial steel layout with a local periodic array occupying a volume $\bar{V}_0$ with boundary $\partial\bar{V}_0$ in the initial configuration as illustrated in Figure 3.1. In the current configuration the corresponding volume and surface will be denoted $\bar{V}$ and $\partial\bar{V}$, respectively.

If a spatial (Eulerian) description of motion is adopted, and if $\underset{\sim}{\bar{x}}$ denotes the global position vector of material particles, then the basic conservation equations of each constituent are:

$$D\bar{\rho}^{(\alpha)}/D\bar{t} + \bar{\rho}^{(\alpha)}\underset{\sim}{\nabla}.\underset{\sim}{\bar{v}}^{(\alpha)} = 0 \quad \text{in } \bar{V} \ , \tag{3-1}$$

$$\underset{\sim}{\nabla}.\underset{\sim}{\bar{\sigma}}^{(\alpha)} + \underset{\sim}{\bar{f}}^{(\alpha)} = \bar{\rho}^{(\alpha)}D\underset{\sim}{\bar{v}}^{(\alpha)}/D\bar{t} \quad \text{in } \bar{V} \ , \tag{3-2a}$$

$$\underset{\sim}{\bar{T}}^{\nu(\alpha)} = \underset{\sim}{\nu}^{(\alpha)}.\underset{\sim}{\bar{\sigma}}^{(\alpha)} \quad \text{on } \partial\bar{V}^{(\alpha)} \ , \tag{3-2b}$$

$$\underset{\sim}{\bar{\sigma}}^{(\alpha)} = \underset{\sim}{\bar{\sigma}}^{(\alpha)T} \quad \text{in } \bar{V} \ , \tag{3-3}$$

$$\bar{\rho}^{(\alpha)}D\bar{e}^{(\alpha)}/D\bar{t} = -\underset{\sim}{\nabla}.\underset{\sim}{\bar{q}}^{(\alpha)} + \bar{\rho}^{(\alpha)}\bar{q}^{(\alpha)} + \underset{\sim}{\bar{\sigma}}^{(\alpha)}:\underset{\sim}{\bar{d}}^{(\alpha)} \ , \quad \text{in } \bar{V} \tag{3-4}$$

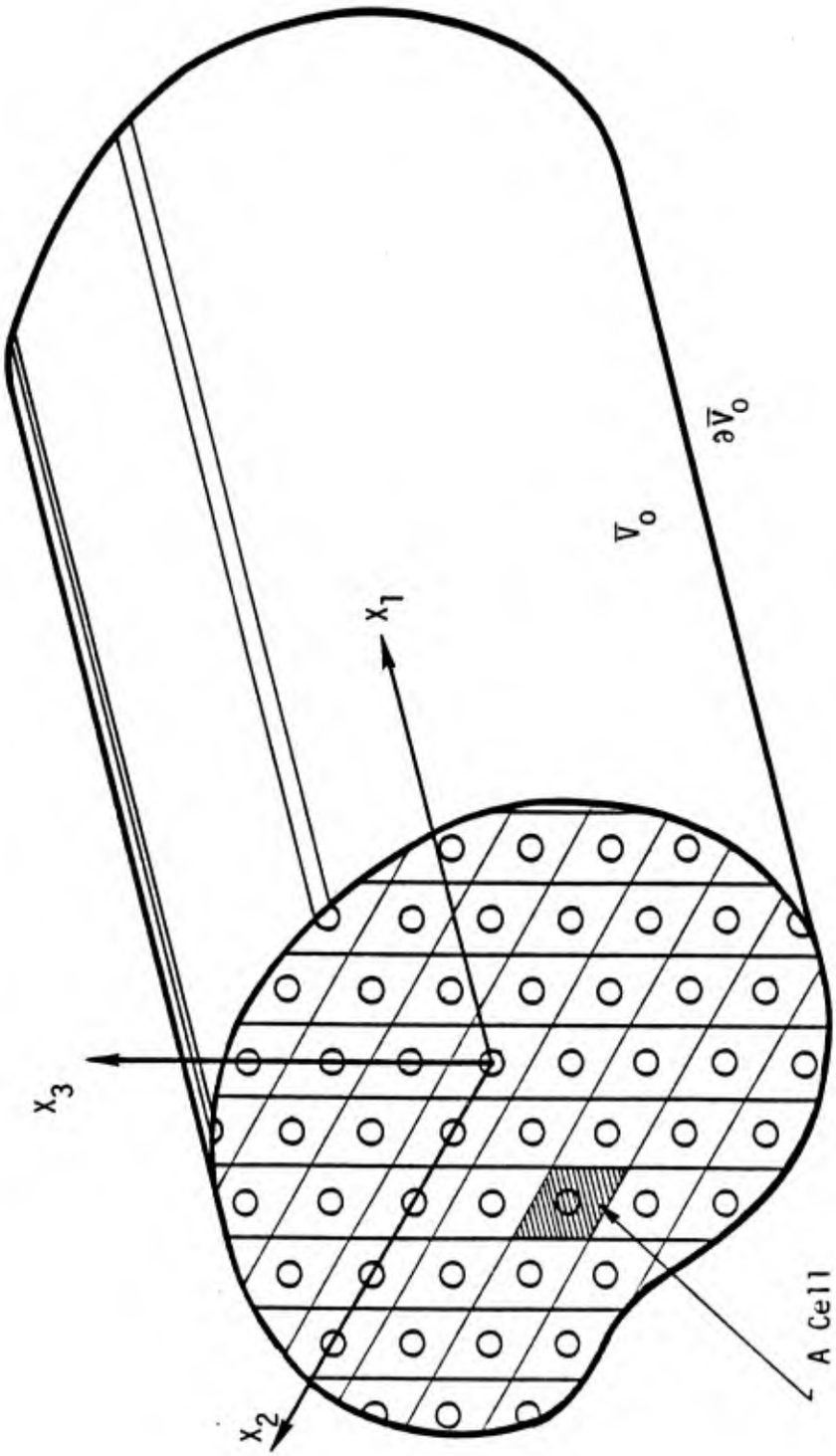


Figure 3.1. Densely reinforced concrete; initial configuration.

where $\bar{\nabla}$ is the gradient operator with respect to $\bar{x}$, $\bar{v}$ is the velocity vector, $\bar{d}_{ij} \equiv 1/2(\bar{v}_{i,j} + \bar{v}_{j,i})$ is the rate-of-deformation tensor, $\bar{\sigma}$ denotes the Cauchy stress tensor, $\bar{\rho}$ denotes material density, $\bar{f}$ is a body force per unit (current) volume, $\bar{T}$ is the traction vector acting on the surface $\partial\bar{V}$ with unit outer normal $\nu$, $\bar{e}$ denotes internal energy per unit mass, $\bar{\mathcal{J}}$ is the heat flux vector per unit time and current area, $\bar{q}$ is a heat source rate per unit time and mass, superscript $\alpha = 1,2$ denotes material $\alpha$ with $\alpha = 1$ representing steel and $\alpha = 2$ concrete, $(\ )^T$ denotes transposition of the tensor indices, $D(\ )/Dt$ is the material time derivative, and $\bar{V}^{(\alpha)}$ is the current volume occupied by material $\alpha$ with boundary $\partial\bar{V}^{(\alpha)}$. In the sequel both the direct and index notations will be used. Lower case indices refer to a fixed rectangular Cartesian coordinate system and repeated subscripts are summed. Superscripts do not refer to tensor components. Repetition of unbracketed superscripts implies summation. Bracketed superscripts are not summed. Thus, $\alpha$ is not summed in the foregoing equations. Equations (3-1) - (3-4) represent the conservation of mass, linear momentum, angular momentum, and energy, respectively. In (3-2), the components of $\bar{\nabla}\cdot\bar{\sigma}$ and $\bar{\nu}\cdot\bar{\sigma}$ are $\bar{\sigma}_{ji,j}$ and $\bar{\nu}_j\bar{\sigma}_{ji}$ respectively. In (3-4) the components of $\bar{\sigma}:\bar{d}$ are $\bar{\sigma}_{ij}\bar{d}_{ij}$.

In what follows, attention will be focused upon physical processes that occur over time intervals that are short compared to typical thermal diffusion times. Consequently, an adiabatic premise will be adopted. Accordingly, in (3-4) one sets

$$\bar{q}^{(\alpha)} \simeq 0, \bar{\mathcal{J}}^{(\alpha)} \simeq 0 \quad . \tag{3-5}$$

The conservation equations must be supplemented by appropriate constitutive relations. A reasonably general class of constitutive behaviors may be characterized by assuming[20] that an objective stress rate relates linearly to the rate-of-deformation tensor, i.e.,

$$\overset{\nabla}{\underset{\sim}{\sigma}}{}^{(\alpha)} = \overline{\underset{\sim}{\mathscr{D}}}^{(\alpha)} : \overline{\underset{\sim}{d}}^{(\alpha)} \tag{3-6}$$

where $\overline{\underset{\sim}{\mathscr{D}}}^{(\alpha)}$ is the instantaneous elastic-plastic modulus tensor for material $\alpha$ and the componenbts of $\overline{\underset{\sim}{\mathscr{D}}} : \overline{\underset{\sim}{d}}$ are $\overline{\mathscr{D}}_{ijk\ell}\overline{d}_{k\ell}$. The tensor $\overline{\underset{\sim}{\mathscr{D}}}^{(\alpha)}$ is assumed to be independent of the stress rate and the rate of deformation, but may depend upon the current stress state, internal energy, and certain deformation measures. Isotropy of $\overline{\underset{\sim}{\mathscr{D}}}^{(\alpha)}$ may not be assumed in general due to plastic flow and/or prior cracking of the concrete. While $\overline{\underset{\sim}{\mathscr{D}}}^{(\alpha)}$ is symmetric with respect to the exchange of i and j, and k and $\ell$, it is not, in general, symmetric with respect to the exchange of ij and k$\ell$.

The stress rate in (3-6) deserves comment. The Jaumann rate corotational with the material is most frequently adopted in constitutive relations of the type (3-6). In this case

$$\overset{\nabla}{\underset{\sim}{\sigma}}{}^{(\alpha)} \equiv D\overline{\underset{\sim}{\sigma}}^{(\alpha)}/D\overline{t} - \overline{\underset{\sim}{w}}^{(\alpha)} \cdot \overline{\underset{\sim}{\sigma}}^{(\alpha)} + \overline{\underset{\sim}{\sigma}}^{(\alpha)} \cdot \overline{\underset{\sim}{w}}^{(\alpha)} \quad , \tag{3-7}$$

where components of, say, $\overline{\underset{\sim}{w}} \cdot \overline{\underset{\sim}{\sigma}}$ are $\overline{w}_{ik}\overline{\sigma}_{kj}$. However, a number of other objective stress rates have been introduced by various authors[20]. While each rate is admissible from the standpoint of being objective, each leads to a different constitutive relation. An appropriate choice depends upon the problem under consideration.

The constitutive form (3-3) covers a wide class of elastic-plastic and elastic-plastic-brittle fracture behavior. Yet, it is not intended to be comprehensive. Rather, it is selected for instructional purposes. Other constitutive relations can be incorporated into the theoretical development to follow if necessary.

A remark concerning the foregoing Eulerian description of motion is in order at this point. For computational purposes it is often convenient to employ an "updated Lagrangian" description of motion. Accordingly, the Kirchhoff stress is adopted as the stress measure and the <u>current</u> configuration is used as the reference. In view of the latter,

$$\bar{\underset{\sim}{\tau}} = \bar{\underset{\sim}{\sigma}} \tag{3-8}$$

where $\bar{\underset{\sim}{\tau}}$ denotes the Kirchhoff stress tensor. However, $D\bar{\underset{\sim}{\tau}}/D\bar{t} \neq D\bar{\underset{\sim}{\sigma}}/D\bar{t}$ since

$$D\bar{\underset{\sim}{\tau}}/D\bar{t} = D\bar{\underset{\sim}{\sigma}}/D\bar{t} + d\,\bar{\sigma} \quad , \quad d = \bar{\underset{\sim}{\nabla}}.\,\bar{\underset{\sim}{v}} \tag{3-9}$$

Thus, for an updated Lagrangian description, one need only replace $\bar{\underset{\sim}{\sigma}}$ by $\bar{\underset{\sim}{\tau}}$ in the conservation equations (3-1) - (3-4) and interpret $D(\ )/D\bar{t}$ as a material time derivative. However, the constitutive relation (3-6) must be altered. For this purpose (3-6) is replaced by

$$\overset{\nabla}{\underset{\tau}{}}{}^{(\alpha)} = \bar{\mathscr{L}}^{(\alpha)} : \bar{\underset{\sim}{d}}^{(\alpha)} \quad . \tag{3-10}$$

From (3-6), (3-8) and (3-9), one finds

$$\bar{\underset{\sim}{D}}^{(\alpha)} = \bar{\underset{\sim}{\mathscr{L}}}^{(\alpha)} - \underset{\sim}{g}^{(\alpha)}\underset{\sim}{\delta} \quad , \quad \text{or} \quad \bar{\underset{\sim}{\mathscr{L}}}^{(\alpha)} = \bar{\underset{\sim}{D}}^{(\alpha)} + \bar{\underset{\sim}{\tau}}^{(\alpha)}\underset{\sim}{\delta} \quad , \tag{3-11}$$

where $\underset{\sim}{g}\underset{\sim}{\delta}$ denotes the tensor product, i.e., components of $\underset{\sim}{g}\underset{\sim}{\delta}$ are $\sigma_{ij}\delta_{k\ell}$ (this product is often written $\underset{\sim}{g} \otimes \underset{\sim}{\delta}$).

In addition to the above conservation and constitutive equations, relations between tractions and velocities for each constituent across the steel-concrete interface must be specified. For modeling purposes this interface is idealized as smooth. Let $\bar{\mathscr{I}}^*$ denote that part of $\partial\bar{V}^{(1)}$ in contact with $\partial\bar{V}^{(2)}$, where both are smooth. Then, continuity of the traction vector requires that

$$\overset{\nu}{\underset{\sim}{T}}{}^{(1)} = -\overset{\nu}{\underset{\sim}{T}}{}^{(2)} \equiv \underset{\sim}{T}^* \text{ on } \bar{\mathscr{I}} \quad . \tag{3-12}$$

With respect to displacements, relative slip across $\bar{\mathscr{I}}$ must be allowed to simulate steel-concrete bond slip and dowel action. Accordingly, a relative velocity $[\bar{\underset{\sim}{v}}]$ is defined by

$$\underset{\sim}{\bar{v}}^{(2)} - \underset{\sim}{\bar{v}}^{(1)} \equiv [\underset{\sim}{\bar{v}}] \text{ on } \bar{\mathscr{I}} \tag{3-13}$$

An interface "constitutive law" is next postulated in the form of a linear relation between an objective traction rate and the relative velocity, i.e.,

$$\overset{0}{\underset{\sim}{\bar{T}}}{}^{*} = \underset{\sim}{\bar{\mathscr{B}}}\,[\underset{\sim}{\bar{v}}] \text{ on } \bar{\mathscr{I}} \ , \tag{3-14a}$$

$$\overset{0}{\underset{\sim}{\bar{T}}}{}^{*} \equiv D\underset{\sim}{\bar{T}}{}^{*}/D\bar{t} - \underset{\sim}{\bar{w}} \cdot \underset{\sim}{\bar{T}}{}^{*} \ , \tag{3-14b}$$

where $\underset{\sim}{\bar{\mathscr{B}}}$ is a second rank tangent modulus tensor which may depend on the current states of stress and relative slip on $\bar{\mathscr{I}}$.

It should be noted that the normal component of velocity (to the surface $\bar{\mathscr{I}}$) may be discontinuous as well as the tangential component in (3-9) and (3-10). This degree of freedom is necessary to allow proper simulation of actual steel-concrete interaction under certain conditions using the idealized smooth surface $\bar{\mathscr{I}}$.

If contact between $\partial\bar{V}^{(1)}$ and $\partial\bar{V}^{(2)}$ is lost, then one sets $\underset{\sim}{\overset{\vee}{T}}{}^{(2)} = 0$, $\underset{\sim}{\overset{\vee}{T}}{}^{(1)} = 0$ over those segments of $\partial\bar{V}^{(1)}$ and $\partial\bar{V}^{(2)}$ corresponding to no contact. This situation can also be incorporated into the form (3-14a) by a suitable choice of $\underset{\sim}{\bar{\mathscr{B}}}$.

The foregoing relations (3-1) - (3-14), must be supplemented by initial conditions at $\bar{t} = 0$ and boundary conditions on $\partial\bar{V}$.

## Scaling

It will be convenient to nondimensionalize the basic equations. For this purpose let

$\bar{\Lambda}$ = typical macrosignal wavelength

$\bar{\Delta}$ = typical steel spacing

$\bar{c}_{(m)}, \bar{\rho}_{(m)}$ = reference wave velocity and macrodensity

$\bar{E}_{(m)} = \bar{\rho}_{(m)}\bar{c}^2_{(m)}$ = reference modulus

$\bar{t}_{(m)}$ = typical macrosignal travel time ($= \bar{\Lambda}/\bar{c}_{(m)}$)

$\varepsilon \quad = \bar{\Delta}/\bar{\Lambda}$ = ratio of micro-to-macrodimensions.

With the aid of the above notation, nondimensional variables are now introduced according to

$$\underset{\sim}{x} = \bar{\underset{\sim}{x}}/\bar{\Lambda} \quad , \quad t = \bar{t}/\bar{t}_{(m)} \quad ,$$

$$\underset{\sim}{v} = \bar{\underset{\sim}{v}}/c_{(m)} \quad , \underset{\sim}{\sigma} = \bar{\underset{\sim}{\sigma}}/\bar{E}_{(m)} \quad ,$$

$$\varepsilon[\dot{\underset{\sim}{v}}] = [\dot{\bar{\underset{\sim}{v}}}]/\bar{c}_{(m)} \quad , \underset{\sim}{T}^* = \bar{\underset{\sim}{T}}^*/\bar{E}_{(m)} \quad , \tag{3-15}$$

$$\underset{\sim}{\mathcal{D}} = \bar{\underset{\sim}{\mathcal{D}}}/\bar{E}_{(m)} \quad , \quad \frac{1}{\varepsilon}\underset{\sim}{\mathcal{B}} = \bar{\underset{\sim}{\mathcal{B}}}/(\bar{E}_{(m)}\bar{\Delta}) \quad ,$$

$$\rho = \bar{\rho}/\rho_{(m)} \quad , \quad \tilde{\underset{\sim}{f}} = (\bar{\Lambda}/\bar{E}_m)\bar{\underset{\sim}{f}} \quad .$$

In terms of the nondimensional variables, the basic equations take the following form:

(a) Conservation Relations

$$D\rho^{(\alpha)}/Dt + \rho^{(\alpha)}\underset{\sim}{\nabla}\cdot\underset{\sim}{v}^{(\alpha)} = 0 \text{ in } V^{(\alpha)} \tag{3-16}$$

$$\underset{\sim}{\nabla}\cdot\underset{\sim}{\sigma}^{(\alpha)} + \underset{\sim}{f}^{(\alpha)} = 0 \quad , \underset{\sim}{f}^{(\alpha)} \equiv \tilde{\underset{\sim}{f}}^{(\alpha)} - \rho D\underset{\sim}{v}^{(\alpha)}/Dt \text{ in } V^{(\alpha)} \tag{3-17a}$$

$$\overset{\nu}{\underset{\sim}{T}}{}^{(\alpha)} = \underset{\sim}{\nu}^{(\alpha)}\cdot\underset{\sim}{\sigma}^{(\alpha)} \text{ on } \partial V^{(\alpha)} \tag{3-17b}$$

$$\underset{\sim}{\sigma}^{(\alpha)} = \underset{\sim}{\sigma}^{(\alpha)T} \text{ on } V^{(\alpha)} \tag{3-18}$$

$$\rho^{(\alpha)}De^{(\alpha)}/Dt = \underset{\sim}{\sigma}^{(\alpha)}:\underset{\sim}{d}^{(\alpha)} \text{ in } V^{(\alpha)} \tag{3-19}$$

(b) Constitutive Relations

$$\overset{\nabla}{\underset{\sim}{\sigma}}{}^{(\alpha)} = \underset{\sim}{\mathscr{D}}^{(\alpha)} : \underset{\sim}{d}^{(\alpha)} \quad , \quad \underset{\sim}{d}^{(\alpha)} = \frac{1}{2}(\underset{\sim}{\nabla v}^{(\alpha)} + \underset{\sim}{\nabla}^{T}\underset{\sim}{v}^{(\alpha)}) \text{ in } V^{(\alpha)} \tag{3-20}$$

(c) Interface Relations

$$\overset{v}{\underset{\sim}{T}}(1) = -\overset{v}{\underset{\sim}{T}}(2) \equiv \underset{\sim}{T}^{*} \text{ on } \mathscr{I} \tag{3-21}$$

$$\overset{0}{\underset{\sim}{T}}{}^{*} = \underset{\sim}{\mathscr{B}}.[\underset{\sim}{v}] \quad , \quad [\underset{\sim}{v}] \equiv \underset{\sim}{v}^{(2)} - \underset{\sim}{v}^{(1)} \text{ on } \mathscr{I} \tag{3-22}$$

(e) Initial Conditions at t = 0, Boundary Data on $\partial V$.

Microcoordinates

It is expected that stress and deformation fields will vary significantly with respect to two basic length scales: (1) a "global" or "macro" length typical of the body size or loading condition, and (2) a "micro" length typical of a "cell" planar dimensions as depicted in Figure 3.2. These macro and micro dimensions will be associated with the variables $\bar{\Lambda}$, $\bar{\lambda}$ respectively. Further, it is expected that these scales will differ by at least one order of magnitude in most cases. This suggests the use of multivariable asymptotic techniques.[7] This approach commences by introducing new independent variables* according to

$$\begin{aligned} \underset{\sim}{x}^{*} &= \phi_{1}^{-1}(\varepsilon)\underset{\sim}{x} \quad , \ \phi(\varepsilon) > 0 \text{ as } \varepsilon > 0, \\ \underset{\sim}{x} &= \psi(\varepsilon)\underset{\sim}{x} \quad , \ \psi(\varepsilon) > 1 \text{ as } \varepsilon > 0 . \end{aligned} \tag{3-23}$$

For the present analysis it will suffice to set

$$\phi(\varepsilon) = \varepsilon \ , \ \psi(\varepsilon) = 1 \tag{3-24}$$

*In what follows, it is implicitly assumed that the cell aspect ratio is of order one.

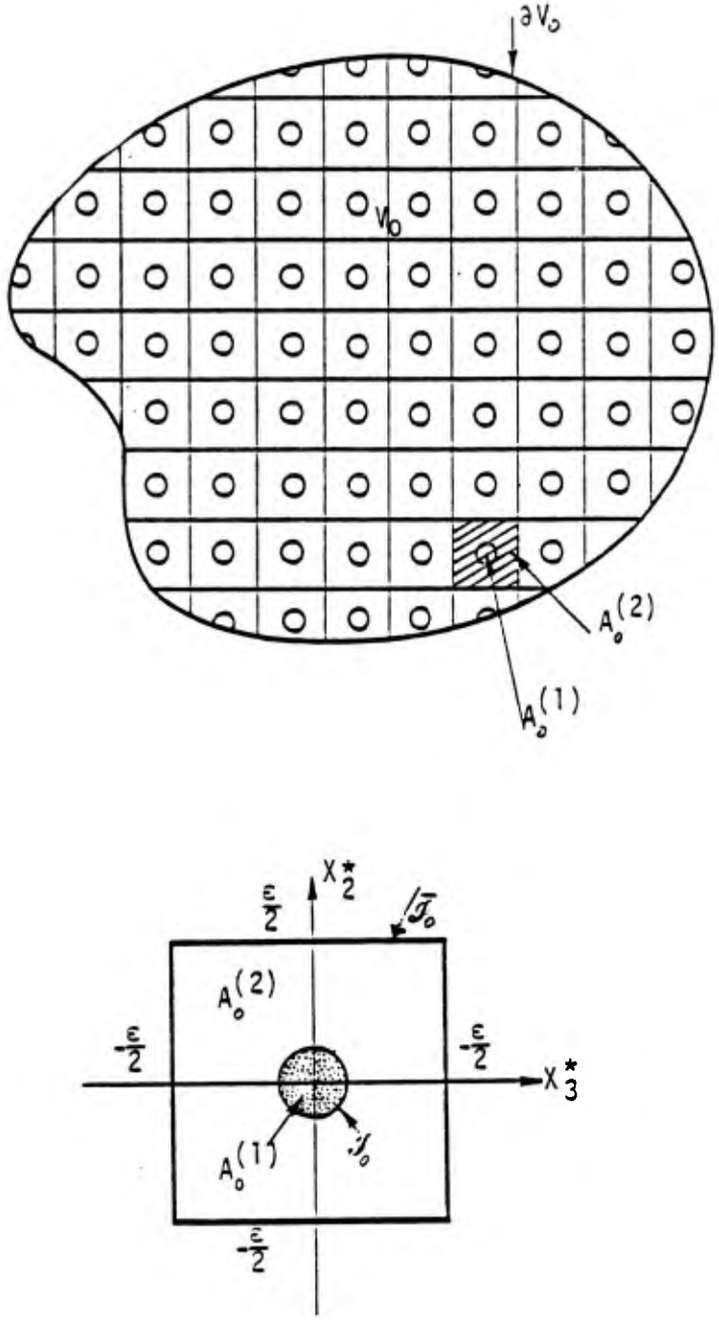


Figure 3.2. Cell geometry for densely reinforced concrete (shown in initial configuration).

Thus, all field variables $f(\underset{\sim}{x},t)$ are now functions of the "microcoordinates" $x^*$ as well as the "macrocoordinates" $\underset{\sim}{\tilde{x}} \equiv \underset{\sim}{x}$, i.e.,

$$f(\underset{\sim}{x},t) = F(\underset{\sim}{x},t;\underset{\sim}{x}^*;\varepsilon) \quad . \tag{3-25a}$$

Spatial derivatives of a function $f(\underset{\sim}{x},t)$ then take the form

$$\underset{\sim}{\nabla} f = \underset{\sim}{\nabla} F + \varepsilon^{-1} \underset{\sim}{\nabla}^* F \quad . \tag{3-25b}$$

For notational convenience in the following development, the functions f and F will both be written as f.

For some problems it is necessary to introduce time-microvariables as well as the foregoing space-microvariables. These additional variables will not be advantageous for the present formulation, however.

It is noted that, for the present unidirectional steel layout, it is appropriate to constrain the vector $\underset{\sim}{x}^*$ according to

$$\underset{\sim}{x}^* . \underset{\sim}{t} = 0 \tag{3-25c}$$

where $\underset{\sim}{t}$ denotes the tangent vector to the steel centerline.

## Synthesized Field Equations

The operations (3-25), when applied to all field variables, lead to the following "synthesized" governing field equations:

(a) Conservation Relations

$$D\rho^{(\alpha)}/Dt + \rho^{(\alpha)} \underset{\sim}{\nabla} . \underset{\sim}{v}^{(\alpha)} + \frac{1}{\varepsilon} \underset{\sim}{\nabla}^* . (\rho^{(\alpha)} \underset{\sim}{v}^{(\alpha)}) = 0 \text{ in } V^{(\alpha)} \tag{3-26}$$

$$\underset{\sim}{\nabla} . \underset{\sim}{\sigma}^{(\alpha)} + \frac{1}{\varepsilon} \underset{\sim}{\nabla}^* . \underset{\sim}{\sigma}^{(\alpha)} + \underset{\sim}{f}^{(\alpha)} = 0 \quad \text{in } V^{(\alpha)} \quad , \tag{3-27a}$$

$$\underset{\sim}{T}^{\nu(\alpha)} = \underset{\sim}{\nu}^{(\alpha)} . \underset{\sim}{\sigma}^{(\alpha)} \text{ on } \partial V^{(\alpha)} \quad , \tag{3-27b}$$

$$\underset{\sim}{\sigma}^{(\alpha)} = \underset{\sim}{\sigma}^{(\alpha)^T} \text{ in } V^{(\alpha)} \quad , \tag{3-28}$$

$$\rho^{(\alpha)} De^{(\alpha)}/Dt + \frac{1}{\varepsilon}\underset{\sim}{v}^{(\alpha)} \cdot \underset{\sim}{\nabla}^* e^{(\alpha)} = \underset{\sim}{\sigma}^{(\alpha)} : (\underset{\sim}{d}^{(\alpha)} + \underset{\sim}{d}^{*(\alpha)}) \text{ in } V^{(\alpha)} \quad ,$$

$$\underset{\sim}{d}^{*(\alpha)} \equiv \frac{1}{2\varepsilon} (\underset{\sim}{\nabla}^* \underset{\sim}{v} + \underset{\sim}{\nabla}^{*T} \underset{\sim}{v}) \quad . \tag{3-29}$$

(b) Constitutive Relation

$$\overset{\nabla}{\underset{\sim}{\sigma}}{}^{(\alpha)} = \underset{\sim}{\mathscr{D}}^{(\alpha)} : (\underset{\sim}{d}^{(\alpha)} + \underset{\sim}{d}^{*(\alpha)}) \text{ in } V^{(\alpha)} \quad . \tag{3-30}$$

(c) Interface Relations

$$\overset{v}{\underset{\sim}{T}}{}^{(1)} = - \overset{v}{\underset{\sim}{T}}{}^{(2)} \equiv T^* \text{ on } \mathscr{I} \tag{3-31a}$$

$$\overset{0}{\underset{\sim}{T}}{}^* = \underset{\sim}{\mathscr{B}} . [\underset{\sim}{v}] \quad ,$$

$$[\underset{\sim}{v}] \equiv v^{(2)} - v^{(1)} \quad \text{on } \mathscr{I} \tag{3-31b}$$

(c) Initial Conditions at t = 0, Boundary Data on $\partial V$.

In the above, $\underset{\sim}{\nabla}^*$ is the gradient operator with respect to $\underset{\sim}{x}^*$, e.g., components of $\underset{\sim}{\nabla}^* \underset{\sim}{v}$ are $\partial v_i/\partial x^*_j$. The material derivative D( )/Dt refers to the macrovariables $x_i$ only.

## Constraints

In what follows, attention will be restricted to processes in which:

(1) The constitutive and interface relations do not depend on the internal energy.

(2) The micro-deformation gradient is sufficiently small that micro-flux or micro-convection terms may be neglected in the material derivative.

(3) The micro-rotation is sufficiently small that its contribution to the stress rate may be neglected.

(4) The micro-deformation is sufficiently small that microvariations in the mass density may be neglected.

Under the above constraints, which are considered to be appropriate for the analysis of reinforced concrete, the last term in (3-26) can be neglected, the energy equation (3-29) need not be treated, and the material and stress-rate derivatives are to be interpreted in terms of the macrocoordinates only.

## Periodicity Condition

At this point a local periodicity condition is introduced. This condition consists of the premise that local periodicity in the microvariable $\underset{\sim}{x}^*$ may be invoked for all field variables. This premise allows one to analyze a single cell in an effort to determine the distribution of any field variable with respect to the mirocoordinate $\underset{\sim}{x}^*$. A typical such cell is illustrated in Figure 3.2.

The local periodicity premise is motivated by extrapolation from linear analysis.[7] It is expected to provide a good representation of the field variables for dense steel layouts.

## Variational Principle for Synthesized Fields

A variational principle is now constructed for the synthesized field variables. For this purpose consider the relation

$$\int_V \left\{ \sum_{\alpha=1}^{2} \int_{A(\alpha)} \left( \underset{\sim}{\nabla}.\underset{\sim}{\sigma}^{(\alpha)} + \varepsilon^{-1} \underset{\sim}{\nabla}^*.\underset{\sim}{\sigma}^{(\alpha)} + \underset{\sim}{f}^{(\alpha)} \right) . \delta \underset{\sim}{v}^{(\alpha)} dA^* \right\} dV$$

$$+ \int_{\partial V} \left\{ \sum_{\alpha=1}^{2} \int_{A(\alpha)} \left( \overset{\nu}{\underset{\sim}{T}} - \underset{\sim}{\nu}.\underset{\sim}{\sigma} \right)^{(\alpha)} . \delta \underset{\sim}{v}^{(\alpha)} dA^* \right\} dS$$

$$+ \int_V \left\{ \sum_{\alpha=1}^{2} \oint_{\mathscr{I}} \varepsilon^{-1} (\underset{\sim}{\overset{\nu}{T}} - \underset{\sim}{\nu} \cdot \underset{\sim}{\sigma}^{(\alpha)}) \cdot \delta \underset{\sim}{v}^{(\alpha)} ds^* \right\} dV$$

$$+ \int_V \left\{ \oint_{\partial A^{(2)}} \varepsilon^{-1} (-\underset{\sim}{\nu}^{(2)} \cdot \underset{\sim}{\sigma}^{(2)}) \cdot \delta \underset{\sim}{v}^{(2)} ds^* \right\} dV = 0 \quad . \tag{3-33}$$

In the above, $d\underset{\sim}{A}^* = dA^* \underset{\sim}{t}$, where $\underset{\sim}{t}$ is the unit tangent vector to the steel centerline in a given cell. Thus, if a plane with normal $\underset{\sim}{t}$ intersects the steel centerline within a cell, then $A^{(\alpha)}$ is the projected area of material $\alpha$ on this plane. The integration is carried out over the microcoordinates, e.g., if $x^*_k$, $k = 2,3$ denote local Cartesian coordinates in the above plane, then $dA^* = dx^*_2 dx^*_3$. The quantity $\mathscr{I} \equiv \partial A^{(1)}$, i.e., $\mathscr{I}$ is the projection of the steel-concrete boundary on this plane.

Let the boundary $\partial V = \partial V_T + \partial V_u$. Then, the following is assumed:

$$\begin{aligned} &\underset{\sim}{\overset{\nu}{T}}{}^{(\alpha)} \text{ prescribed on } \partial V_T \\ &\delta \underset{\sim}{v}^{(\alpha)} = 0 \text{ on } \partial V_u \quad . \end{aligned} \tag{3-34}$$

In addition, let

$$\underset{\sim}{\overset{\nu}{T}}(1) = - \underset{\sim}{\overset{\nu}{T}}(2) \equiv \underset{\sim}{T}^* \text{ on } \mathscr{I} \equiv \partial A^{(1)} \tag{3-35}$$

where $\underset{\sim}{T}^*$ is prescribed. Finally, let

$$\begin{aligned} &\delta \underset{\sim}{v}^{(\alpha)} \in C' \text{ on } A^{(\alpha)} \text{ with respect to } \underset{\sim}{x}, \underset{\sim}{x}^*, \\ &\delta \underset{\sim}{v}^{(\alpha)} \in \underset{\sim}{x}^* \text{ - periodic} \quad . \end{aligned} \tag{3-36}$$

If $\delta \underset{\sim}{v}^{(\alpha)}$ is the variation of the exact velocity field, then the first term of (3-33) vanishes due to (3-27a), the second vanishes due to (3-27b) and (3-34), the third vanishes due to (3-27b), and the last term vanishes due to (3-32). Thus, the validity of (3-33) is established if $\underset{\sim}{v}^{(\alpha)}$ is the exact velocity field.

If $\underset{\sim}{v}^{(\alpha)}$ is not the exact field, then (3-33) corresponds to a weighted residual procedure for generating weak solutions of the governing equations. The weighting functions are $\delta\underset{\sim}{v}^{(\alpha)}$. In the latter case the solutions are of course approximate.

With the aid of Gauss' Theorem, and (3-34) - (3-36), (3-33) can be placed in the following form:

$$\int_V \left\{ \sum_{\alpha=1}^{2} \int_{A^{(\alpha)}} \underset{\sim}{\sigma}:(\underset{\sim}{\nabla}\delta\underset{\sim}{v}^{(\alpha)} + \varepsilon^{-1}\underset{\sim}{\nabla}^*\delta\underset{\sim}{v}^{(\alpha)})dA^* + \varepsilon^{-1}\int_{\mathscr{I}} \underset{\sim}{T}^*.\delta[\underset{\sim}{v}]ds) \right\} dV \tag{3-37}$$

$$= \int_V \left\{ \sum_{\alpha=1}^{2} \int_{A^{(\alpha)}} \underset{\sim}{f}^{(\alpha)}.\delta\underset{\sim}{v}^{(\alpha)}\, dA^* \right\} dV + \int_{\partial V_T} \left\{ \sum_{\alpha=1}^{2} \int_{A^{(\alpha)}} \overset{\nu}{\underset{\sim}{T}}{}^{(\alpha)}.\delta\underset{\sim}{v}^{(\alpha)} dA^* \right\} dS.$$

Equation (3-37) corresponds to the Principle of Virtual Work for the synthesized fields. This relation constitutes an important tool, in the form of a variational principle, for generating mixture field equations for the highly nonlinear class of problems of interest herein.

## Test Functions

Kantorovich's direct variational method is now used to generate the desired mixture equations. The trial velocity field (test functions) is selected in the form

$$\underset{\sim}{v}^{(\alpha)}(\underset{\sim}{x},t;\underset{\sim}{x}^*;\varepsilon) = \underset{\sim}{\dot{U}}^{(\alpha)}(\underset{\sim}{x},t) + \varepsilon\underset{\sim}{\dot{S}}^{K(\alpha)}(\underset{\sim}{x},t)g^{K(\alpha)}(\underset{\sim}{x}^*) + O(\varepsilon^2). \tag{3-38}$$

The "weight" functions $g^{K(\alpha)}(\underset{\sim}{x}^*)$ are to be prescribed for each material ($\alpha = 1,2$). The vector $\underset{\sim}{\dot{U}}^{(\alpha)}$ reflects the macro contribution to the velocity field whereas the vectors $\underset{\sim}{\dot{S}}^{K(\alpha)}$ reflect the micro contribution; these variables play the role of new dependent-type displacement variables. In the above, and in what follows, the summation convention is used with respect to the index K with range 1 to n.

## Equations of Motion, Boundary Conditions

Substitution of the test functions (3-38) into the variational principle (3-34) furnishes, after some algebraic manipulation and integrations by parts, the following relation:

$$\int_{\partial V_T} \left[ \sum_{\alpha=1}^{2} \delta \dot{\underset{\sim}{U}}^{(\alpha)} \cdot (\overset{\nu}{\underset{\sim}{T}}{}^{p(\alpha)} - \underset{\sim}{\nu} \cdot \underset{\sim}{N}^{(\alpha)}) + \delta \dot{\underset{\sim}{S}}^{k(\alpha)} \cdot (\overset{\nu}{\underset{\sim}{T}}{}^{k(\alpha)} - \underset{\sim}{\nu} \cdot \underset{\sim}{M}^{k(\alpha)}) \right] dS$$

$$+ \int_V \left\{ \sum_{\alpha=1}^{2} \delta \dot{\underset{\sim}{U}}^{(\alpha)} \cdot (\underset{\sim}{\nabla} \cdot \underset{\sim}{N}^{(\alpha)} + \underset{\sim}{F}^{(\alpha)} + (-1)^{1+\alpha} \underset{\sim}{P}) \right.$$

$$\left. + \delta \dot{S}^{k(\alpha)} \cdot (\underset{\sim}{\nabla} \cdot \underset{\sim}{M}^{k(\alpha)} - \underset{\sim}{\overline{N}}^{k(\alpha)} + \underset{\sim}{F}^{k(\alpha)} + (-1)^{1+\alpha} \underset{\sim}{Q}^{k}) \right\} dV = 0 \quad . \tag{3-39}$$

In (3-39), the following quantities have been defined:

$$(\underset{\sim}{F}^{(\alpha)}, \underset{\sim}{F}^{k(\alpha)}) \equiv \int_{A^{(\alpha)}} (1, \varepsilon g^{k(\alpha)}) \underset{\sim}{f}^{(\alpha)} dA^* \quad , \tag{3-40}$$

$$(\underset{\sim}{N}^{(\alpha)}, \underset{\sim}{M}^{k(\alpha)}) \equiv \int_{A^{(\alpha)}} (1, \varepsilon g^{k(\alpha)}) \underset{\sim}{\sigma}^{(\alpha)} dA^* \quad , \tag{3-41}$$

$$\underset{\sim}{\overline{N}}^{k(\alpha)} \equiv \int_{A^{(\alpha)}} \varepsilon \underset{\sim}{\sigma}^{(\alpha)} \cdot \underset{\sim}{\nabla}^* g^{k(\alpha)} dA^* \quad , \tag{3-42}$$

$$\left( \overset{\nu}{\underset{\sim}{T}}{}^{(\alpha)}, \overset{\nu}{\underset{\sim}{T}}{}^{k(\alpha)} \right) \equiv \int_{A^{(\alpha)}} (1, \varepsilon g^{k(\alpha)}) \overset{\nu}{\underset{\sim}{T}}{}^{(\alpha)} \, dA^* \quad , \tag{3-43}$$

$$\underset{\sim}{P} \equiv \frac{1}{\varepsilon} \oint_{\mathscr{I}} \underset{\sim}{T}^* ds^* \quad , \quad \underset{\sim}{Q}^k \equiv \oint_{\mathscr{I}} \underset{\sim}{T}^* \, g^{k(\alpha)} ds^* \quad (\alpha = 1 \text{ or } 2) \quad . \tag{3-44}$$

The Euler-Lagrange equations associated with the variational equation (3-39) are

$$\underset{\sim}{\nabla} \cdot \underset{\sim}{N}^{(\alpha)} + \underset{\sim}{F}^{(\alpha)} + (-1)^{1+\alpha} \underset{\sim}{P} = 0 \quad \text{in } V \quad , \tag{3-45}$$

$$\underset{\sim}{\nabla} \cdot \underset{\sim}{M}^{k(\alpha)} - \underset{\sim}{\overline{N}}^{k(\alpha)} + \underset{\sim}{F}^{k(\alpha)} + (-1)^{1+\alpha} \underset{\sim}{Q}^{k} = 0 \text{ in } V \quad . \tag{3-46}$$

The boundary conditions are

$$\overset{\nu}{\underset{\sim}{T}}{}^{(\alpha)} = \underset{\sim}{\nu}.\underset{\sim}{N}^{(\alpha)} \quad \text{or} \quad \delta\dot{\underset{\sim}{U}}^{(\alpha)} = 0 \quad \text{on } \partial V_T \ , \tag{3-47}$$

$$\overset{\nu}{\underset{\sim}{T}}{}^{k(\alpha)} = \underset{\sim}{\nu}.\underset{\sim}{M}^{k(\alpha)} \quad \text{or} \quad \delta\dot{\underset{\sim}{S}}^{k(\alpha)} = 0 \quad \text{on } \partial V_T . \tag{3-48}$$

Equations (3-45) are the "smoothed" equilibrium relations. They have the form of a binary mixture. The dependent variables $\underset{\sim}{N}^{(\alpha)}$ represent "partial stress" tensors, i.e., stress averages over the cell area occupied by the appropriate constituent. The quantity $\underset{\sim}{P}$ represents a stress interaction vector which reflects stress transfer between the steel and the concrete across the interface $\mathscr{I}$.

In addition to direct averages of the stress field over the cell, weighted averages also enter the formulation via the variational principle. Equation (3-46) governs these new dependent variables.

The variational principle provides appropriate boundary conditions for the displacement-type variables $\dot{\underset{\sim}{U}}^{(\alpha)}$, $\dot{\underset{\sim}{S}}^{k(\alpha)}$ and the stress-type variables $\underset{\sim}{N}^{(\alpha)}$, $\underset{\sim}{M}^{k(\alpha)}$. These conditions are expressed by (3-47) and (3-48).

## Mixture Constitutive Relations

The test functions (3-38) furnish the following rate-of-deformation tensor:

$$\underset{\sim}{d}^{(\alpha)} = \dot{\underset{\sim}{\mathscr{E}}}^{(\alpha)} + \varepsilon g^{k(\alpha)} \dot{\underset{\sim}{\mathscr{K}}}^{k(\alpha)} + \underset{\sim}{d}^{*(\alpha)} \tag{3-49}$$

where

$$\dot{\underset{\sim}{\mathscr{E}}}^{(\alpha)} \equiv \frac{1}{2}(\underset{\sim}{\nabla}\dot{\underset{\sim}{U}}^{(\alpha)} + \underset{\sim}{\nabla}^{T}\dot{\underset{\sim}{U}}^{(\alpha)}) \ , \tag{3-50a}$$

$$\dot{\underset{\sim}{\mathscr{K}}}^{k(\alpha)} \equiv \frac{1}{2}(\underset{\sim}{\nabla}\dot{\underset{\sim}{S}}^{k(\alpha)} + \underset{\sim}{\nabla}^{T}\dot{\underset{\sim}{S}}^{k(\alpha)}) \ , \tag{3-50b}$$

$$d^{*(\alpha)} \equiv \frac{1}{2}(\underset{\sim}{S}^{k(\alpha)}\underset{\sim}{\nabla}^{*}g^{k(\alpha)} + \underset{\sim}{S}^{k(\alpha)}\underset{\sim}{\nabla}^{*T}g^{k(\alpha)}) \quad . \tag{3-50c}$$

Substitution of (3-49) into the constitutive relation (3-40), and the latter into (3-41), gives

$$\dot{\underset{\sim}{N}}^{(\alpha)} = \underset{\sim}{E}^{(\alpha)}:\dot{\underset{\sim}{\mathscr{E}}}^{(\alpha)} + \underset{\sim}{A}^{k(\alpha)}:\dot{\mathscr{K}}^{k(\alpha)} + \underset{\sim}{B}^{k(\alpha)}:\dot{\underset{\sim}{S}}^{k(\alpha)} \tag{3-51a}$$

$$\dot{M}^{k(\alpha)} = \underset{\sim}{A}^{k(\alpha)}:\dot{\underset{\sim}{\mathscr{E}}}^{(\alpha)} + \underset{\sim}{G}^{KL(\alpha)}:\dot{\mathscr{K}}^{L} + \underset{\sim}{C}^{KL(\alpha)}.\dot{\underset{\sim}{S}}^{L(\alpha)} \qquad K, = 1 \text{ to } n \tag{3-51b}$$

where

$$\underset{\sim}{E}^{(\alpha)} \equiv \int_{A^{(\alpha)}} \underset{\sim}{D}^{(\alpha)} dA^{*} \quad , \quad \underset{\sim}{A}^{k(\alpha)} \equiv \int_{A^{(\alpha)}} \varepsilon \underset{\sim}{D}^{(\alpha)} g^{k(\alpha)} dA^{*}, \tag{3.52a,b}$$

$$\underset{\sim}{B}^{k(\alpha)} \equiv \int_{A^{(\alpha)}} \underset{\sim}{D}^{(\alpha)}.\underset{\sim}{\nabla}^{*}g^{k(\alpha)} dA^{*} \quad , \tag{3-53}$$

$$G^{kL(\alpha)} \equiv \int_{A^{(\alpha)}} \varepsilon^{2} g^{k(\alpha)} g^{L(\alpha)} \underset{\sim}{D}^{(\alpha)} dA^{*} \quad , \tag{3-54}$$

$$\underset{\sim}{C}^{kL(\alpha)} \equiv \int_{A^{(\alpha)}} \varepsilon g^{k(\alpha)} \underset{\sim}{D}^{(\alpha)}.\underset{\sim}{\nabla}^{*}g^{L(\alpha)} \, dA^{*} \quad . \tag{3-55}$$

In addition, (3-49), (3-30) and (3-45) give

$$\dot{\underset{\sim}{N}}^{k(\alpha)} = \underset{\sim}{a}^{k(\alpha)}:\dot{\underset{\sim}{\mathscr{E}}}^{(\alpha)} + \underset{\sim}{b}^{kL(\alpha)}:\dot{\mathscr{K}}^{L} + \underset{\sim}{c}^{kL(\alpha)}.\dot{\underset{\sim}{S}}^{L(\alpha)} \tag{3-56}$$

where

$$\underset{\sim}{a}^{k(\alpha)} \equiv \int_{A^{(\alpha)}} \varepsilon \underset{\sim}{\nabla}^{*}g^{k(\alpha)}.\underset{\sim}{D}^{(\alpha)} dA^{*} \quad , \tag{3-57a}$$

$$\underset{\sim}{b}^{kL(\alpha)} = \int_{A^{(\alpha)}} \varepsilon^{2} g^{k(\alpha)} \underset{\sim}{\nabla}^{*}g^{k(\alpha)}.\underset{\sim}{D}^{(\alpha)} dA^{*} \quad , \tag{3-57b}$$

$$\underset{\sim}{c}^{kL(\alpha)} = \int_{A^{(\alpha)}} \varepsilon \underset{\sim}{\nabla}^{*}g^{k(\alpha)}.\underset{\sim}{D}^{(\alpha)}.\underset{\sim}{\nabla}^{*}g^{L(\alpha)} dA^{*} \quad . \tag{3-57c}$$

Interaction Terms

Using (3-44a), (3-38) and (3-31b), the interaction term $\underset{\sim}{P}$ can be expressed in the form

$$\overset{\nabla}{\underset{\sim}{P}} \approx \underset{\sim}{\mathscr{L}}.[\dot{\underset{\sim}{U}}] \quad , \mathscr{L} \equiv \frac{1}{\varepsilon} \oint_{\mathscr{I}} \mathscr{B}\, ds \tag{3-58}$$

In deriving (3-58), terms of $O(\varepsilon)$ were neglected in (3-38).

In a similar manner, (3-44b), (3-38) and (3-31b) furnish

$$\overset{\nabla}{\underset{\sim}{Q}}{}^{k} \approx \underset{\sim}{\mathscr{M}}{}^{k}.[U] \quad , \underset{\sim}{\mathscr{M}}{}^{k} \equiv \oint_{\mathscr{I}} \underset{\sim}{\mathscr{B}} g^{k(1)} ds^{*} \quad . \tag{3-59}$$

Summary of Mixture Equations

The basic equations of the mixture model for dense, uniaxially reinforced concrete are now summarized below.

(a) Equations of Motion

$$\underset{\sim}{\nabla}.\underset{\sim}{N}^{(\alpha)} + \underset{\sim}{F}^{(\alpha)} + (-1)^{1+\alpha}\underset{\sim}{P} = 0 \quad , \tag{3-60}$$

$$\underset{\sim}{\nabla}.\underset{\sim}{M}^{k(\alpha)} - \underset{\sim}{N}^{k(\alpha)} + \underset{\sim}{F}^{k(\alpha)} + (-1)^{1+\alpha}\underset{\sim}{Q}^{k} = 0 \quad ; \tag{3-61}$$

(b) Constitutive Equations

$$\overset{\nabla}{\underset{\sim}{N}}{}^{(\alpha)} = \underset{\sim}{E}^{(\alpha)}:\dot{\underset{\sim}{\mathscr{E}}}^{(\alpha)} + \underset{\sim}{A}^{k(\alpha)}:\dot{\mathscr{K}}^{k(\alpha)} + \underset{\sim}{B}^{k(\alpha)}:\dot{\underset{\sim}{S}}^{k(\alpha)} \quad , \tag{3-62a}$$

$$\overset{\nabla}{\underset{\sim}{M}}{}^{k(\alpha)} = \underset{\sim}{A}^{k(\alpha)}:\dot{\underset{\sim}{\mathscr{E}}}^{(\alpha)} + \underset{\sim}{G}^{kL(\alpha)}:\dot{\mathscr{K}}^{L(\alpha)} + \underset{\sim}{C}^{kL(\alpha)}.\dot{\underset{\sim}{S}}^{L(\alpha)} \quad , \tag{3-62b}$$

$$\overset{\nabla}{\underset{\sim}{N}}{}^{k(\alpha)} = \underset{\sim}{a}^{k(\alpha)}:\dot{\underset{\sim}{\mathscr{E}}}^{(\alpha)} + \underset{\sim}{b}^{kL(\alpha)}:\dot{\mathscr{K}}^{L(\alpha)} + \underset{\sim}{c}^{kL(\alpha)}.\dot{\underset{\sim}{S}}^{L(\alpha)} \tag{3-62c}$$

(c) Interaction Terms

$$\overset{\nabla}{\underset{\sim}{P}} = \underset{\sim}{\mathscr{L}}.[\dot{\underset{\sim}{U}}] \quad , \quad \overset{\nabla}{\underset{\sim}{Q}}{}^{k} = \underset{\sim}{\mathscr{M}}{}^{k}.[\dot{\underset{\sim}{U}}] \tag{3-63}$$

(d) Boundary Conditions on $\partial V$

$$\overset{\nu}{\underset{\sim}{T}}{}^{(\alpha)} = \underset{\sim}{\nu}.\underset{\sim}{N}^{(\alpha)} \quad \text{or} \quad \delta\dot{\underset{\sim}{U}}^{(\alpha)} = 0 \quad \text{on } \partial V_{T} \quad , \tag{3-64a}$$

$$\overset{\nu}{\underset{\sim}{T}}{}^{k(\alpha)} = \underset{\sim}{\nu}.\underset{\sim}{M}^{k(\alpha)} \quad \text{or} \quad \delta\dot{\underset{\sim}{S}}^{k(\alpha)} = 0 \quad \text{on } \partial V_{T} \quad , \tag{3-64b}$$

(e) Kinematic Relations

$$\dot{\underset{\sim}{\mathscr{E}}}^{(\alpha)} \equiv \frac{1}{2}(\underset{\sim}{\nabla}\dot{\underset{\sim}{U}}^{(\alpha)} + \underset{\sim}{\nabla}^{T}\dot{\underset{\sim}{U}}^{(\alpha)}) \quad , \tag{3-65a}$$

$$\dot{\underset{\sim}{\mathscr{K}}}^{k(\alpha)} \equiv \frac{1}{2}(\underset{\sim}{\nabla}\dot{\underset{\sim}{S}}^{k(\alpha)} + \underset{\sim}{\nabla}^{T}\dot{\underset{\sim}{S}}^{k(\alpha)}) \quad , \tag{3-65b}$$

(f) Averages

$$(\underset{\sim}{E}^{(\alpha)}, \underset{\sim}{A}^{k(\alpha)}, \underset{\sim}{B}^{k(\alpha)}, \underset{\sim}{G}^{kL(\alpha)}, \underset{\sim}{C}^{kL(\alpha)}) \equiv \int_{A^{(\alpha)}} (\underset{\sim}{D}^{(\alpha)}, \varepsilon\underset{\sim}{D}^{(\alpha)} g^{k(\alpha)}, \tag{3-66a}$$

$$\underset{\sim}{D}^{(\alpha)} \cdot \underset{\sim}{\nabla}^{*} g^{k(\alpha)}, \varepsilon^{2} g^{k(\alpha)} g^{L(\alpha)} \underset{\sim}{D}^{(\alpha)}, \varepsilon g^{k(\alpha)} \underset{\sim}{D}^{(\alpha)} \cdot \underset{\sim}{\nabla}^{*} g^{L(\alpha)}) dA^{*} \quad ,$$

$$(\underset{\sim}{a}^{k(\alpha)}, \underset{\sim}{b}^{kL(\alpha)}, \underset{\sim}{c}^{kL(\alpha)}) \equiv \int_{A^{(\alpha)}} (\varepsilon\underset{\sim}{\nabla}^{*} g^{k(\alpha)} \cdot \underset{\sim}{D}^{(\alpha)}, \varepsilon^{2} g^{k(\alpha)} \underset{\sim}{\nabla}^{*} g^{k(\alpha)} \cdot \underset{\sim}{D}^{(\alpha)}, \tag{3-66b}$$

$$\varepsilon\underset{\sim}{\nabla}^{*} g^{k(\alpha)} \cdot \underset{\sim}{D}^{(\alpha)} \cdot \underset{\sim}{\nabla}^{*} g^{L(\alpha)}) dA^{*}$$

$$(\underset{\sim}{\mathscr{L}}\underset{\sim}{\mathscr{M}}^{k}) \equiv \oint_{\mathscr{I}} (\frac{1}{\varepsilon}\underset{\sim}{\mathscr{B}}, \underset{\sim}{\mathscr{B}} g^{k(1)}) ds^{*} \tag{3-66c}$$

Weighting Functions

In order to utilize the preceeding mixture equations, the weighting functions $g^{K(\alpha)}(\underset{\sim}{x}^{*})$ must be selected. For the dense steel layout, weighting functions are introduced in conjunction with a "concentric cylinders approximation."[5] Accordingly, the outer cell boundary is approximate by a circle which is defined based upon equal area of the original and approximate cell. This procedure is depicted in Figure 3.3 (for a hexagonal steel array).

Subsequent to the introduction of the approximate cell, the weighting functions are defined as follows:

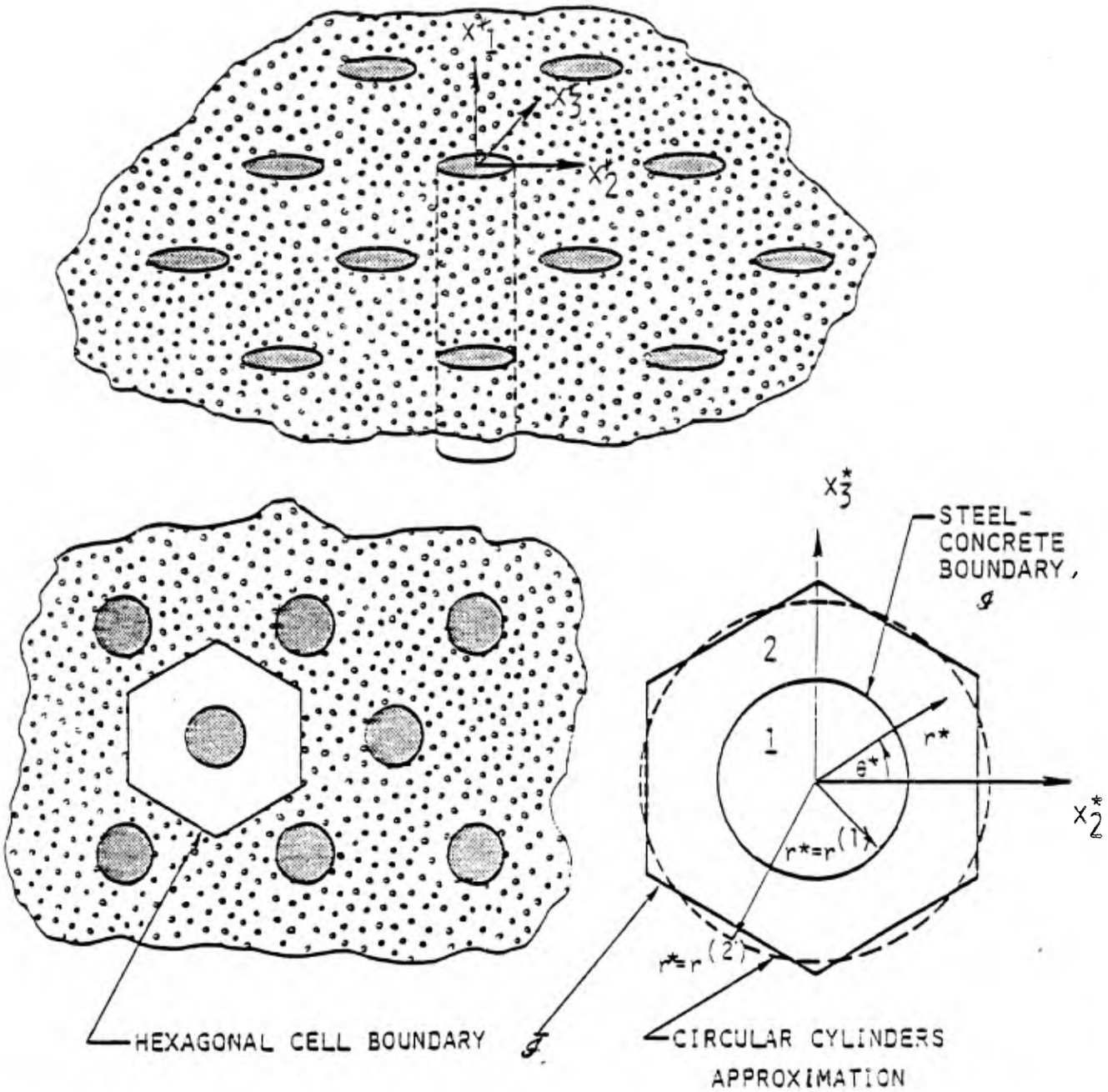


Figure 3.3. Circular cylinders approximation (shown for periodic hexagonal steel array).

$$g_2^{(1)}(x_2^*,x_3^*) = x_2^*/n^{(1)} \quad ,$$

$$g_2^{(2)}(x_2^*,x_3^*) = -\left(x_2^* - \frac{x_2^*}{x_2^{*2} + x_3^{*2}}\right)\Big/ n^{(2)} \quad , \qquad (3\text{-}67)$$

$$g_3^{(1)}(x_2^*,x_3^*) = x_3^*/n^{(1)} \quad ,$$

$$g_3^{(2)}(x_2^*,x_3^*) = -\left(x_3^* - \frac{x_3^*}{x_2^{*2} + x_3^{*2}}\right)\Big/ n^{(2)} .$$

The relations (3-65) satisfy the $\underset{\sim}{x}^*$ - periodicity condition on the (approximate) outer cell boundary.

The form (3-67) represents the first relevant terms of a Taylor expansion in the singly connected region $A^{(1)}$ and a Laurent expansion in the annular region $A^{(2)}$.

The quantities $n^{(1)}$, $n^{(2)}$ denote, respectively, the volume fractions of the steel and concrete. If $r^{(1)}$, $r^{(2)}$ represent the current steel and cell radii, respectively, then $n^{(1)} = (r^{(1)}/r^{(2)})^2$, $n^{(2)} = 1 - n^{(1)}$. The dimension $2r^{(2)}$ represents essentially the steel spacing.

Additional Constraints

For some applications, it may be appropriate to introduce the constraint:

$$\underset{\sim}{S}^{k(1)} = \underset{\sim}{S}^{k(2)} \quad . \qquad (3\text{-}68a)$$

In accordance with the reduction of the number of dependent variables represented by (3-68a), the relation (3-61) is replaced by

$$\underset{\sim}{\nabla}.\underset{\sim}{M}^K - \underset{\sim}{N}^K + \underset{\sim}{F}^k = 0 \qquad (3\text{-}68b)$$

where

$$(\underset{\sim}{M}^K, \underset{\sim}{N}^k, \underset{\sim}{F}^k) \equiv \sum_{\alpha=1}^{2} (\underset{\sim}{M}^{k(\alpha)}, \underset{\sim}{N}^{k(\alpha)}, \underset{\sim}{F}^{k(\alpha)}) \quad . \tag{3-68c}$$

Constitutive equations for the new dependent variables $\underset{\sim}{M}^k$, $\underset{\sim}{N}^k$ are obtained by adding (3-63) for $\alpha = 1,2$ or by adding (3-64) for $\alpha = 1,2$. The result is

$$\overset{\nabla}{\underset{\sim}{M}}{}^k = \sum_{\alpha=1}^{2} [\underset{\sim}{A}^{k(\alpha)} : \underset{\sim}{\mathscr{E}}^{(\alpha)} + G^{kL(\alpha)} \underset{\sim}{\mathscr{K}}^{L(\alpha)} + \underset{\sim}{C}^{KL(\alpha)} \cdot \dot{\underset{\sim}{S}}^L] \tag{3-69a}$$

$$\overset{\nabla}{\underset{\sim}{N}}{}^k = \sum_{\alpha=1}^{2} [\underset{\sim}{a}^{k(\alpha)} : \underset{\sim}{\mathscr{E}}^{(\alpha)} + \underset{\sim}{b}^{kL(\alpha)} : \underset{\sim}{\mathscr{K}}^{L(\alpha)} + \underset{\sim}{c}^{kL(\alpha)} \cdot \dot{\underset{\sim}{S}}^L] \tag{3-69b}$$

## Remarks on Coordinate Systems

The mixture relations (3-60) - (3-66) are based on the assumption that the current configuration is also the reference configuration. Otherwise, the equations are general with respect to coordinate systems. In particular, since direct notation has been used, the mixture relations are valid for arbitrary coordinate systems.

## Remarks on Curvilinear Steel Layouts

In the construction of the mixture model, a rectilinear, unidirectional dense steel such as is depicted in Figure 3.4(a) was envisaged in which the cell geometry was constant. However, if the cell geometry (e.g., the steel and concrete volume fractions) varies sufficiently slowly with respect to the microcoordinates, then the governing equations can also be used to model a curvilinear, unidirectional dense steel array, as depicted in Figure 3.4(b). This opens the door to the simulation of a number of practical steel layouts.

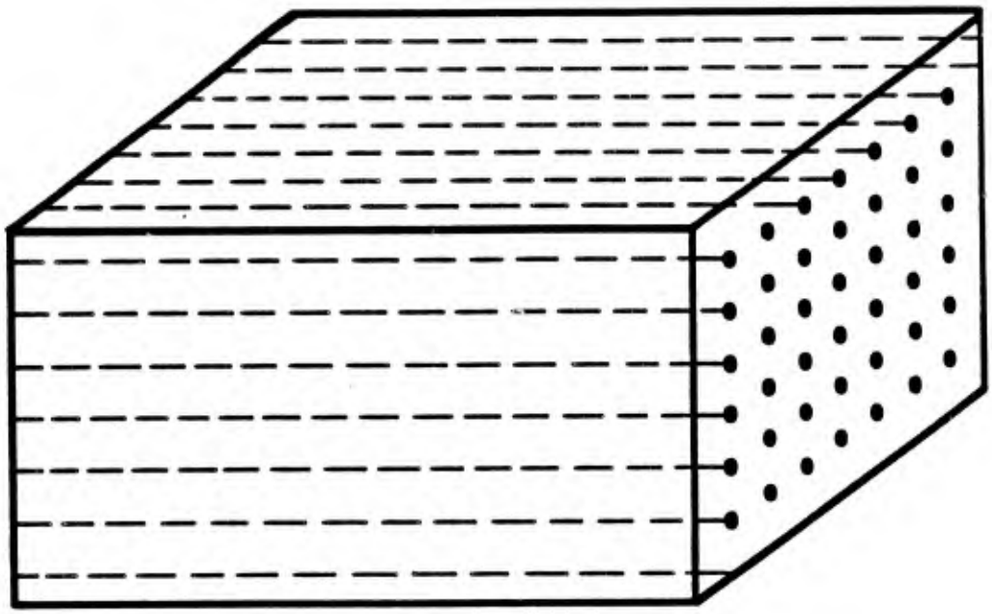

(a) Rectilinear

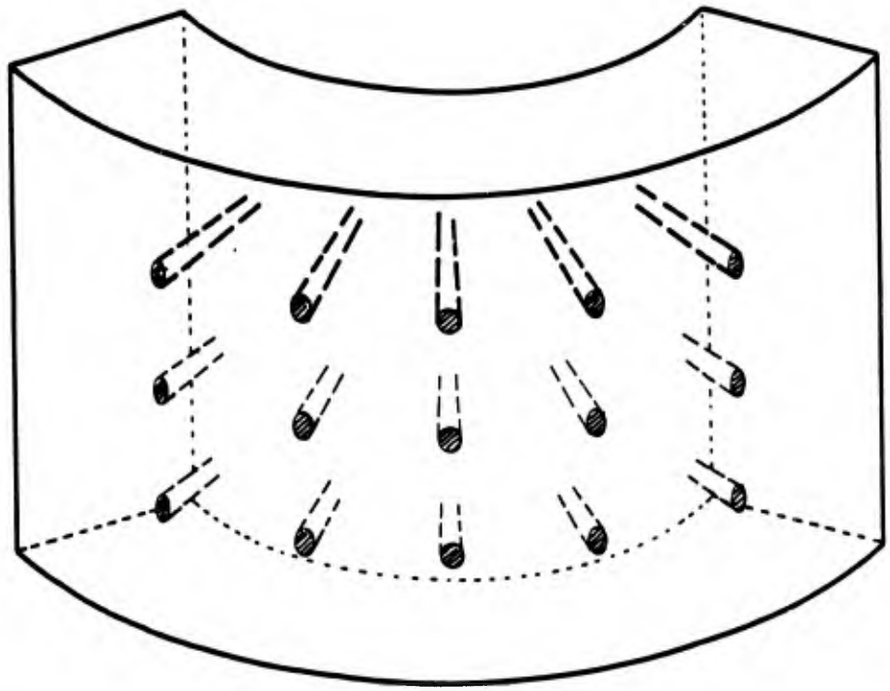

(b) Curvilinear

Figure 3.4. Unidirectional dense steel arrays.

Mixture Equations - Compoment Form

The mixture relations (3-60) - (3-66) can be written in compoment form once the reference base vectors are selected. For later use, we list below the compoments referred to fixed rectangular Cartesian base vectors (in which case the description becomes Eulerian).

(a) Equations of Motion

$$N^{(\alpha)}_{ji,j} + F^{(\alpha)}_i + (-1)^{1+\alpha} P_i = 0 \quad , \tag{3-70a}$$

$$M^{k(\alpha)}_{ji,j} - \overline{N}^{k(\alpha)}_i + F^{k(\alpha)}_i + (-1)^{1+\alpha} Q^k_i = 0 \quad ; \tag{3-70b}$$

(b) Constitutive Equations

$$\overset{\nabla}{N}{}^{(\alpha)}_{ij} = E^{(\alpha)}_{ijk\ell}\, \mathscr{E}^{(\alpha)}_{k\ell} + A^{k(\alpha)}_{ijk\ell}\, \dot{\mathscr{K}}^{k(\alpha)}_{k\ell} + B^{k(\alpha)}_{ijk}\, \dot{S}^{k(\alpha)}_k \quad , \tag{3-71a}$$

$$\overset{\nabla}{M}{}^{k(\alpha)}_{ij} = A^{k(\alpha)}_{ijk}\, \dot{\mathscr{E}}^{(\alpha)}_{k\ell} + G^{kL(\alpha)}_{ijk\ell}\, \dot{\mathscr{K}}^{L(\alpha)}_{k\ell} + C^{kL(\alpha)}_{ijk}\, \dot{S}^{L(\alpha)}_k \quad , \tag{3-71b}$$

$$\overset{\nabla}{\overline{N}}{}^{k(\alpha)}_{ij} = a^{k(\alpha)}_{ijk\ell}\, \dot{\mathscr{E}}^{(\alpha)}_{k\ell} + b^{kL(\alpha)}_{ijk\ell}\, \dot{\mathscr{K}}^{L(\alpha)}_{k\ell} + C^{kL(\alpha)}_{ijk}\, \dot{S}^{L(\alpha)}_k \tag{3-71c}$$

(c) Interaction Terms

$$\overset{\nabla}{P}_i = \mathscr{L}_{ij}\,[\dot{U}_j] \quad , \quad \overset{\nabla}{Q}{}^k_i = \mathscr{M}^k_{ij}[\dot{U}_j] \tag{3-72}$$

(d) Boundary Conditions on $\partial V_T$

$$\overset{\nu}{T}{}^{(\alpha)}_i = N^{(\alpha)}_{ji}\, \nu_j \quad \text{or} \quad \delta \dot{U}^{(\alpha)}_i = 0 \quad \text{on } \partial V_T \quad . \tag{3-73}$$

$$\overset{\nu}{T}{}^{k(\alpha)}_i = M^{k(\alpha)}_{ji}\, \nu_j \quad \text{or} \quad \delta S^{k(\alpha)}_i = 0 \quad \text{on } \partial V_T \tag{3-74}$$

(e) Kinematic Relations

$$\dot{\mathscr{E}}^{(\alpha)}_{ij} \equiv \frac{1}{2}\,(\dot{U}^{(\alpha)}_{i,j} + \dot{U}^{(\alpha)}_{j,i}) \quad , \tag{3-75}$$

$$\dot{\mathscr{H}}^{k(\alpha)} \equiv \frac{1}{2}(\dot{S}^{k(\alpha)}_{i,j} + \dot{S}^{k(\alpha)}_{j,i}) \ . \qquad (3\text{-}76)$$

## 3.2 MIXTURE RELATIONS FOR SPARSE STEEL

In this section a mixture model is formulated for the case of a sparse steel layout. This work represents an extension of our previous model[4,5]. The new formulation incorporates arbitrary curvilinear rebar geometry and finite deformations.

The work on the sparse mixture model forms the basis for a new finite element rebar element that properly models progressive cracking of the concrete, steel-concrete bond degradation and slip, and dowel action.

In what follows <u>two</u> formulations of the sparse steel case are presented. The first formulation employs the <u>current</u> configuration as the reference state. The second formulation utilizes the <u>initial</u> configuration as the reference. The former is more convenient from a theoretical standpoint. The latter may be more useful for certain numerical applications.

### Geometry

With reference to Figure 3.5(a), we consider a single steel reinforcing bar together with surrounding concrete cover. The geometry of the resulting composite element is a matter of modeling convenience at the time of discretization, i.e., at the time a finite element mesh is created. However, if possible, the cell should be constructed in such a manner that the aspect ratio is one.

The geometry depicted in Figure 3.5 represents the <u>current</u> configuration of a rebar plus cover segment. The position of a material point in the cell is defined by the position vector $\underset{\sim}{r} = \underset{\sim}{x} + \underset{\sim}{x}^*$ where $\underset{\sim}{x}$ denotes the position of the steel centerline and $\underset{\sim}{x}^* = \underset{\sim}{e}_k \xi_k$ $(k = 2,3)$. The vectors $\underset{\sim}{e}_2$ and $\underset{\sim}{e}_3$ are unit base vectors

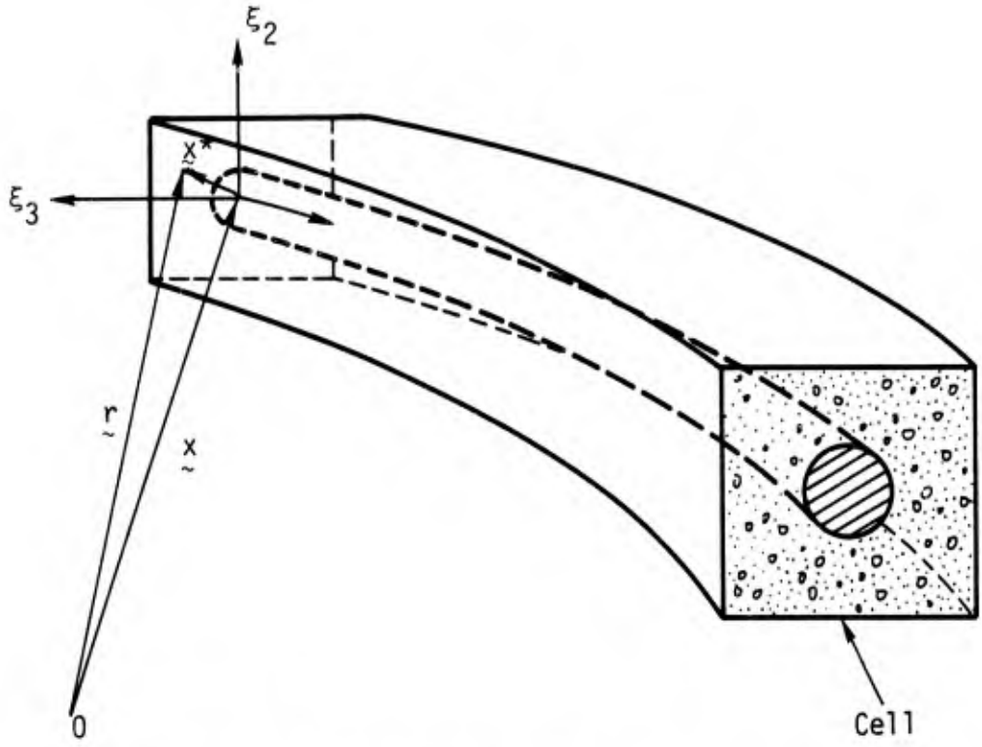


Figure 3.5(a). Geometry for sparse array.

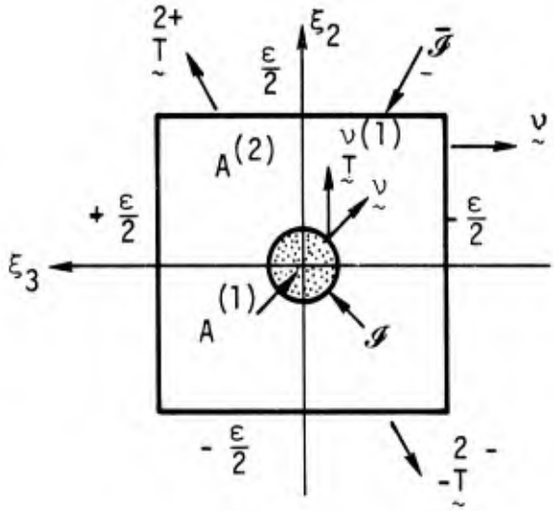


Figure 3.5(b). Cross-sectional geometry.

(see Fig. 3.5). The coordinate $\xi_1$ is a convected coordinate directed along the steel centerline. The coordinates $\xi_2$ and $\xi_3$ are convected coordinates in a plane with normal in the direction of $\xi_1$.

In what follows, finite deformations of the rebar element will be allowed. However, cross-sectional deformations will be restricted to be sufficiently small that the current cross-sectional geometry may be approximated by the initial cross-sectional geometry.

## Variational Principle

The formulation of the sparse-case mixture model is based upon the use of a variational principle. This principle can be constructed as follows: With the current configuration selected as the reference, and using the notation described in Section 3.1, the Principle of Virtual Work for the steel can be written (note that the cell in Figure 3.5(b) has been nondimensionalized in a manner similar to that described in Section 3.1)

$$\int_0^{\ell}\left(\int_{A^{(1)}} \underset{\sim}{f}^{(1)}\cdot\delta\underset{\sim}{v}^{(1)}\,dA + \oint_{\mathscr{I}} \underset{\sim}{T}^{\nu(1)}\cdot\delta\underset{\sim}{v}^{(1)}\,ds\right) d\xi_1 + \left[\int_{A^{(1)}} \underset{\sim}{T}^{1(1)}\cdot\delta\underset{\sim}{v}^{(1)}\,dA\right]_{\xi_1=0}^{\xi_1=\ell} \tag{3-77}$$

$$= \int_0^{\ell}\left(\int_{A^{(1)}} \underset{\sim}{\sigma}^{(1)}:\delta\underset{\sim}{d}^{(1)}\,dA\right) d\xi_1$$

where $\underset{\sim}{d}^{(\alpha)} \equiv (\underset{\sim}{\nabla}\,\underset{\sim}{v}^{(\alpha)} + \underset{\sim}{\nabla}^{T}\underset{\sim}{v}^{(\alpha)})/2$ and $dA = d\xi_2 d\xi_3$. Similarly, for the concrete one has

$$\int_0^{\ell}\left(\int_{A^{(2)}} \underset{\sim}{f}^{(2)}\cdot\delta\underset{\sim}{v}^{(2)}\,dA + \oint_{\mathscr{I}} \underset{\sim}{T}^{\nu(2)}\cdot\delta\underset{\sim}{v}^{(2)}\,ds - \oint_{\mathscr{I}} \underset{\sim}{T}^{\nu(2)}\cdot\delta\underset{\sim}{v}^{(2)}\,ds\right) d\xi_1 \tag{3-78}$$

$$+ \left[\int_{A^{(2)}} \underset{\sim}{T}^{1(2)}\cdot\delta\underset{\sim}{v}^{(2)}\,dA\right]_{\xi_1=0}^{\xi_1=\ell} = \int_0^{\ell}\left(\int_{A^{(2)}} \underset{\sim}{\sigma}^{(2)}:\delta\underset{\sim}{d}^{(2)}\,dA\right) d\xi_1 \ .$$

On the steel-concrete interface, in general

$$\underset{\sim}{\overset{\nu}{T}}(1) = - \underset{\sim}{\overset{\nu}{T}}(2) \equiv \underset{\sim}{T}^* \quad \text{on } \mathscr{I} \tag{3-79}$$

$$\underset{\sim}{v}^{(1)} \neq \underset{\sim}{v}^{(2)} \quad \text{on } \mathscr{I}. \tag{3-80}$$

Let us define the "slip" as

$$[\underset{\sim}{v}] \equiv \underset{\sim}{v}^{(2)} - \underset{\sim}{v}^{(1)} \quad \text{on } \mathscr{I}. \tag{3-81}$$

If one now adds (3-77) and (3-78), then the Principle of Virtual Work for the composite element becomes

$$\int_0^{\ell} \left( \sum_{\alpha=1}^{2} \int_{A(\alpha)} \underset{\sim}{f}^{(\alpha)} \cdot \delta \underset{\sim}{v}^{(\alpha)} dA + \oint_{\mathscr{I}} \underset{\sim}{\overset{\nu}{T}}(2) \cdot \delta \underset{\sim}{v}^{(2)} ds \right) d\xi_1$$

$$+ \left[ \sum_{\alpha=1}^{2} \int_{A(\alpha)} \overset{1}{T}^{(\alpha)} \cdot \delta v^{(\alpha)} dA \right]_{\xi_1=0}^{\xi_1=\ell} \tag{1-82}$$

$$= \int_0^{\ell} \left( \sum_{\alpha=1}^{2} \int_{A(\alpha)} \underset{\sim}{\sigma}^{(\alpha)} : \delta \underset{\sim}{d}^{(\alpha)} dA + \oint_{\mathscr{I}} \underset{\sim}{\overset{\nu}{T}}^* \cdot \delta [\underset{\sim}{v}] ds \right) d\xi_1 \quad .$$

The additional virtual work term $\underset{\sim}{\overset{\nu}{T}}^* \cdot \delta[\underset{\sim}{v}]$ in (3-82) depends upon the particular interface constitutive law specified. However, it is possible to develop a mixture model of the composite cell without direct reference to this law if the slip $[\underset{\sim}{v}]$ is treated as a dependent displacement-type variable.

## Test Functions

In a manner similar to that described in Section 3.1, the following test functions are now introduced and Kantorovich's direct variational method is used to derive a set of "lowest order" mixture relations:

$$\underset{\sim}{v}^{(\alpha)}(\underset{\sim}{x}, \underset{\sim}{x}^*, t) \doteq \underset{\sim}{\dot{U}}^{(\alpha)}(\underset{\sim}{x}, t) + \dot{S}^{K(\alpha)}(\underset{\sim}{x}, t) g^{K(\alpha)}(\underset{\sim}{x}^*) \tag{3-83}$$

where K ranges from 1 to n (summation on K is implied), the quantities $\underset{\sim}{S}^{K(\alpha)}$ denotes the Kth director for material $\alpha$, and $g^{K(\alpha)}(\underset{\sim}{x}^*)$ denotes a "weight" function for each K and $\alpha$.

As a result of (3-83), and assumed continuity of the $g^{K(\alpha)}(\underset{\sim}{x}^*)$ across the steel-concrete interface,

$$[\underset{\sim}{v}] = \dot{\underset{\sim}{U}}^{(2)} - \dot{\underset{\sim}{U}}^{(1)} = [\dot{\underset{\sim}{U}}] \tag{3-84}$$

and

$$\underset{\sim}{d}^{(\alpha)} = \dot{\underset{\sim}{\mathscr{E}}}^{(\alpha)} + g^{K(\alpha)}\dot{\underset{\sim}{\mathscr{K}}}^{K(\alpha)} + \underset{\sim}{d}^{*(\alpha)} \tag{3-85}$$

where

$$\dot{\underset{\sim}{\mathscr{E}}}^{(\alpha)} \equiv \frac{1}{2}(\underset{\sim}{\nabla}_x \dot{\underset{\sim}{U}}^{(\alpha)} + \underset{\sim}{\nabla}_x^T \dot{\underset{\sim}{U}}^{(\alpha)}) \quad , \tag{3-86a}$$

$$\dot{\underset{\sim}{\mathscr{K}}}^{K(\alpha)} \equiv \frac{1}{2}(\underset{\sim}{\nabla}_x \dot{\underset{\sim}{S}}^{K(\alpha)} + \underset{\sim}{\nabla}_x^T \dot{\underset{\sim}{S}}^{K(\alpha)}) \quad , \tag{3-86b}$$

$$\underset{\sim}{d}^{*(\alpha)} \equiv \frac{1}{2}(\dot{\underset{\sim}{S}}^{(\alpha)} \underset{\sim}{\nabla}_* g^{K(\alpha)} + \dot{\underset{\sim}{S}}^{(\alpha)} \underset{\sim}{\nabla}_*^T g^{K(\alpha)}) \quad . \tag{3-86c}$$

The gradient operators $\underset{\sim}{\nabla}_x$ and $\underset{\sim}{\nabla}_*$ in the above equations are defined according to

$$\underset{\sim}{\nabla}_x \equiv \underset{\sim}{g}^1 \frac{\partial}{\partial \xi_1} \quad , \quad \underset{\sim}{\nabla}_* \equiv \underset{\sim}{g}^K \frac{\partial}{\partial \xi_k} \quad (k = 2,3) \tag{3-87}$$

where $\underset{\sim}{g}^i$ denote the contravariant base vectors associated with the coordinates $\xi_i$.

## Equations of Motion, Boundary Conditions

Substitution of (3-83) - (3-86) into (3-82) and integration by parts gives

$$\int_0^{\ell} \Bigg\{ \sum_{\alpha=1}^{2} \delta\dot{\underset{\sim}{U}}^{(\alpha)} \cdot \left( \underset{\sim}{\nabla}_x \cdot \underset{\sim}{N}^{(\alpha)} + \underset{\sim}{F}^{(\alpha)} + (-1)^{1+\alpha} \underset{\sim}{P} + \delta_{\alpha 2} \underset{\sim}{\bar{Q}} \right)$$

$$+ \delta\dot{\underset{\sim}{S}}^{K(\alpha)} \cdot \left( \underset{\sim}{\nabla}_x \cdot \underset{\sim}{M}^{K(\alpha)} - \underset{\sim}{\bar{N}}^{K(\alpha)} + \underset{\sim}{F}^{K(\alpha)} + \delta_{\alpha 2} \underset{\sim}{\bar{Q}}^{K} + (-1)^{1+} \underset{\sim}{Q}^{K} \right) \Bigg\} d\xi_1 \qquad (3\text{-}88)$$

$$+ \left[ \sum_{\alpha=1}^{2} \delta\dot{\underset{\sim}{U}}^{(\alpha)} \cdot \left( \underset{\sim}{T}^{(\alpha)} - \underset{\sim}{\nu}_1 \cdot \underset{\sim}{N}^{(\alpha)} \right) + \delta\dot{\underset{\sim}{S}}^{K(\alpha)} \cdot \left( \underset{\sim}{T}^{K(\alpha)} - \underset{\sim}{\nu}_1 \cdot \underset{\sim}{M}^{K(\alpha)} \right) \right]_{\xi_1=0}^{\xi_1=\ell} = 0,$$

where

$$\left( \underset{\sim}{F}^{(\alpha)}, \underset{\sim}{F}^{K(\alpha)} \right) = \int_{A^{(\alpha)}} (1, g^{K(\alpha)}) \underset{\sim}{f}^{(\alpha)} dA \quad , \qquad (3\text{-}89a)$$

$$\left( \underset{\sim}{N}^{(\alpha)}, \underset{\sim}{M}^{K(\alpha)} \right) \equiv \int_{A^{(\alpha)}} (1, g^{K(\alpha)}) \underset{\sim}{\sigma}^{(\alpha)} \quad , \qquad (3\text{-}89b)$$

$$\underset{\sim}{\bar{N}}^{K(\alpha)} \equiv \int_{A^{(\alpha)}} \underset{\sim}{\sigma}^{(\alpha)} \cdot \underset{\sim}{\nabla}_* g^{K(\alpha)} dA \quad , \qquad (3\text{-}89c)$$

$$\left( \underset{\sim}{\bar{T}}^{(\alpha)}, \underset{\sim}{T}^{K(\alpha)} \right) \equiv \int_{A^{(\alpha)}} (1, g^{K(\alpha)}) \underset{\sim}{T}^{(\alpha)} \, dA \quad , \qquad (3\text{-}89d)$$

$$\underset{\sim}{P} \equiv \oint_{\mathscr{I}} T^* ds \quad , \quad (\underset{\sim}{\bar{Q}}, \underset{\sim}{\bar{Q}}^{K}) \equiv \oint_{\mathscr{I}} (1, g^{K(2)}) \underset{\sim}{T}^{\nu(2)} ds \qquad (3\text{-}89e)$$

$$\underset{\sim}{Q}^{K} \equiv \oint_{\mathscr{I}} T^* g^{K(\alpha)} ds \qquad (\alpha = 1 \text{ or } 2) \qquad (3\text{-}89f)$$

The Euler-Lagrange equations of (1-88) on $0 < \xi_1 < \ell$ are:

$$\underset{\sim}{\nabla}_x \cdot \underset{\sim}{N}^{(\alpha)} + \underset{\sim}{F}^{(\alpha)} + \delta_{\alpha 2} \underset{\sim}{\bar{Q}} + (-1)^{1+\alpha} \underset{\sim}{P} = 0 \quad , \qquad (3\text{-}90a)$$

$$\underset{\sim}{\nabla}_x \cdot M^{K(\alpha)} - \underset{\sim}{\bar{N}}^{K(\alpha)} + \underset{\sim}{F}^{K(\alpha)} + \delta_{\alpha 2} \underset{\sim}{\bar{Q}}^{K} + (-1)^{1+\alpha} \underset{\sim}{Q}^{K} = 0 \quad , \qquad (3\text{-}90b)$$

Further, at $\xi_1 = 0$ and $\xi_1 = \ell$, we have

$$\delta\dot{\underset{\sim}{U}}^{(\alpha)} = 0 \quad \text{or} \quad \overset{1}{\underset{\sim}{T}}^{(\alpha)} = \underset{\sim}{\nu}_1 \cdot \underset{\sim}{N}^{(\alpha)} \tag{3-91a}$$

$$\delta\dot{\underset{\sim}{S}}^{K(\alpha)} = 0 \quad \text{or} \quad \overset{1}{\underset{\sim}{T}}^{K(\alpha)} = \underset{\sim}{\nu}_1 \cdot \underset{\sim}{M}^{K(\alpha)} \tag{3-91b}$$

Equations (3-90a,b) are the desired mixture equations of motion for the composite cell. Equations (3-91a,b) represent boundary conditions at the cell termini.

## Mixture Constitutive Relations

The mixture constitutive relations are obtained by substitution of the rate-of-deformation tensor $\underset{\sim}{d}^{(\alpha)}$, defined by (3-85), into the definitions (3-89b,c) for $\underset{\sim}{N}^{(\alpha)}$, $\underset{\sim}{M}^{k(\alpha)}$, and $\underset{\sim}{\bar{N}}^{k(\alpha)}$. The result is

$$\dot{\underset{\sim}{N}}^{(\alpha)} = \underset{\sim}{E}^{(\alpha)} : \dot{\underset{\sim}{\mathscr{E}}}^{(\alpha)} + \underset{\sim}{A}^{K(\alpha)} : \dot{\underset{\sim}{\mathscr{K}}}^{K(\alpha)} + \underset{\sim}{B}^{K(\alpha)} : \dot{\underset{\sim}{S}}^{K(\alpha)} \quad , \tag{3-92a}$$

$$\dot{\underset{\sim}{M}}^{K(\alpha)} = \underset{\sim}{A}^{K(\alpha)} : \dot{\underset{\sim}{\mathscr{E}}}^{(\alpha)} + \underset{\sim}{G}^{KL(\alpha)} : \dot{\underset{\sim}{\mathscr{K}}}^{L} + \underset{\sim}{C}^{KL(\alpha)} \cdot \dot{\underset{\sim}{S}}^{L(\alpha)} \quad , \tag{3-92b}$$

$$\dot{\underset{\sim}{\bar{N}}}^{K(\alpha)} = \underset{\sim}{a}^{K(\alpha)} : \dot{\underset{\sim}{\mathscr{E}}}^{(\alpha)} + \underset{\sim}{b}^{KL(\alpha)} \dot{\underset{\sim}{\mathscr{K}}}^{L} + \underset{\sim}{c}^{KL(\alpha)} \cdot \underset{\sim}{S}^{L(\alpha)} \tag{3-92c}$$

where

$$(\underset{\sim}{E}^{(\alpha)}, \underset{\sim}{A}^{K(\alpha)}, \underset{\sim}{B}^{K(\alpha)}, \underset{\sim}{G}^{KL(\alpha)}, \underset{\sim}{C}^{KL(\alpha)}) \equiv \int_{A^{(\alpha)}} (\underset{\sim}{D}^{(\alpha)}, \underset{\sim}{D}^{(\alpha)} g^{K(\alpha)}, \underset{\sim}{D}^{(\alpha)} \cdot \underset{\sim}{\nabla}_* g^{K(\alpha)}$$

$$g^{K(\alpha)} g^{L(\alpha)} \underset{\sim}{D}^{(\alpha)}, \; g^{K(\alpha)} \underset{\sim}{D}^{(\alpha)} \cdot \underset{\sim}{\nabla}_* g^{L(\alpha)}) \, dA^* \quad , \tag{3-93a}$$

$$(\underset{\sim}{a}^{K(\alpha)}, \underset{\sim}{b}^{KL(\alpha)}, \underset{\sim}{c}^{kL(\alpha)}) \equiv \int_{A^{(\alpha)}} (\underset{\sim}{\nabla}_* g^{K(\alpha)} \cdot \underset{\sim}{D}^{(\alpha)}, g^{K(\alpha)} \underset{\sim}{\nabla}_* g^{K(\alpha)} \cdot \underset{\sim}{D}^{(\alpha)} \quad ,$$

$$\underset{\sim}{\nabla}_* g^{K(\alpha)} \cdot \underset{\sim}{D}^{(\alpha)} \cdot \underset{\sim}{\nabla}_* g^{L(\alpha)}) dA^* \quad . \tag{3-93b}$$

Steel-Concrete Interaction Terms

With use of the interface constitutive relation (3-31b), the trial displacement function (3-83), and the definition of the interaction term $\underset{\sim}{P}$ from the first of (3-89e), the interaction term $\underset{\sim}{P}$ can be written

$$\overset{\nabla}{\underset{\sim}{P}} \simeq \underset{\sim}{\mathscr{L}}.[\dot{\underset{\sim}{U}}] \quad , \underset{\sim}{\mathscr{L}} = \int_{\mathscr{I}} \underset{\sim}{\mathscr{B}} ds \tag{3-94}$$

In a similar manner, from the second of (3-89e), (3-31b), and (3-83), one obtains

$$\overset{\nabla}{\underset{\sim}{Q}}{}^{K} \simeq \underset{\sim}{M}^{K}.[\dot{\underset{\sim}{U}}] \quad , \underset{\sim}{\mathscr{M}}^{K} \equiv \int_{\mathscr{I}} \mathscr{B} g^{K(1)} ds \, . \tag{3-95}$$

Crack Interface Relations

Consider a crack $\mathscr{D}$ in the concrete. Across such a crack surface the traction vector $\overset{\nu}{T}$ must be continuous. Thus, if $\underset{\sim}{\nu}$ is the unit normal to $\mathscr{D}$ (Figure 3.6), then

$$\underset{\sim}{T}^{\nu}(2)^{+} = - \underset{\sim}{T}^{\nu}(2)^{-} \equiv \underset{\sim}{T}^{\nu}(2) \quad \text{on} \quad \mathscr{D} \, . \tag{3-96}$$

As was noted in the case of the dense steel layout, a reasonably wide class of crack phenomena, including crack dilatancy, can be modeled using incremental relations of the form

$$\overset{\nabla}{T}(2) = \underset{\sim}{\mathscr{G}}\left( \underset{\sim}{T}^{\nu}(2), [\underset{\sim}{U}^{(2)}]_{\mathscr{D}} \right).[\dot{\underset{\sim}{U}}^{(2)}]_{\mathscr{D}} \tag{3-97}$$

The notation $[U]_{\mathscr{D}} \equiv \underset{\sim}{U}^{(2)+} - \underset{\sim}{U}^{(2)-}$, and $\underset{\sim}{\mathscr{G}}$ denotes a second rank tensor. Specific forms of (3-97) will be treated later.

Summary of Mixture Equations

The basic equations of the mixture model for a sparse steel layout can be summarized as follows:

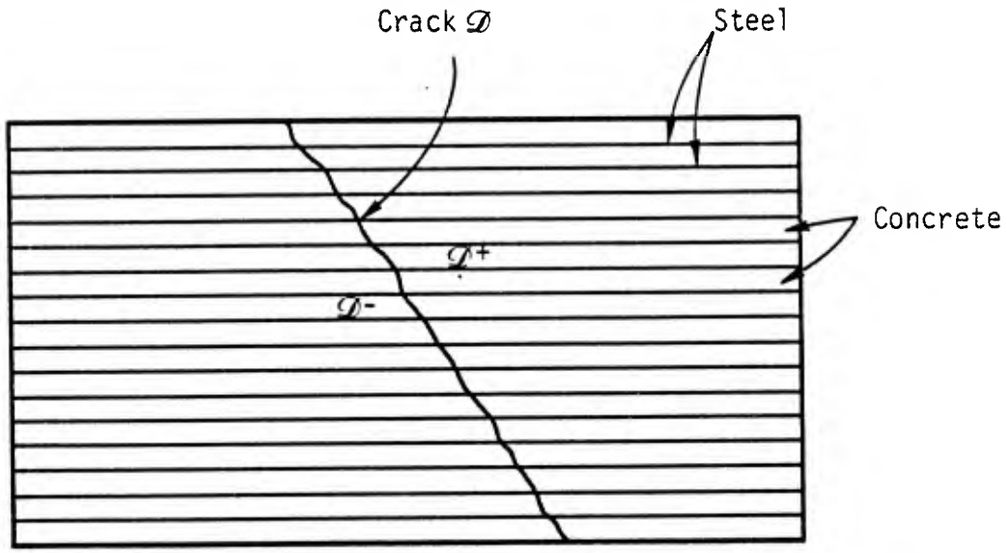


Figure 3.6. A cracked reinforced concrete with dense steel layout.

(a) Equations of Motion

$$\underset{\sim}{\nabla}_x \cdot \underset{\sim}{N}^{(\alpha)} + \underset{\sim}{F}^{(\alpha)} + \delta_{\alpha 2}\,\overline{\underset{\sim}{Q}} + (-1)^{1+\alpha}\underset{\sim}{P} = 0 \qquad (3\text{-}98a)$$

$$\underset{\sim}{\nabla}_x \cdot \underset{\sim}{M}^{K(\alpha)} - \underset{\sim}{N}^{K(\alpha)} + \underset{\sim}{F}^{K(\alpha)} + \delta_{\alpha 2}\underset{\sim}{Q}^{K} + (-1)^{1+\alpha}\underset{\sim}{Q}^{K} = 0 \qquad (3\text{-}98b)$$

(b) Constitutive Equations

$$\overset{\nabla}{\underset{\sim}{N}}{}^{(\alpha)} = \underset{\sim}{E}^{(\alpha)} : \dot{\underset{\sim}{\mathscr{E}}}^{(\alpha)} + \underset{\sim}{A}^{K(\alpha)} : \dot{\mathscr{K}}^{K(\alpha)} + \underset{\sim}{B}^{K(\alpha)} : \dot{\underset{\sim}{S}}^{K(\alpha)} \quad , \qquad (3\text{-}99a)$$

$$\overset{\nabla}{\underset{\sim}{M}}{}^{K(\alpha)} = \underset{\sim}{A}^{K(\alpha)} : \dot{\underset{\sim}{\mathscr{E}}}^{(\alpha)} + \underset{\sim}{G}^{KL(\alpha)} : \dot{K}^{L} + \underset{\sim}{C}^{KL(\alpha)} \cdot \dot{\underset{\sim}{S}}^{L(\alpha)} \quad , \qquad (3\text{-}99b)$$

$$\overset{\nabla}{\underset{\sim}{N}}{}^{K(\alpha)} = \underset{\sim}{a}^{K(\alpha)} : \dot{\underset{\sim}{\mathscr{E}}}^{(\alpha)} + \underset{\sim}{b}^{KL(\alpha)} : \dot{K}^{L} + \underset{\sim}{c}^{KL(\alpha)} \cdot \dot{\underset{\sim}{S}}^{L(\alpha)} \qquad (3\text{-}99c)$$

(c) Interaction Terms

$$\overset{\nabla}{\underset{\sim}{P}} = \underset{\sim}{\mathscr{L}} \cdot [\dot{\underset{\sim}{U}}] \quad , \quad \overset{\nabla}{\underset{\sim}{Q}}{}^{K} = \underset{\sim}{\mathscr{M}}{}^{K} \cdot [\dot{\underset{\sim}{U}}] \qquad (3\text{-}100)$$

(d) Crack Interface Terms

$$\overset{\nu}{\underset{\sim}{T}}{}^{(2)+} = -\overset{\nu}{\underset{\sim}{T}}{}^{(2)-} \equiv \overset{\nu}{\underset{\sim}{T}}{}^{(2)} \quad \text{on} \quad \mathscr{D} \quad , \qquad (3\text{-}101)$$

$$\overset{\nabla}{\underset{\sim}{T}}{}^{(2)} = \underset{\sim}{\mathscr{G}} \cdot [\dot{\underset{\sim}{U}}^{(2)}]_{\mathscr{D}} \quad \text{on} \quad \mathscr{D} \quad .$$

(e) Boundary Conditions on $\xi_1 = 0$ and $\xi_1 = \ell$.

$$\overset{1}{\underset{\sim}{T}}{}^{(\alpha)} = \underset{\sim}{\nu}_1 \cdot \underset{\sim}{N}^{(\alpha)} \quad \text{or} \quad \delta\dot{\underset{\sim}{U}}^{(\alpha)} = 0 \qquad (3\text{-}102a)$$

$$\overset{1}{\underset{\sim}{T}}{}^{K(\alpha)} = \underset{\sim}{\nu}_1 \cdot \underset{\sim}{M}^{K(\alpha)} \quad \text{or} \quad \delta\dot{\underset{\sim}{S}}^{K(\alpha)} = 0 \qquad (3\text{-}102b)$$

(f) Kinematic Relations

$$\dot{\underset{\sim}{\mathscr{E}}}^{(\alpha)} \equiv \frac{1}{2}\left(\underset{\sim}{\nabla}_x \dot{\underset{\sim}{U}}^{(\alpha)} + \underset{\sim}{\nabla}_x^{T} \dot{\underset{\sim}{U}}^{(\alpha)}\right) \quad , \qquad (3\text{-}103)$$

$$\dot{\underset{\sim}{\mathscr{K}}}^{K(\alpha)} \equiv \frac{1}{2}\left(\underset{\sim}{\nabla}_x \underset{\sim}{S}^{K(\alpha)} + \underset{\sim}{\nabla}_x^{T} \dot{\underset{\sim}{S}}^{K(\alpha)}\right) \quad , \qquad (3\text{-}104)$$

(g) Averages

$$\left(\underset{\sim}{E}^{(\alpha)}, \underset{\sim}{A}^{K(\alpha)}, \underset{\sim}{B}^{K(\alpha)}, G^{KL(\alpha)}, \underset{\sim}{C}^{KL(\alpha)}\right) \equiv \int_{A^{(\alpha)}} \left(\underset{\sim}{\mathscr{D}}^{(\alpha)}, \underset{\sim}{\mathscr{D}}^{(\alpha)} g^{K(\alpha)}, \underset{\sim}{\mathscr{D}}^{(\alpha)} \cdot \underset{\sim}{\nabla}_* g^{K(\alpha)} \right.$$

$$\left. g^{K(\alpha)} g^{L(\alpha)} \underset{\sim}{\mathscr{D}}^{(\alpha)}, \; g^{K(\alpha)} \underset{\sim}{\mathscr{D}}^{(\alpha)} \cdot \underset{\sim}{\nabla}_* g^{L(\alpha)}\right) dA \qquad (3\text{-}105)$$

$$(\underset{\sim}{a}^{K(\alpha)}, \underset{\sim}{b}^{KL(\alpha)}, \underset{\sim}{c}^{KL(\alpha)}) \equiv \int_{A^{(\alpha)}} (\underset{\sim}{\nabla}_* g^{K(\alpha)} \cdot \underset{\sim}{\mathscr{D}}^{(\alpha)}, g^{K(\alpha)} \underset{\sim}{\nabla}_* g^{K(\alpha)} \cdot \underset{\sim}{\mathscr{D}}^{(\alpha)}, \underset{\sim}{\nabla}_* g^{K(\alpha)} \underset{\sim}{\mathscr{D}}^{(\alpha)} \cdot \underset{\sim}{\nabla}_* g^{L(\alpha)}) dA \qquad (3\text{-}106)$$

$$(\underset{\sim}{\mathscr{L}}\underset{\sim}{\mathscr{M}}^{K}) \equiv \oint_{\mathscr{J}} (\underset{\sim}{\mathscr{B}} \cdot \underset{\sim}{\mathscr{B}} g^{K(1)}) ds \qquad (3\text{-}107)$$

Remarks

Equations (3-98) - (3-107) are similar in form to Equations (3-60) - (3-66) for the dense periodic steel layout. An important difference, however, concerns the terms $\bar{\underset{\sim}{Q}}$, $\bar{\underset{\sim}{Q}}^{K}$. These variables are the result of (weighted) tractions integrated around the outer cell boundary $\mathscr{J}$ (see Equation (3-89e)). Such terms vanish in the dense case due to the assumed local periodicity condition. Their presence in the sparse steel problem renders the mixture equilibriums equations "nonsymmetric" with respect to materials "1" and "2".

The dependent variables $\underset{\sim}{N}^{(\alpha)}$ in the mixture relations are, again, "partial stresses". The dependent variables $\underset{\sim}{M}^{K(\alpha)}$, represent weighted averages of the stresses $\underset{\sim}{\sigma}^{(\alpha)}$ over the cell area $A^{(\alpha)}$ occupied by material "α".

As in the case of a dense steel layout, the quantities $\underset{\sim}{U}^{(\alpha)}$, $\underset{\sim}{S}^{K(\alpha)}$ represent displacement-type dependent variables which are introduced by the displacement field (3-83) which, in turn, is utilized as a test function in the Principle of Virtual Work.

Weighting Functions

For the case of a sparse steel layout, the following elementary weighting functions appear to be adequate:

$$g_2^{(1)} = g_2^{(2)} = \xi_2 \quad , \quad g_3^{(1)} = g_3^{(2)} = \xi_3 \qquad (3\text{-}108)$$

## Additional Constraints

As in the dense steel discussion, it is appropriate for some problems to introduce the constraint

$$\underset{\sim}{S}^{K(1)} = \underset{\sim}{S}^{K(2)} \quad . \tag{3-109}$$

And, as before, in accordance with the reduction of the number of dependent variables, the relation (3-98b) is replaced by

$$\underset{\sim}{\nabla}_x \cdot \underset{\sim}{M}^K - \underset{\sim}{\bar{N}}^K + \underset{\sim}{F}^K + \delta_{\alpha 2}\, \underset{\sim}{\bar{Q}}^K = 0 \tag{3-110}$$

where

$$(\underset{\sim}{M}^K, \underset{\sim}{\bar{N}}^K, \underset{\sim}{F}^K) \equiv \sum_{\alpha=1}^{2} (\underset{\sim}{M}^{K(\alpha)}, \underset{\sim}{\bar{N}}^{K(\alpha)}, \underset{\sim}{F}^{K(\alpha)}) \quad . \tag{3-111}$$

Constitutive relations for $\underset{\sim}{M}^K, \underset{\sim}{N}^K$ are obtained by addition of (3-99b) or (3-99c) for $\alpha = 1,2$. The result is given by (3-66d,e).

## Mixture Equations - Compcnent Form

For later use, we list below the compoments of the mixture equations under the restrictions that (1) the initial geometry is rectilinear, (2) the deformations are small, and (3) the constraint (3-109) applies:

(a) Equations of Motion

$$N^{(1)}_{1i,1} + F^{(1)}_i + P_i = 0 \quad , \tag{3-112a}$$

$$N^{(2)}_{1i,1} + F^{(2)}_i + Q_i - P_i = 0 \tag{3-112b}$$

$$M^2_{1i,1} + F^2_i + \bar{Q}^2_i - (N^{(1)}_{2i} + N^{(2)}_{2i}) = 0 \quad , \tag{3-113a}$$

$$M^3_{1i,1} + F^3_i + \bar{Q}^3_i - (N^{(1)}_{3i} + N^{(2)}_{3i}) = 0 \tag{3-113b}$$

(b) Constitutive Equations

$$\dot{N}_{ij}^{(\alpha)} = E_{ijk\ell}^{(\alpha)} \dot{\mathscr{E}}_{k\ell}^{(\alpha)} + A_{ijk\ell}^{K(\alpha)} \dot{\mathscr{K}}_{k\ell}^{K(\alpha)} + B_{ijk}^{K(\alpha)} \dot{S}_k^K \tag{3-114a}$$

$$\dot{M}_{ij}^{K} = \sum_{\alpha=1}^{2} A_{ijk\ell}^{K(\alpha)} \dot{\mathscr{E}}_{k\ell}^{(\alpha)} + G_{ijk\ell}^{KL(\alpha)} \dot{\mathscr{K}}_{k\ell}^{L} + C_{ijk}^{KL(\alpha)} \dot{S}_k^L \tag{3-114b}$$

$$\dot{\overline{N}}_{ij}^{K(\alpha)} = \sum_{\alpha=1}^{2} a_{ijk\ell}^{K(\alpha)} \dot{\mathscr{E}}_{k\ell}^{(\alpha)} + b_{ijk\ell}^{KL(\alpha)} \dot{\mathscr{K}}_{k\ell}^{L} + C_{ijk}^{KL(\alpha)} \dot{S}_k^L \tag{3-114c}$$

(c) Steel-Concrete Interface Law

$$\dot{P}_i = \mathscr{L}_{ij} [\dot{U}_j] \tag{3-115}$$

(d) Crack Interface Law

$$\dot{\overset{\nu}{T}}_i^{(2)} = \mathscr{G}_{ij} [\dot{U}_j^{(2)}] \quad \text{on crack } \mathscr{D} \tag{3-116}$$

(e) Boundary Conditions on $\xi_1 = 0, \ell$.

$$\delta U_i^{(1)} = 0 \quad \text{or} \quad N_{1i}^{(1)} = \overset{1}{\overset{\sim}{T}}_i^{(1)} \tag{3-117a}$$

$$\delta U_i^{(2)} = 0 \quad \text{or} \quad N_{1i}^{(2)} = \overset{1}{\overset{\sim}{T}}_i^{(2)} \quad , \tag{3-117b}$$

$$\delta S_i^2 = 0 \quad \text{or} \quad M_{1i}^2 = \overset{1}{T}_i^2 \tag{3-117c}$$

$$\delta S_i^3 = 0 \quad \text{or} \quad M_{1i}^3 = \overset{1}{T}_i^3 \tag{1-117d}$$

(f) Boundary Terms

$$(\overline{Q}_i, \overline{Q}_i^K) \equiv \int_{\mathscr{J}} (1, g^{K(2)}) \overset{\nu}{T}_i^{(2)} \, ds \tag{3-118}$$

where $\overset{\nu}{T}_i^{(2)}$ must be specified.

## 3.3 OTHER DESCRIPTIONS OF THE MIXTURE RELATIONS

In Sections 3.1 and 3.2, mixture relations for dense and sparse steel layouts were constructed based upon the use of the

current configuration as the reference configuration. For some problem types, it may be more convenient from a computational standpoint to employ a Lagrangian description of motion wherein the initial configuration serves as the reference state. In view of this, a Lagrangian formulation of the mixture model for the sparse case is constructed in this section. The derivation for the dense case follows in a similar manner.

### 3.3.1 Sparse Steel

#### Geometry

As before, we consider a single steel reinforcing bar together with the surrounding concrete cover, Figure 3.7. In this case, however, the initial configuration of the cell is selected as the reference state. With reference to Figure 3.7, let $\underset{\sim}{R}$ denote the steel centerline in the initial configuration, $\mathscr{C}_{(0)}$. The vector $\underset{\sim}{X}^*$ lies in the plane whose normal is tangent to this centerline at the location defined by the vector $\underset{\sim}{R}$. Thus, material points in $\mathscr{C}_{(0)}$ are located by the position vector $\underset{\sim}{X} = \underset{\sim}{R} + \underset{\sim}{X}^*$. The quantities $A_0^{(1)}$, $A_0^{(2)}$, $S_0^+$, $S_0^-$, L in Figure 3.7 denote steel, concrete cross-sectional areas, steel-concrete interface, outer cell boundary, and cell length, respectively -- all with respect to $\mathscr{C}_{(0)}$. Normals to the areas $A_0^{(1)}$, $A_0^{(2)}$ are tangent to the steel centerline.

#### Variational Principle

In a manner similar to that outlined in Section 3.2, one begins the analysis by constructing a variational principle for the composite cell. This is accomplished by first writing the Principle of Virtual Work for both compoments. When the initial configuration is used as the reference, the appropriate forms are:

$$\int_{S_0^{(\alpha)}} \left( \underset{\sim}{T}_0^{(\alpha)} \cdot \delta \underset{\sim}{u}^{(\alpha)} \right) dS_0^{(\alpha)} + \int_{V_0^{(\alpha)}} \left( \rho_0 \underset{\sim}{f}_0^{(\alpha)} \cdot \delta u^{(\alpha)} \right) = \int_{V_0^{(\alpha)}} \left( \underset{\sim}{\tau} : \delta \underset{\sim}{E} \right) dV_0^{(\alpha)} \qquad (\alpha = 1,2) \qquad (3\text{-}119)$$

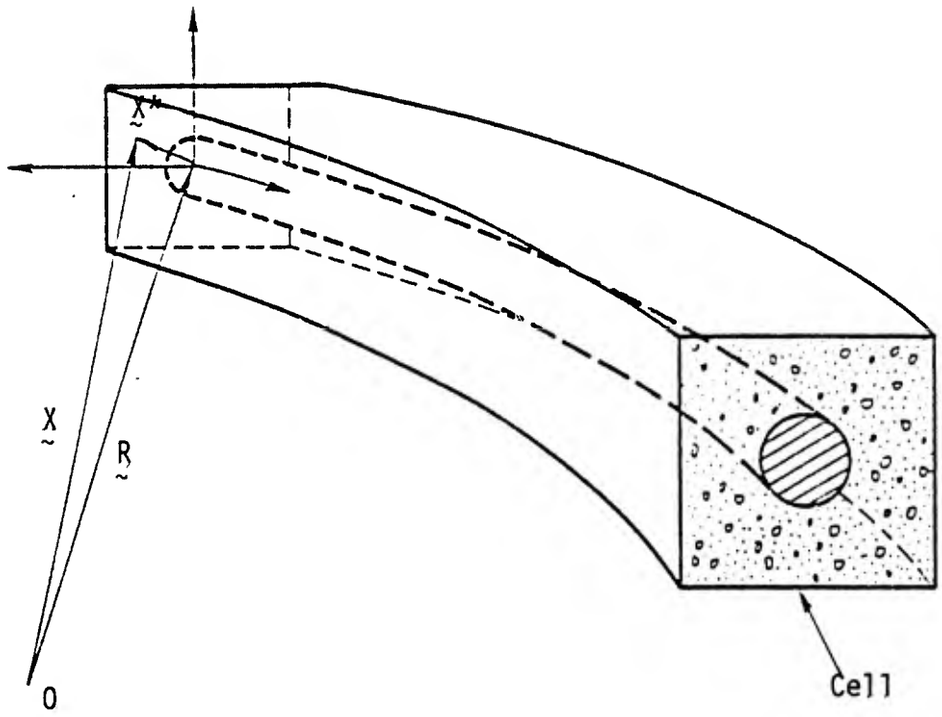


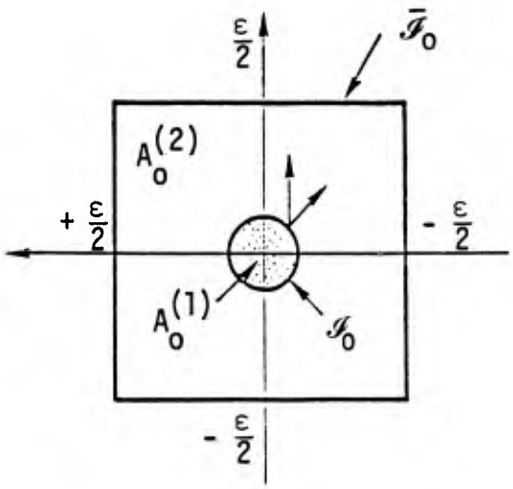


Figure 3.7. Initial configuration of cell.

where $\underset{\sim}{\tau}$ is the Piola-Kirchoff stress tensor of the second kind, $\underset{\sim}{E}$ is the Green's strain tensor

$$\underset{\sim}{E} = \frac{1}{2}\left(\underset{\sim}{\nabla}_X \underset{\sim}{u} + \underset{\sim}{\nabla}_X^T \underset{\sim}{u} + \underset{\sim}{\nabla}_X \underset{\sim}{u} \cdot \underset{\sim}{\nabla}_X^T u\right) , \tag{3-120}$$

$\overset{n}{\underset{\sim}{T}}_0$ is the pseudo-traction vector, $\underset{\sim}{f}_0$ is a body force per unit mass which includes inertial terms, $\underset{\sim}{u}$ is the displacement vector, and $S_0$, $V_0$ denote surface area and volume, respectively.

On the steel-concrete interface $S^*_0$:

$$\overset{n}{\underset{\sim}{T}}_0^{(1)} = - \overset{n}{\underset{\sim}{T}}_0^{(2)} \equiv \overset{n}{\underset{\sim}{T}}{}^*_0 \quad \text{on } S^*_0 \tag{3-121}$$

results from continuity of the traction vector. However, continuity of the displacement $\underset{\sim}{u}$ may not be assumed. To account for displacement discontinuities, we define the "slip" $[\underset{\sim}{u}]$ as follows:

$$[\underset{\sim}{u}] \equiv \underset{\sim}{u}^{(2)} - \underset{\sim}{u}^{(1)} \quad \text{on } S^*_0. \tag{3-122}$$

Upon addition of (3-119) for $\alpha = 1$, $\alpha = 2$ with use of (3-121) and (3-122), the Principle of Virtual Work for the composite cell becomes:

$$\sum_{\alpha=1}^{2}\left\{\int_{V_0^{(\alpha)}} \rho_0^{(\alpha)} \underset{\sim}{f}_0^{(\alpha)} \cdot \delta\underset{\sim}{u}^{(\alpha)} dV_0 + \int_{S_0^{(\alpha)} - S^*_0} \overset{n}{\underset{\sim}{T}}_0^{(\alpha)} \cdot \delta\underset{\sim}{u}^{(\alpha)} dS_0\right\}$$

$$= \sum_{\alpha=1}^{2}\left\{\int_{V_0^{(\alpha)}} \underset{\sim}{\tau}^{(\alpha)} : \delta\underset{\sim}{E}^{(\alpha)} dS_0 + \int_{S^*_0} \underset{\sim}{T}{}^*_0 \cdot \delta[\underset{\sim}{u}] dS_0\right\} \tag{3-123}$$

With the application of Gauss' Theorem, equation (3-123) can also be written

$$\sum_{\alpha=1}^{2} \left\{ \int_{V_o^{(\alpha)}} [\nabla_X \cdot (\underset{\sim}{\tau} \cdot \underset{\sim}{F}^T) + \rho_o \underset{\sim}{f}_o]^{(\alpha)} \cdot \delta \underset{\sim}{u}^{(\alpha)} dV_o \right.$$

$$\left. + \int_{S_o^{(2)} - S_o^*} [\underset{\sim}{T}_o - \underset{\sim}{n} \cdot \underset{\sim}{\tau} \cdot \underset{\sim}{F}^T]^{(\alpha)} \cdot \delta \underset{\sim}{u}^{(2)} dS_o = \int_{S_o^*} T_o^* \cdot \delta [\underset{\sim}{u}] dS_o \right\} \qquad (3\text{-}124)$$

where

$$F \equiv \nabla_X^T \underset{\sim}{X} \quad , \quad \underset{\sim}{F}^T \equiv \nabla_X \underset{\sim}{x} \qquad (3\text{-}125)$$

defines the deformation gradient, $\underset{\sim}{F}$ and its transpose $\underset{\sim}{F}^T$.

The operator $\nabla_X$ is given by

$$\nabla_X \equiv \underset{\sim}{G}^k \frac{\partial}{\partial \theta_k} \qquad (3\text{-}126)$$

where $\underset{\sim}{G}^k$ are the contravariant base vectors of the coordinate system and $\theta_k$ are the coordinates. Thus, $\underset{\sim}{G}^k \cdot \underset{\sim}{G}_s = \delta_s^k$ where $\underset{\sim}{G}_s \equiv \partial \underset{\sim}{X} / \partial \theta_s$ and $\delta_s^k$ is the Kronecker delta.

Since the current position vector $\underset{\sim}{x}$ and the initial position vector $\underset{\sim}{X}$ are related by

$$\underset{\sim}{x} = \underset{\sim}{X} + \underset{\sim}{u} \quad , \qquad (3\text{-}127)$$

The deformation gradient can be written

$$\underset{\sim}{F}^T = \underset{\sim}{I} + \nabla_X \underset{\sim}{u} \qquad (3\text{-}128)$$

where $\underset{\sim}{I}$ is the unit tensor with Cartesian compoments $\delta_{ij}$.

In addition, since $\underset{\sim}{X} = \underset{\sim}{R} + \underset{\sim}{X}^*$, one can write

$$\nabla_X = \nabla_R + \nabla_{X^*} \qquad (3\text{-}129)$$

where

$$\underset{\sim}{\nabla}_R \equiv \underset{\sim}{G}^i \frac{\partial}{\partial \bar{\theta}_i} \quad , \quad \underset{\sim}{\nabla}_{X^*} \equiv \underset{\sim}{G}^i \frac{\partial}{\partial \theta^*_i} \quad . \tag{3-130}$$

The coordinates $\bar{\theta}_i$, $\theta^*_i$ are defined by

$$d\underset{\sim}{R} = \underset{\sim}{G}^i d\bar{\theta}_i \quad , \quad d\underset{\sim}{X^*} = \underset{\sim}{G}^i d\theta^*_i \tag{3-131}$$

## Test Functions

A trial displacement field is now assumed in the form

$$\underset{\sim}{u}^{(\alpha)}(\underset{\sim}{X},t) \cong \underset{\sim}{U}^{(\alpha)}(\underset{\sim}{R},t) + \underset{\sim}{S}^{K(\alpha)}(\underset{\sim}{R},t) g^{K(\alpha)}(\underset{\sim}{X^*}) \quad (K = 1 \text{ to } N) \tag{3-132}$$

(K summed, no sum on $\alpha$)

where $g^{K(\alpha)}(\underset{\sim}{X^*})$ are weight functions which are continuous across the steel-concrete interface $S^*_o$. Thus

$$[\underset{\sim}{u}] = \underset{\sim}{U}^{(2)} - \underset{\sim}{U}^{(1)} \equiv [\underset{\sim}{U}] \text{ on } S^*_o \tag{3-133}$$

## Equations of Motion, Boundary Conditions

Upon combining (3-128), (3-129), and (3-132), one finds

$$\begin{aligned} \underset{\sim}{\nabla}_X \cdot (\underset{\sim}{\tau} \cdot \underset{\sim}{F}^T) \cdot \delta\underset{\sim}{u} &= \underset{\sim}{\nabla}_R \cdot (\underset{\sim}{\tau} \cdot \underset{\sim}{F}^T) \cdot \delta\underset{\sim}{U} + \underset{\sim}{\nabla}_{X^*} \cdot (\underset{\sim}{\tau} \cdot \underset{\sim}{F}^T) \cdot \delta\underset{\sim}{U} \\ &+ \underset{\sim}{\nabla}_R \cdot (\underset{\sim}{\tau} \cdot \underset{\sim}{F}^T) \cdot g^K \delta\underset{\sim}{S}^K + \underset{\sim}{\nabla}_{X^*} \cdot (\underset{\sim}{\tau} \cdot \underset{\sim}{F}^T) \cdot g^K \delta\underset{\sim}{S}^K \end{aligned} \tag{3-134a}$$

where

$$\underset{\sim}{F}^T = \underset{\sim}{I} + \underset{\sim}{\nabla}_R \underset{\sim}{U} + \underset{\sim}{\nabla}_R \underset{\sim}{S}^K g^K + \underset{\sim}{\nabla}_{X^*} g^K \underset{\sim}{S}^K \tag{3-134b}$$

Following substitution of (3-134a,b) into (3-125), one obtains after algebraic manipulation and neglect of $O(g^K)^2$ terms:

$$\sum_{\alpha=1}^{2}\int_{0}^{L}\Big\{\underset{\sim}{\nabla}_R\cdot\Big[\underset{\sim}{N}^{(\alpha)}\cdot(\underset{\sim}{I}+\underset{\sim}{\nabla}_R\underset{\sim}{U}^{(\alpha)})+\underset{\sim}{M}^{K(\alpha)}\cdot\underset{\sim}{\nabla}_R\underset{\sim}{S}^{K(\alpha)}+\overline{\underset{\sim}{N}}^{K(\alpha)}\underset{\sim}{S}^{K(\alpha)}\Big]$$

$$+(-1)^{1+\alpha}\underset{\sim}{P}+\delta_{\alpha 2}\overline{\underset{\sim}{P}}+\underset{\sim}{F}_0^{(\alpha)}\Big\}\cdot\delta\underset{\sim}{U}^{(\alpha)}$$

$$+\Big\{\underset{\sim}{\nabla}_R\cdot\Big[\underset{\sim}{M}^{K(\alpha)}\cdot(\underset{\sim}{I}+\underset{\sim}{\nabla}_R\underset{\sim}{U}^{(\alpha)})+\underset{\sim}{N}^{LK}\underset{\sim}{S}^{L}\Big]-\overline{\underset{\sim}{N}}^{K(\alpha)}\cdot(\underset{\sim}{I}+\underset{\sim}{\nabla}_R\underset{\sim}{U}^{(\alpha)})$$

$$+\underset{\sim}{N}^{KL(\alpha)}\cdot\underset{\sim}{\nabla}_R\underset{\sim}{S}^{L}+\Gamma^{KL(\alpha)}\underset{\sim}{S}^{L(\alpha)}+(-1)^{1+\alpha}\underset{\sim}{Q}^{K}$$

$$+\delta_{\alpha 2}\overline{\underset{\sim}{Q}}^{K}+\underset{\sim}{F}_0^{K(\alpha)}\Big\}\cdot\delta\underset{\sim}{S}^{K(\alpha)}\Big]ds$$

$$+\Big[\Big\{\underset{\sim}{T}_0^{(\alpha)}-\underset{\sim}{n}_1\cdot\Big[\underset{\sim}{N}^{(\alpha)}\cdot(\underset{\sim}{I}+\underset{\sim}{\nabla}_R\underset{\sim}{U}^{(\alpha)})+\underset{\sim}{M}^{K(\alpha)}\cdot\underset{\sim}{\nabla}_R\underset{\sim}{S}^{K(\alpha)}+\overline{\underset{\sim}{N}}^{K(\alpha)}\underset{\sim}{S}^{K(\alpha)}\Big]\Big\}\cdot\delta\underset{\sim}{U}^{(\alpha)}$$

$$+\Big\{\underset{\sim}{T}_0^{K(\alpha)}-\underset{\sim}{n}_1\Big[\underset{\sim}{M}^{K(\alpha)}\cdot(\underset{\sim}{I}+\underset{\sim}{\nabla}_R\underset{\sim}{U}^{(\alpha)})+\underset{\sim}{N}^{LK(\alpha)}\underset{\sim}{S}^{L(\alpha)}\Big]\Big\}\cdot\delta\underset{\sim}{S}^{K(\alpha)}\Big]_0^L=0, \quad (3\text{-}135)$$

where

$$(\underset{\sim}{N}^{(\alpha)},\underset{\sim}{M}^{K(\alpha)})\equiv\int_{A_0^{(\alpha)}}(1,g^{K(\alpha)})\underset{\sim}{T}^{(\alpha)}\,dA_0\,, \quad (3\text{-}136a)$$

$$(\underset{\sim}{F}^{(\alpha)},\underset{\sim}{F}^{K(\alpha)})\equiv\int_{A_0^{(\alpha)}}(1,g^{K(\alpha)})f_0^{(\alpha)}\,dA_0\,, \quad (3\text{-}136b)$$

$$\overline{\underset{\sim}{N}}^{K(\alpha)}\equiv\int_{A_0^{(\alpha)}}\underset{\sim}{T}^{(\alpha)}\cdot\underset{\sim}{\nabla}_{X^*}g^{K(\alpha)}dA_0 \quad (3\text{-}136c)$$

$$(\underset{\sim}{\overset{1}{T}}^{(\alpha)},\overset{1}{T}^{K(\alpha)})\equiv\int_{A_0^{(\alpha)}}(1,g^{K(\alpha)})\underset{\sim}{\overset{1}{T}}^{(\alpha)}\,dA_0\,, \quad (3\text{-}136d)$$

$$\underset{\sim}{N}^{KL(\alpha)} \equiv \int_{A_o^C} g^{L(\alpha)} \nabla_{X^*} g^{K(\alpha)} \cdot \underset{\sim}{T}^{(\alpha)} dA_o \ ,$$

$$\Gamma^{KL(\alpha)} \equiv \int_{A_o} \nabla_{X^*} g^{K(\alpha)} \cdot \underset{\sim}{T}^{(\alpha)} \cdot \nabla_{X^*} g^{L(\alpha)} \ dA_o \ , \qquad (3\text{-}136e)$$

$$(\overline{\underset{\sim}{P}}, \overline{\underset{\sim}{Q}}^K) \equiv \oint_{\mathscr{I}} (1, g^{K(2)}) \underset{\sim}{T}_o^{n(2)} ds_o \ , \qquad (3\text{-}136f)$$

$$(\underset{\sim}{P}, \underset{\sim}{Q}^K) \equiv \oint_{\mathscr{I}} (\underset{\sim}{1}, g^{K(\alpha)}) \underset{\sim}{T}_o^* \ ds_o \ . \qquad (3\text{-}136g)$$
$$(\alpha = 1 \text{ or } 2)$$

The Euler-Lagrange equations of (3-135) are

either $\delta \underset{\sim}{U}^{(\alpha)} \equiv 0$ or

$$\nabla_R \cdot \left[ \underset{\sim}{N}^{(\alpha)} \cdot (\underset{\sim}{I} + \nabla_R \underset{\sim}{U}^{(\alpha)}) + \underset{\sim}{M}^{K(\alpha)} \cdot \nabla_R \underset{\sim}{S}^{K(\alpha)} + \overline{\underset{\sim}{N}}^{K(\alpha)} \underset{\sim}{S}^{K(\alpha)} \right]$$

$$+ (-1)^{1+\alpha} \underset{\sim}{P} + \delta_{\alpha 2} \overline{\underset{\sim}{P}} + \underset{\sim}{F}_o^{(\alpha)} = 0 \ , \qquad (3\text{-}137a)$$

either $\delta \underset{\sim}{S}^{K(\alpha)} \equiv 0$ or

$$\nabla_R \cdot \left[ \underset{\sim}{M}^{K(\alpha)} \cdot (\underset{\sim}{I} + \nabla_R \underset{\sim}{U}^{(\alpha)}) + \underset{\sim}{N}^{LK} \underset{\sim}{S}^{L(\alpha)} \right] - \overline{\underset{\sim}{N}}^{K(\alpha)} \cdot (\underset{\sim}{I} + \nabla_R \underset{\sim}{U}^{(\alpha)})$$

(3-137b)

$$+ \underset{\sim}{N}^{KL(\alpha)} \cdot \nabla_R \underset{\sim}{S}^{L(\alpha)} + \underset{\sim}{\Gamma}^{KL(\alpha)} \underset{\sim}{S}^{L(\alpha)} + (-1)^{1+\alpha} \underset{\sim}{Q}^K + \delta_{\alpha 2} \overline{\underset{\sim}{Q}}^K + \underset{\sim}{F}_o^{K(\alpha)} = 0 \ .$$

The boundary conditions at $s_o = 0$ and $s_o = L$ are

$$\delta \underset{\sim}{U}^{(\alpha)} = 0 \quad \text{or} \quad \underset{\sim}{T}^{(\alpha)} = \underset{\sim}{n}_1 \cdot \left[ \underset{\sim}{N}^{(\alpha)} \cdot (\underset{\sim}{I} + \nabla_R \underset{\sim}{U}^{(\alpha)}) + \underset{\sim}{M}^{K(\alpha)} \cdot \nabla_R S^{K(\alpha)} + \underset{\sim}{N}^{K(\alpha)} S^{K(\alpha)} \right] \quad (3\text{-}138$$

$$\delta \underset{\sim}{S}^{K(\alpha)} = 0 \quad \text{or} \quad \underset{\sim}{T}^{K(\alpha)} = \underset{\sim}{n}_1 \cdot \left[ \underset{\sim}{M}^{K(\alpha)} \cdot (\underset{\sim}{I} + \nabla_R \underset{\sim}{U}^{(\alpha)}) + \underset{\sim}{N}^{LK(\alpha)} \underset{\sim}{S}^{L(\alpha)} \right] \quad (3\text{-}138b)$$

where $n_1$ denotes the normal to the end surfaces.

Equations (3-137a,b) are the mixture equations of motion for the Lagrangian description. Equations (3-138a,b) are the appropriate boundary conditions for the mixture equations.

### 3.3.2 Equations of Motion for Initial Rectilinear Geometry

If the initial geometry is rectilinear, Figure 3.8, then

$$\underset{\sim}{R} = \underset{\sim}{e}_1 X_1 \quad , \quad \underset{\sim}{\nabla}_R = \underset{\sim}{e}_1 \frac{\partial}{\partial X_1} \, , \quad \underset{\sim}{\nabla}_{X^*} = \underset{\sim}{e}_L \frac{\partial}{\partial X_L^*} \quad (L = 2,3) \tag{3-139}$$

where $\underset{\sim}{e}_1$, $\underset{\sim}{e}_2$, $\underset{\sim}{e}_3$ are orthogonal unit base vectors. In addition, if the weight functions (see (3-108))

$$g^{K(\alpha)} \equiv X_k^* \quad (k = 2,3, \quad \alpha = 1,2) \tag{3-140}$$

are selected, then

$$\underset{\sim}{\nabla}_{X^*} g^{K(\alpha)} = \underset{\sim}{e}_L \frac{\partial}{\partial X_L^*} (X_k^*) = \underset{\sim}{e}_L \delta_{LK} = \underset{\sim}{e}_K \tag{3-141}$$

whence

$$\underset{\sim}{N}^{K(\alpha)} = \int_{A_o^{(\alpha)}} (\underset{\sim}{\tau}^{(\alpha)} \cdot \underset{\sim}{\nabla}_{X^*} g^{K(\alpha)}) dA_o = (\int_{A_o^{(\alpha)}} \underset{\sim}{\tau}^{(\alpha)} dA_o) \cdot \underset{\sim}{e}_K = \underset{\sim}{N}^{(\alpha)} \cdot \underset{\sim}{e}_k$$

$$\underset{\sim}{N}^{KL(\alpha)} = \int_{A_o^{(\alpha)}} g^{L(\alpha)} \underset{\sim}{\nabla}_{X^*} g^{K(\alpha)} \cdot \underset{\sim}{\tau}^{(\alpha)} dA_o = \underset{\sim}{e}_K \cdot \int_{A_o^{(\alpha)}} g^{L(\alpha)} \underset{\sim}{\tau}^{(\alpha)} = \underset{\sim}{e}_k \cdot \underset{\sim}{M}^{L(\alpha)} \, ,$$

$$\Gamma^{KL(\alpha)} = \int_{A_o^{(\alpha)}} \underset{\sim}{\nabla}_{X^*} g^{K(\alpha)} \cdot \underset{\sim}{\tau}^{(\alpha)} \cdot \underset{\sim}{\nabla}_{X^*} g^{L(\alpha)} dA_o = \underset{\sim}{e}_k \cdot (\int_{A_o^{(\alpha)}} \underset{\sim}{\tau} dA_o) \cdot \underset{\sim}{e}_L = \underset{\sim}{e}_K \cdot \underset{\sim}{N}^{(\alpha)} \cdot \underset{\sim}{e}_L$$

(3-142)

Under (3-139) and (3-142), the mixture relations (3-137) can be written in compoment form as follows

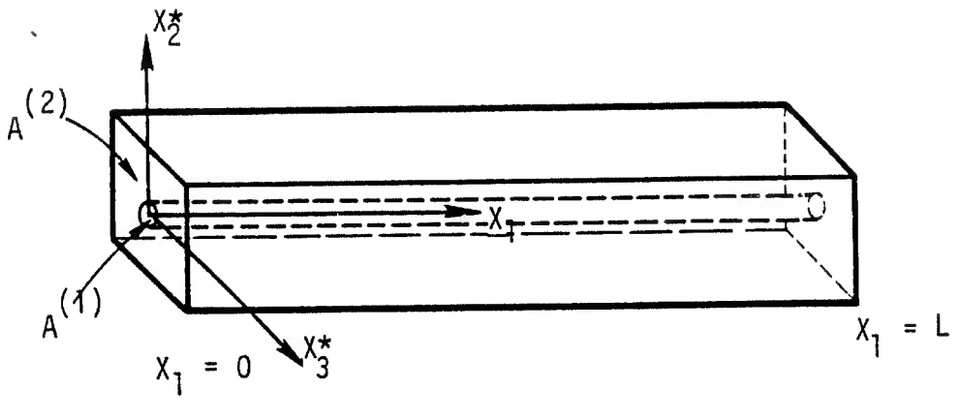


Figure 3.8a. Reinforced concrete cylinder.

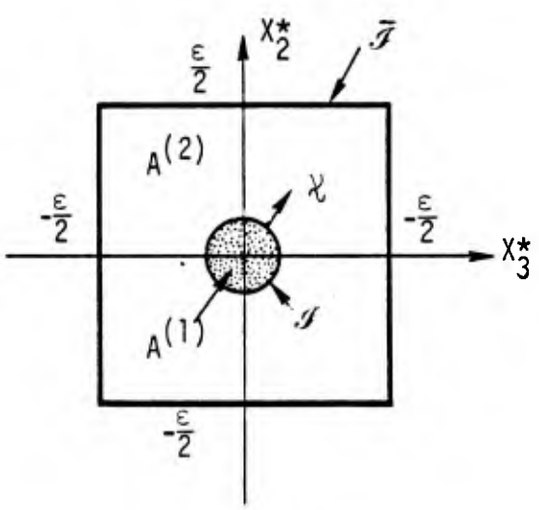


Figure 3.8b. Cross-sectional geometry of the reinforced concrete cylinder.

$$\delta U_i^{(\alpha)} \equiv 0 \quad \text{or}$$

$$\left[N_{1i} + N_{11}U_{i,1} + M_{11}^K S_{i,1}^K + N_{1K}S_i^K\right]_{,1}^{(\alpha)} + (-1)^{1+\alpha}P_i + \delta_{\alpha 2}\bar{P}_i + F_{o_i}^{(\alpha)} = 0, \quad (3\text{-}143a)$$

$$\delta S_i^{K(\alpha)} \equiv 0 \quad \text{or}$$

$$\left[M_{1i}^K + M_{11}^K U_{i,1} + M_{L1}^K S_i^L\right]_{,1}^{(\alpha)} - N_{iK}^{(\alpha)} - N_{1K}U_{i,1} + M_{K1}^L S_{i,1}^L$$

$$+ N_{KL}S_i^L + (-1)^{1+\alpha}Q_i^K + \delta_{\alpha 2}\bar{Q}_i^K + F_{o_i}^{K(\alpha)} = 0 \quad . \qquad (3\text{-}143b)$$

In the above i = 1 to 3; K,L = 1 to 2; $\alpha$ = 1,2 .

The corresponding boundary conditions are

$$\delta U_i^{(\alpha)} = 0 \quad \text{or} \quad \frac{1}{T_i}(\alpha) = [N_{1i} + N_{11}U_{i,1} + M_{11}^K S_{i,1}^K + N_{1K}S_i^K]^{(\alpha)}, \quad (3\text{-}144a)$$

$$\delta S_i^{K(\alpha)} = 0 \quad \text{or} \quad \frac{1}{T_i}K(\alpha) = [M_{1i}^K + M_{11}^K U_{i,1} + M_{L1}^K S_i^L]^{(\alpha)} \qquad (3\text{-}144b)$$

on $X_1$ = 0,L.

### 3.3.3 Dense Steel

An analysis similar to that discussed under Section 1.5.1 may be used to generate the Lagrangian form of the mixture momentum equations for the case of a dense steel layout. The resulting equations can be obtained from (3-137a) by invoking the following changes:

$$\underset{\sim}{\nabla}_R \rightarrow \underset{\sim}{\nabla} \quad , \quad \bar{P} \equiv 0 \quad , \quad \underset{\sim}{\bar{Q}}^K \equiv 0 \, . \qquad (3\text{-}145)$$

The independent spatial variable is the position vector $\underset{\sim}{X}$ and $\underset{\sim}{\nabla} \equiv \underset{\sim}{e}_i \partial/\partial X_i$ if a rectangular Cartesian triad is used.

## 3.4 APPLICATIONS

Several important special cases of the mixture relations developed in the previous sections are considered in this section. The problems investigated are intended to both validate, and demonstrate the modeling capability of, the mixture theory.

### 3.4.1 The Steel Concrete Bond Problem

The "steel-concrete bond problem" is significant from three different viewpoints. First, this problem type reflects a mode of deformation that often dominates the nonlinear behavior of a reinforced concrete structure. Second, it provides a means for validating a segment of the mixture model. Finally, the steel-concrete bond problem is central to the evaluation of a subset of the mixture model parameters.

Below, the general mixture relations are specialized to the steel-concrete bond problem. Subsequent to this, solutions of the resulting equations are compared with experimental data for both monotonic and hysteretic deformations.

#### Problem Definition, Sparse Steel

The steel-concrete bond problem is concerned with initial geometry that is rectilinear (Fig 3.1 for dense steel, Fig 3.8 for sparse steel). While the component (steel, concrete) and interface (steel-concrete) relations may be nonlinear, the deformations are to be sufficiently small that all nonlinear geometric terms may be neglected.

Within the context of the above mentioned rectilinear geometry and small deformations, the steel-concrete bond problem for sparse steel is defined by the constraints:

$$U_2^{(\alpha)} = U_3^{(\alpha)} \equiv 0 \quad , \tag{3-146a}$$

$$F_i^{(\alpha)} = F_i^K \equiv 0 \quad , \tag{3-146b}$$

$$\bar{Q}_i = \bar{Q}_i^K \equiv 0 \quad . \tag{3-146c}$$

Equation (3-146a) indicates that the average displacement is the 2- and 3-directions is zero (recall that $U_i^{(\alpha)}$ represents the cell-averaged displacement in the ith direction). Equation (3-146b) results from the premise that the body force $f_i$ vanishes. Equation (3-146c) results from the premise that the traction vector $\underset{\sim}{\bar{T}}^{(2)}$ vanishes on the cell boundary $\mathscr{I}$ (Fig. 3.8); thus, the cell outer boundary is presumed to be stress free.

Our analysis of the steel-concrete bond problem will be confined to the idealized situation wherein the concrete is elastic-brittle and the steel is elastic-plastic. Further, the influence of Poisson's ratio on the concrete response will be neglected. Under these conditions, and assuming that $\underset{\sim}{S}^{K(\alpha)} = 0$ at $X_1 = 0,\ell$ which in turn implies that the displacement field is uniform in $X_2, X_3$ at the cell termini, then it can be shown (see Reference [5]) that $\underset{\sim}{S}^{K(\alpha)} \equiv 0$. As a consequence of the above, the basic mixture equations (3-98) - (3-100) reduce to the elementary relations:

$$N_{11,1}^{(1)} + P_1 = 0 \quad , \quad N_{11,1}^{(2)} - P_1 = 0 \quad ; \tag{3-147a,b}$$

$$\dot{N}_{11}^{(1)} = 2\bar{\mu}^{(1)}\eta^{(1)}\varepsilon^2\dot{U}_{1,1}^{(1)} \quad , \quad \dot{N}_{11}^{(2)} = 2\mu^{(2)}\eta^{(2)}\varepsilon^2\dot{U}_{1,1}^{(2)} \quad ; \tag{3-147c,d}$$

$$\dot{P}_1 = K^*(\dot{U}_1^{(2)} - \dot{U}_1^{(1)}) \quad , \tag{3-147e}$$

where K* denotes a tangent slip modulus which, in general, depends on the steel-concrete relative slip history, and $\mu^{(2)}$ denotes an elastic-plastic tangent modulus for the steel. The remaining dependent variables vanish, i.e.,

$$U_2^{(a)} = U_3^{(\alpha)} \equiv 0 \quad , \quad N_{ij}^{(\alpha)} \equiv 0 \quad (i,j \neq 1) \quad ,$$

$$\bar{N}_{ij}^{K(\alpha)} \equiv 0 \quad , \quad M_{ij}^{2(\alpha)} = M_{ij}^{3(\alpha)} \equiv 0 \tag{3-147f}$$

Equations (3-147a-e) are the governing relations for the steel-concrete bond problem under the assumption that Poisson's ratio may be neglected, and that the steel layout is sparse.

## Problem Definition, Dense Steel

For dense steel, the steel-concrete bond problem is defined by

$$U_2^{(\alpha)} = U_3^{(2)} \equiv 0 \tag{3-148a}$$

$$F_i^{(\alpha)} = F_i^K \equiv 0 \ . \tag{3-148b}$$

If the concentric cylinder approximation of the cell and the weighting functions (3-167) are adopted, then it can be shown (see Reference [5]) that, if Poisson's ratio is neglected, the basic mixture relations (3-60) - (3-63) reduce to

$$N_{11,1}^{(1)} + P_1 = 0 \ , \ N_{11,1}^{(2)} - P_1 = 0 \ ; \tag{3-149a}$$

$$\dot{N}_{11}^{(1)} = 2\bar{\mu}^{(1)}{}_{\pi}n^{(1)}\dot{U}_{1,1}^{(1)} \ , \ \dot{N}_{11}^{(2)} = 2\mu^{(2)}{}_{\pi}n^{(2)}\dot{U}_{1,1}^{(2)} \ ; \tag{3-149b}$$

$$\dot{P}_1 = K^*(\dot{U}_1^{(2)} - \dot{U}_1^{(1)}) \ . \tag{3-149c}$$

All other dependent variables vanish.

It is evident that, upon neglecting the influence of Poisson's ratio, the mixture equations have the same form for both sparse and dense steel.

## Theory Versus Experiment

Several comparisons will now be made between theory and experiment in an effort to demonstrate the simulation capability of the mixture model. This discussion will be descriptive in nature. For additional details concerning numerics, material properties, and specimen geometries, the reader is referred to References 4, 5, and 21.

The parameters in the mixture equations that must be specified in order to allow a test simulation are: (1) the steel volume fraction, (2) the steel and concrete moduli, (3) the concrete tensile strength, (4) the steel yield point, (5) the initial specimen length, and (6) the coefficient K* in the interaction term. Item 1 results from a knowledge of the steel percentage in the specimen. Items 2 - 4 can be obtained from simple compoment tests. Item (5) is a matter of test specimen geometry. Item 6 must be deduced from a pullout test or a tension test; this subject (in contrast to items 1 - 5) is non-trivial and deserves some discussion.

Typical pullout and tension-test geometries are depicted in Figure 3.9. In order to define the interaction term $P_1$, it is necessary to "back-out" a local bond stress versus relative slip (between steel and concrete) relation from test data, and then to evaluate the interaction term. For this purpose, it has been found that a rigid-perfectly plastic interface description suffices in most cases involving monotonic deformation. The ultimate local bond stress is known to be proportional to $f'_c$ where $f'_c$ denotes the uniaxial compressive strength of the concrete. In terms of the difference of the <u>average</u> constituent displacements, $(U_1^{(1)} - U_1^{(2)})$, the interface behavior becomes <u>elastic</u>-perfectly plastic, Figure 3.10. The elastic segment is determined by a separate elastic analysis and represents no problem. More sophisticated interface constitutive relations can be postulated if necessary. Figure 3.11, for example, shows a fit to experimental data from a pullout test[22] using a piece-wise linear relation. For hysteretic deformations, the rigid-perfectly plastic bond behavior must be extended to allow relative slip reversals; here the incorporation of bond degeneration is necessary. Figure 3.12 illustrates a modified rigid-plastic model that has been successfully applied to problems involving cyclic loading.

Let us turn now to experimental versus theoretical comparisons. The first case to be considered involves a pullout

test. Based upon an analysis of the available experimental literature, the local bond stress versus slip relation depicted in Figure 3.13 was postulated as a general bond constitutive law for monotonic slip. Figure 3.14 shows the simulation accuracy of the mixture model using this law for one set of experiments[22]. Upon consideration of the experimental data scatter, it can be concluded that the simulation accuracy in this example is good. Also shown in Figure 3.14 is the influence of a rigid-plastic bond-slip relation (with the same peak bond strength) on simulation. The use of a simple rigid-plastic bond model appears to provide adequate simulation accuracy. Theoretical versus experimental[22] comparisons for another set of pullout test specimens are shown in Figure 3.15. The bond law shown in Figure 3.13 was again used in the simulation. Agreement in this case is reasonable, but not as good as in the previous example. The primary difference in the test specimens was the degree of concrete cover.

The second case to be examimed concerns tension tests. Figure 3.16 shows simulation versus experimental[23] data for two sizes of tension specimens. Agreement is considered to be satisfactory when one considers the data scatter typical of such tests. Again it is emphasized that the bond slip law defined by Figure 3.13 was used in the simulations. In particular, it is noted that no effort to "tune" the model to the data was made.

The third case to be considered involves monotonic extension of a scaled reinforced concrete specimen with a dense unidirectional steel layout, Figure 3.17. Experimental[24] versus theoretical comparisons for load controlled tests are shown in Figures 3.18 and 3.19. Because of the load-control, the tests in this series were not "clean." In particular, expected sharp drops in global stress due to progressive fracture of the concrete are "smeared" due to the specimen loading procedure. In addition, the method of testing led to significant data scatter. Nevertheless, the experimental-theoretical comparisons shown, which represent essentially monotonic

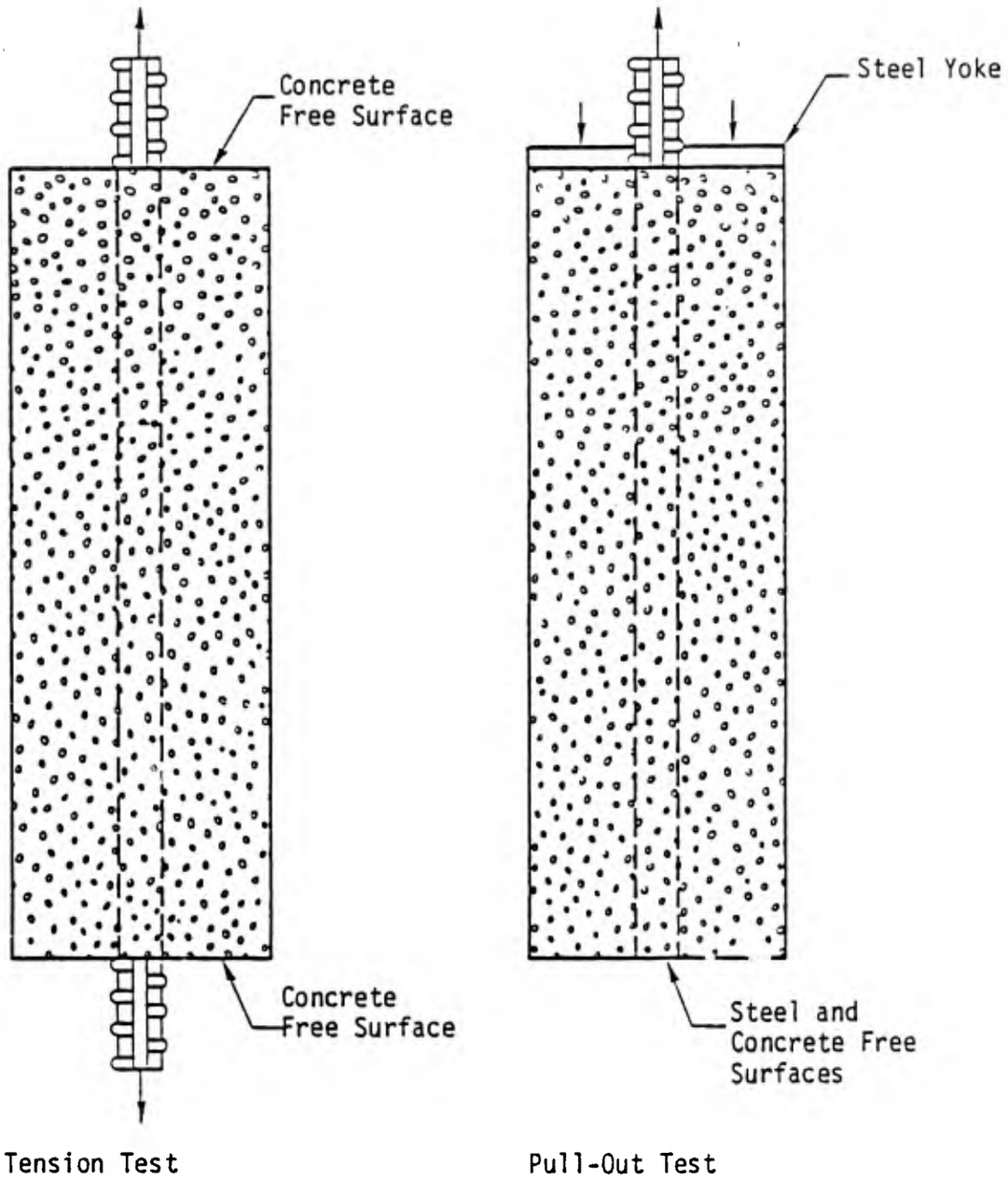


Figure 3.9. Typical tension and pullout test specimens.

extension, demonstrate that the mixture formulation is capable of good simulations for a wide range of steel layouts in all major response stages, Figure 3.20. The latter consists of: elastic response with no cracking, debonding, or slip (State I), progressive cracking with debonding and slip (Stage II), and slip only (Stage III). In addition to global stress-strain response, reasonable agreement has been observed between predicted and observed crack patterns. An example is furnished by Figure 3.21.

The fourth case to be examined involves cyclic loading (tension-compression) of full-scale reinforced concrete masonry specimens[25] with sparse unidirectional steel layouts, Figure 3.22. In contarast to the previous example, the tests in this series were carefully conducted under displacement control. Figures 3.23 and 3.24 indicate typical experimental versus theoretical comparisons. The experimental points in Figure 3.23 represent the (average or global) stress-strain envelope. Figure 3.24 depicts specimen stiffness degradation as measured by average unload-reload slopes. The agrement of test results and theoretical predictions is observed to be excellent. It is noted that both bond slip and progressive cracking of the concrete were active in these tests and simulations.

In addition to the above global stress-strain envelop, detailed comparisons have been made between theory and experiment for each unload-reload cycle. A sample of these comparisons is provided by Figures 3.25 and 3.26. It is evident that the mixture model is capable of simulating complex details concerning the hysteretic response of reinforced concrete within the context of the "steel-concrete bond problem."

### 3.4.2 The Dowel Problem

Dowel action occurs in many problems involving the progressive cracking of reinforced concrete. The term refers to the global contribution of steel rebar penetrating a shear plane to the overall

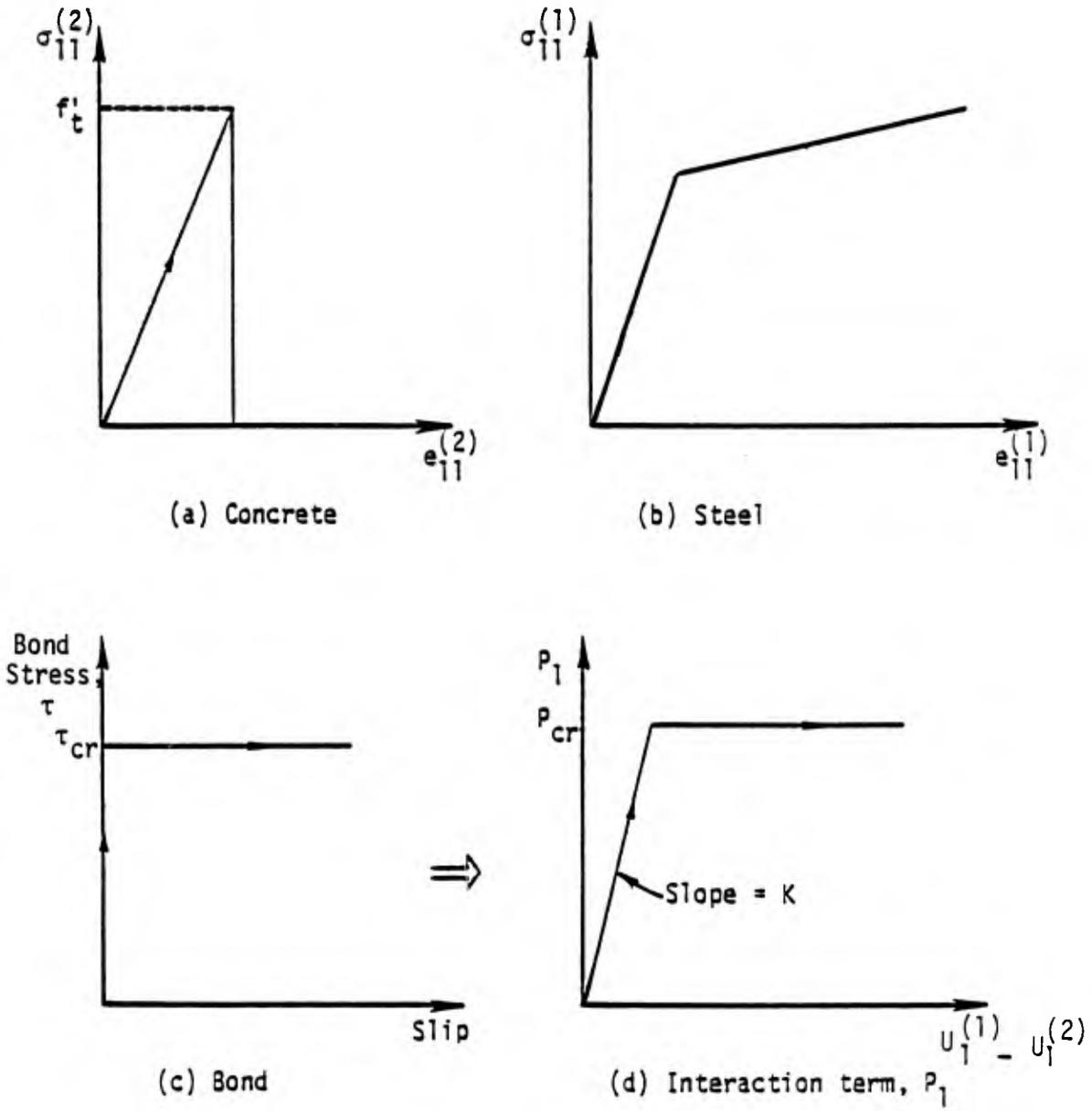


Figure 3.10 Behavior of constituents and steel-concrete interface for monotonic extension example.

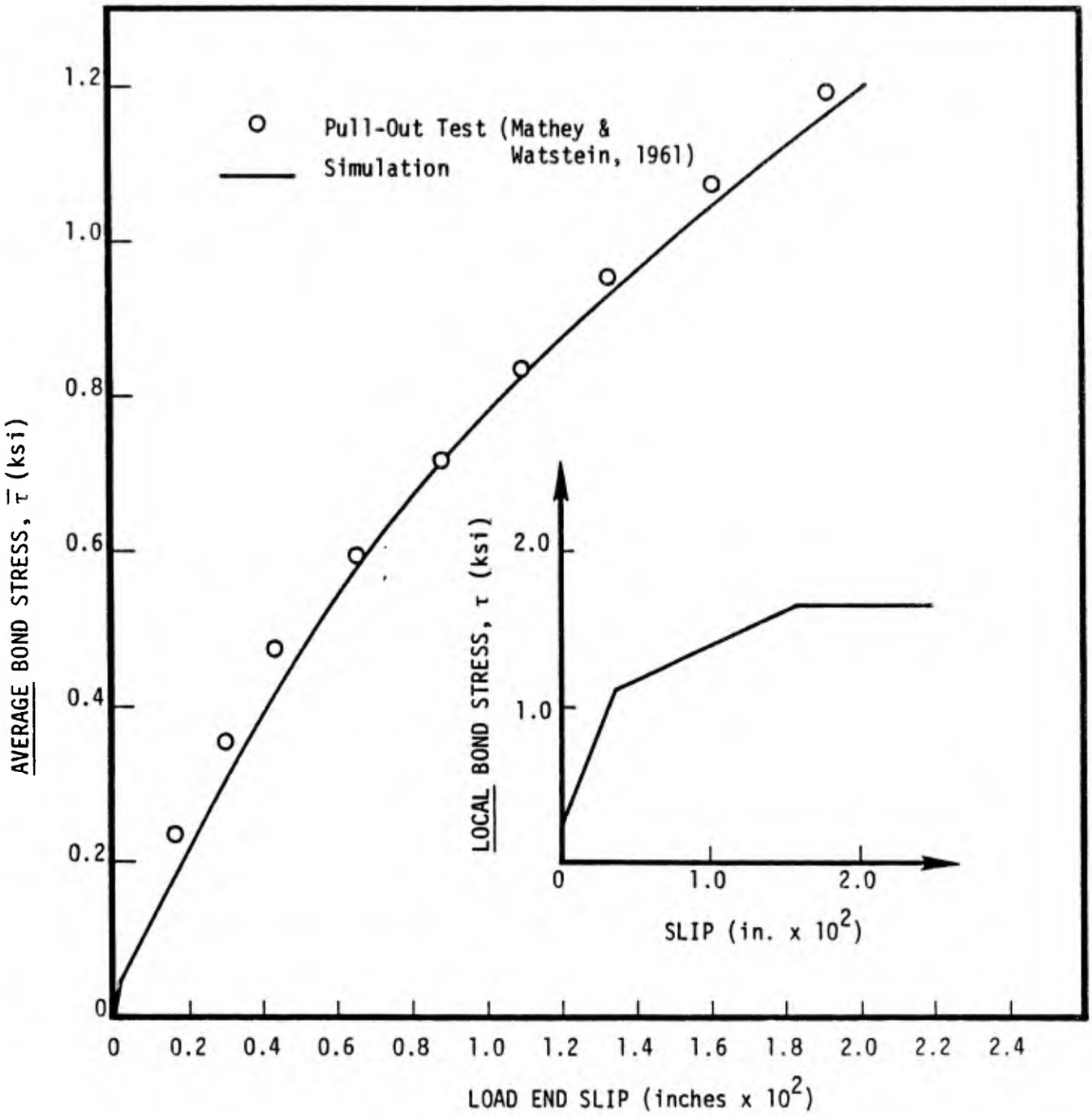


Figure 3.11 Simulation of pull-out test (average bond stress, $\bar{\tau}$, is the pull-out force divided by the steel surface area).

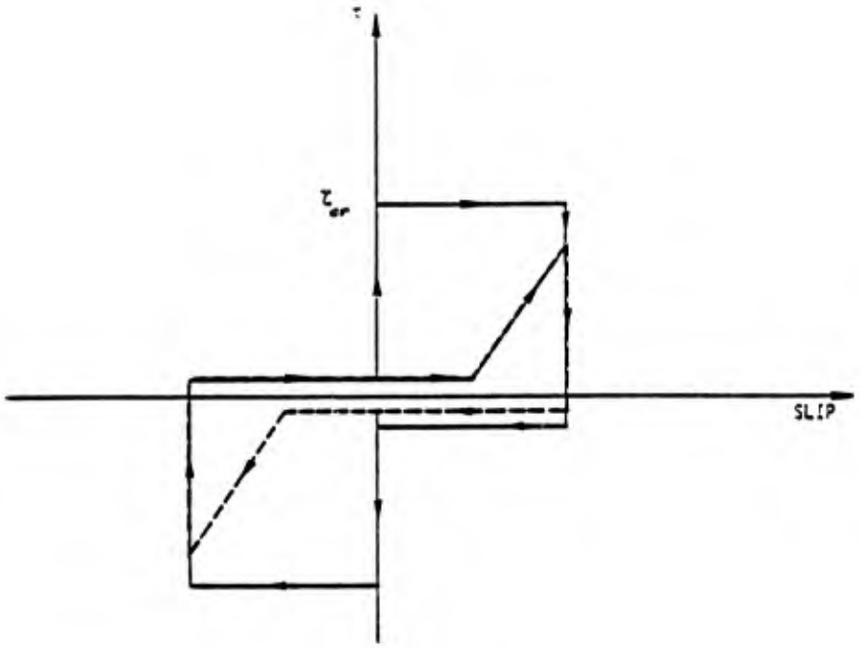


Figure 3.12a Proposed local bond-slip relation for reversed load cycles with fixed slip limits. The first cycle is represented by solid lines, all subsequent cycles by dashed lines.

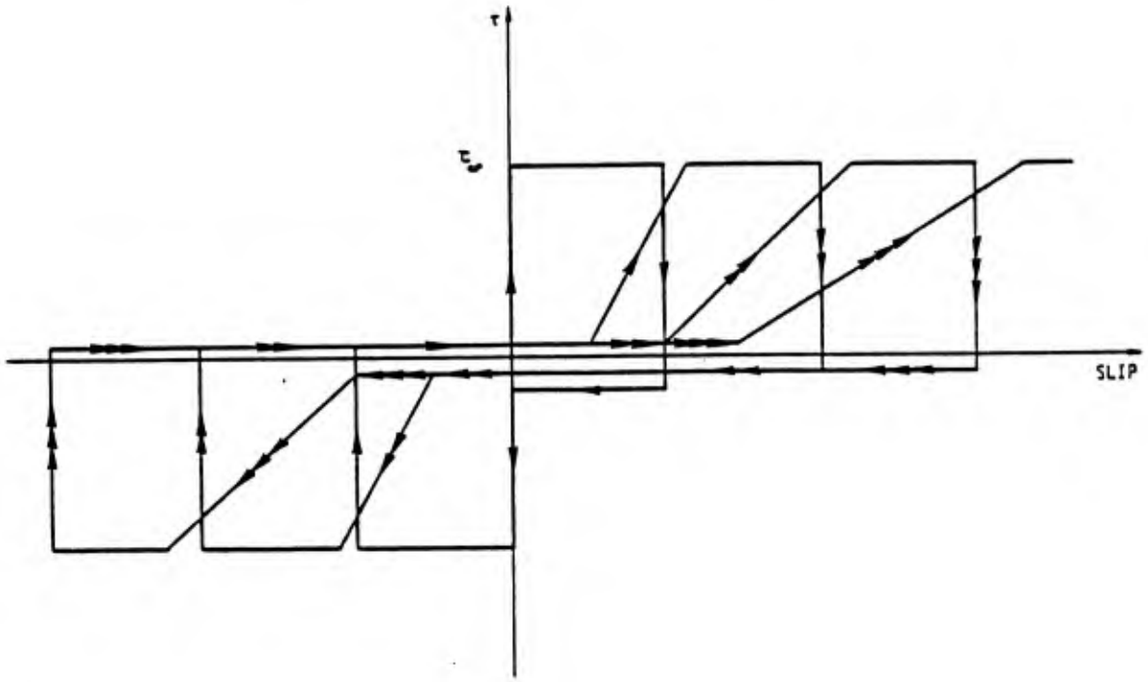


Figure 3.12b Proposed local bond-slip relation for reversed load cycles with increasing slip limits.

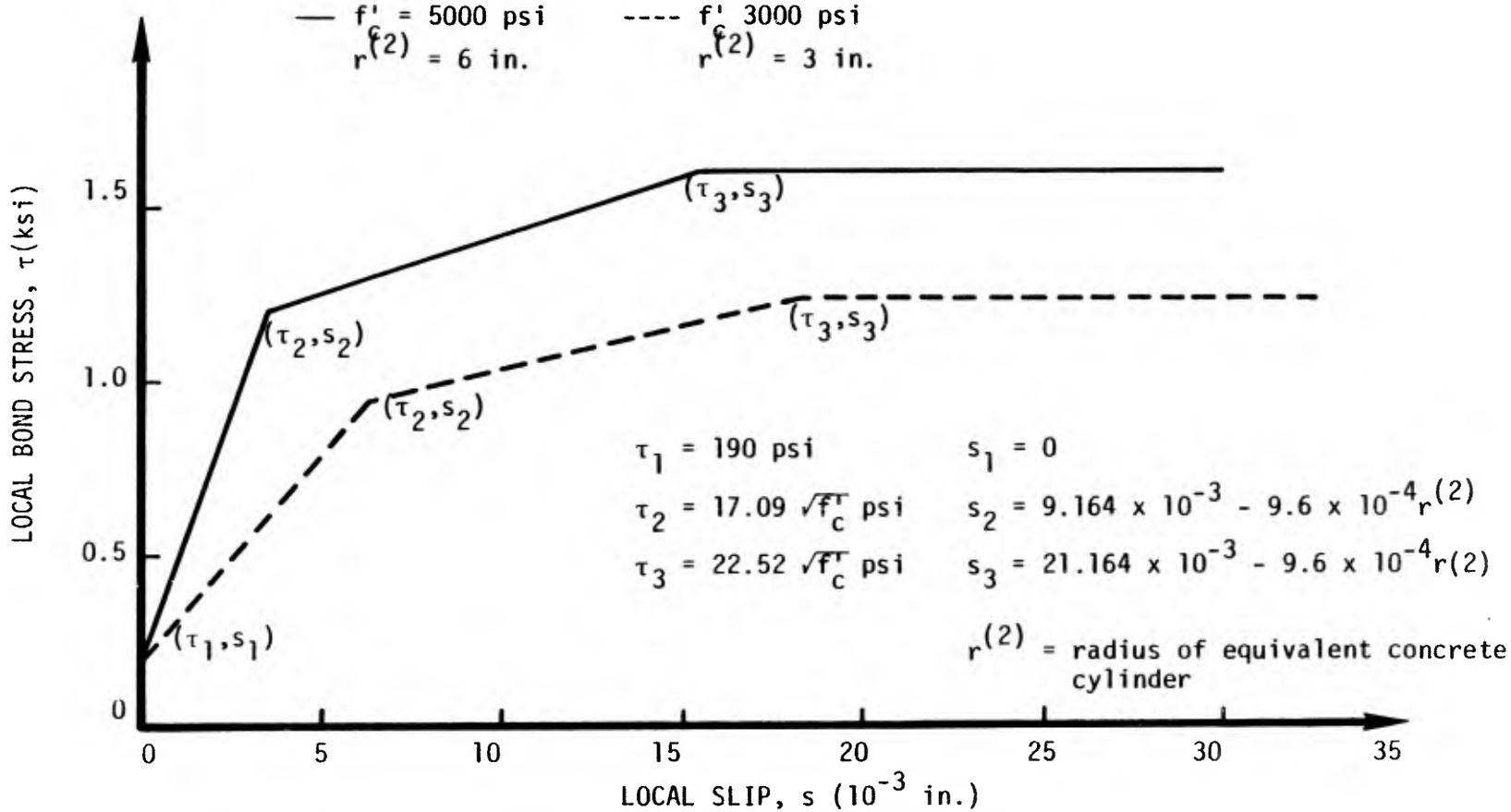


Figure 3.13. Local bond slip relation for specimens axially reinforced with deformed bars as a function of concrete strength and cover.

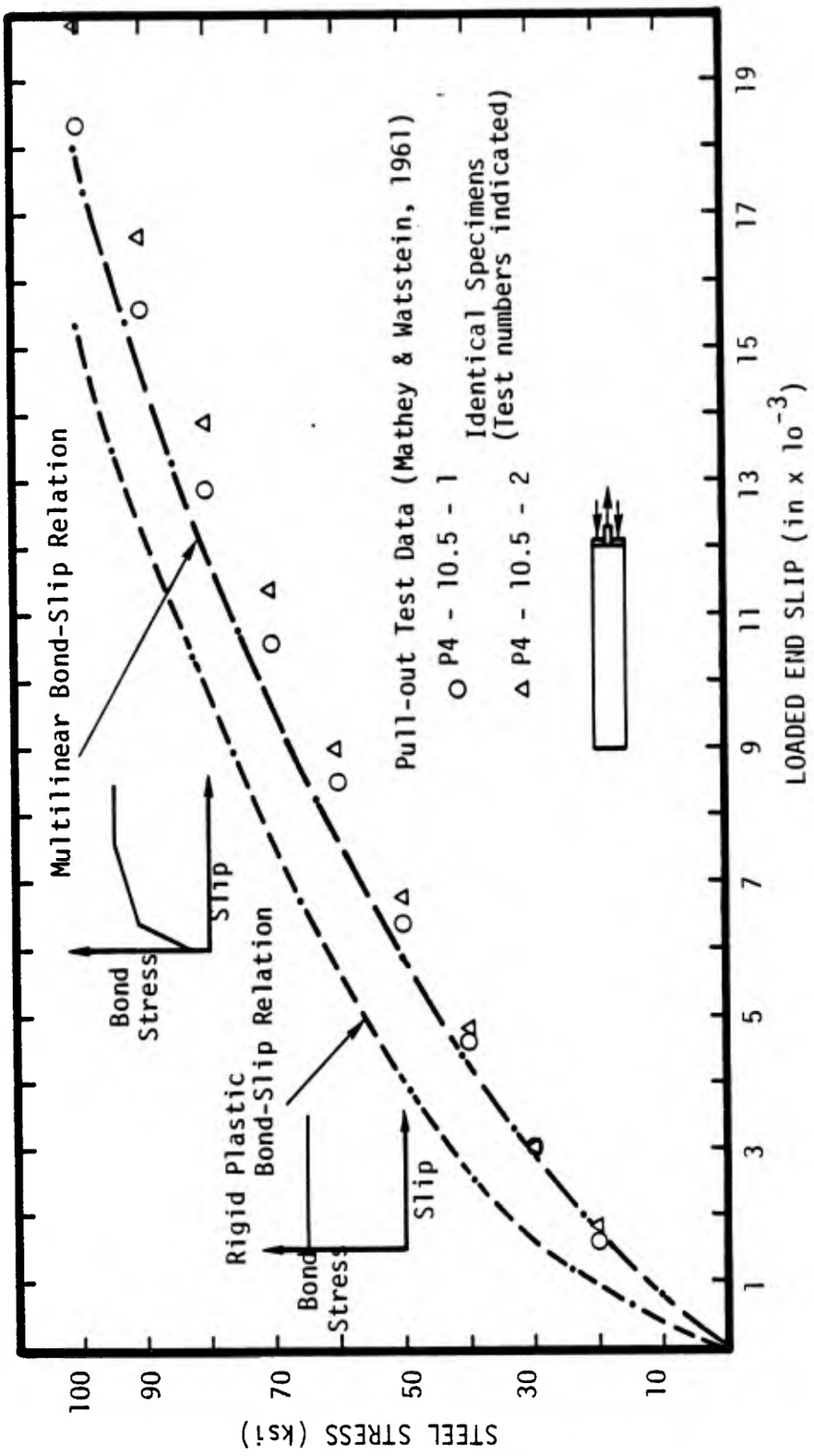


Figure 3.14 Simulation versus experiment for pullout tests.

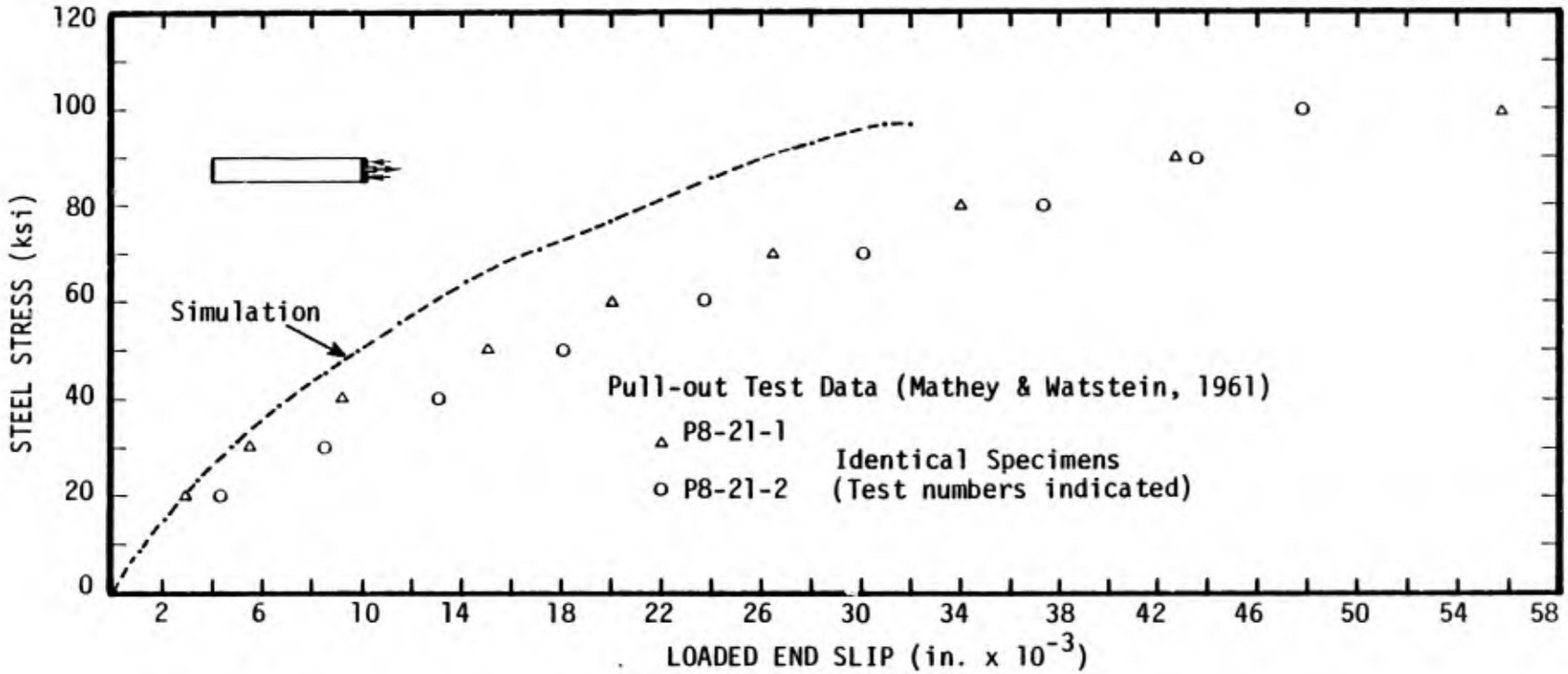


Figure 3.15. Simulation versus experiment for pull-out tests.

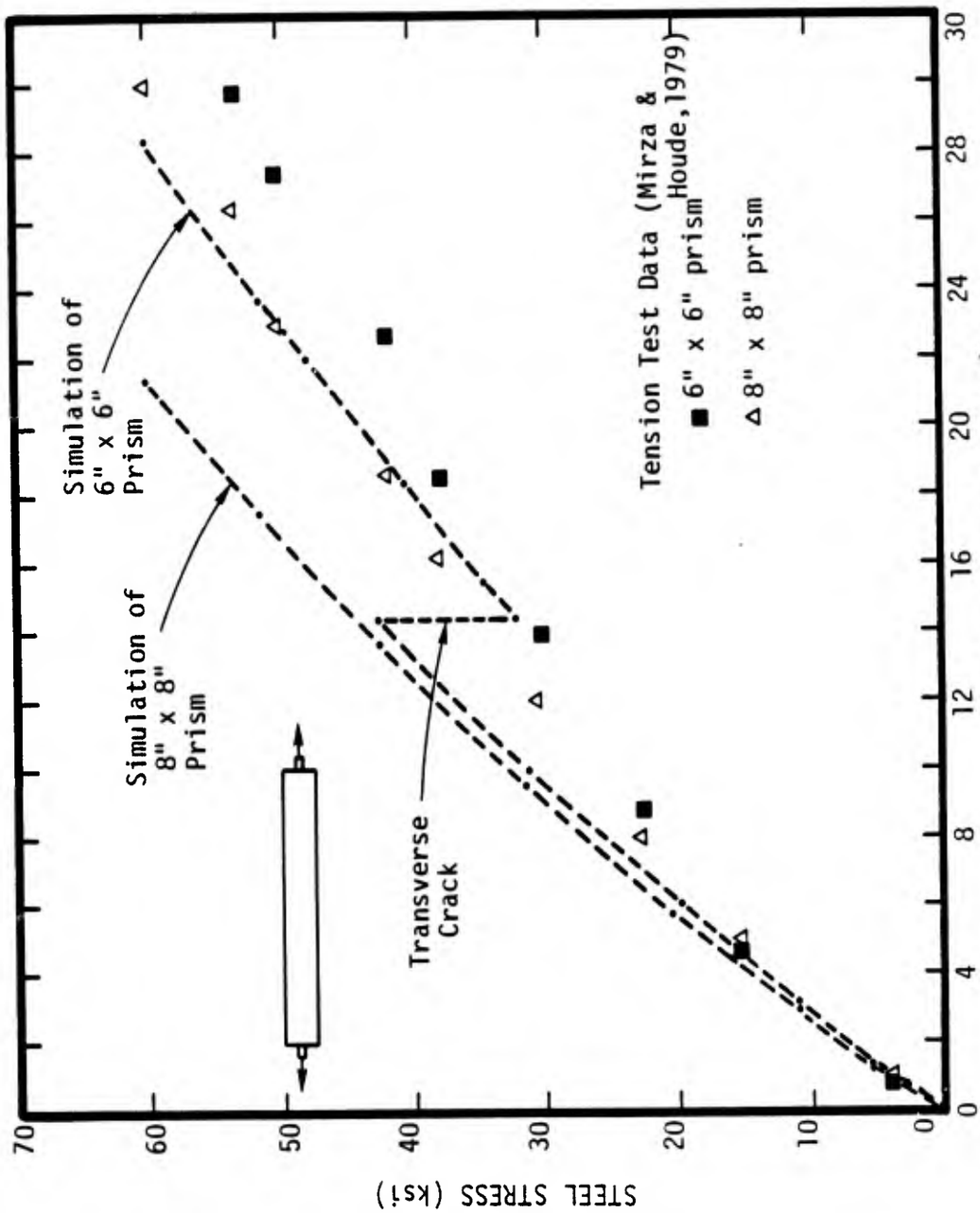


Figure 3.16. Simulation versus experiment for tension tests.

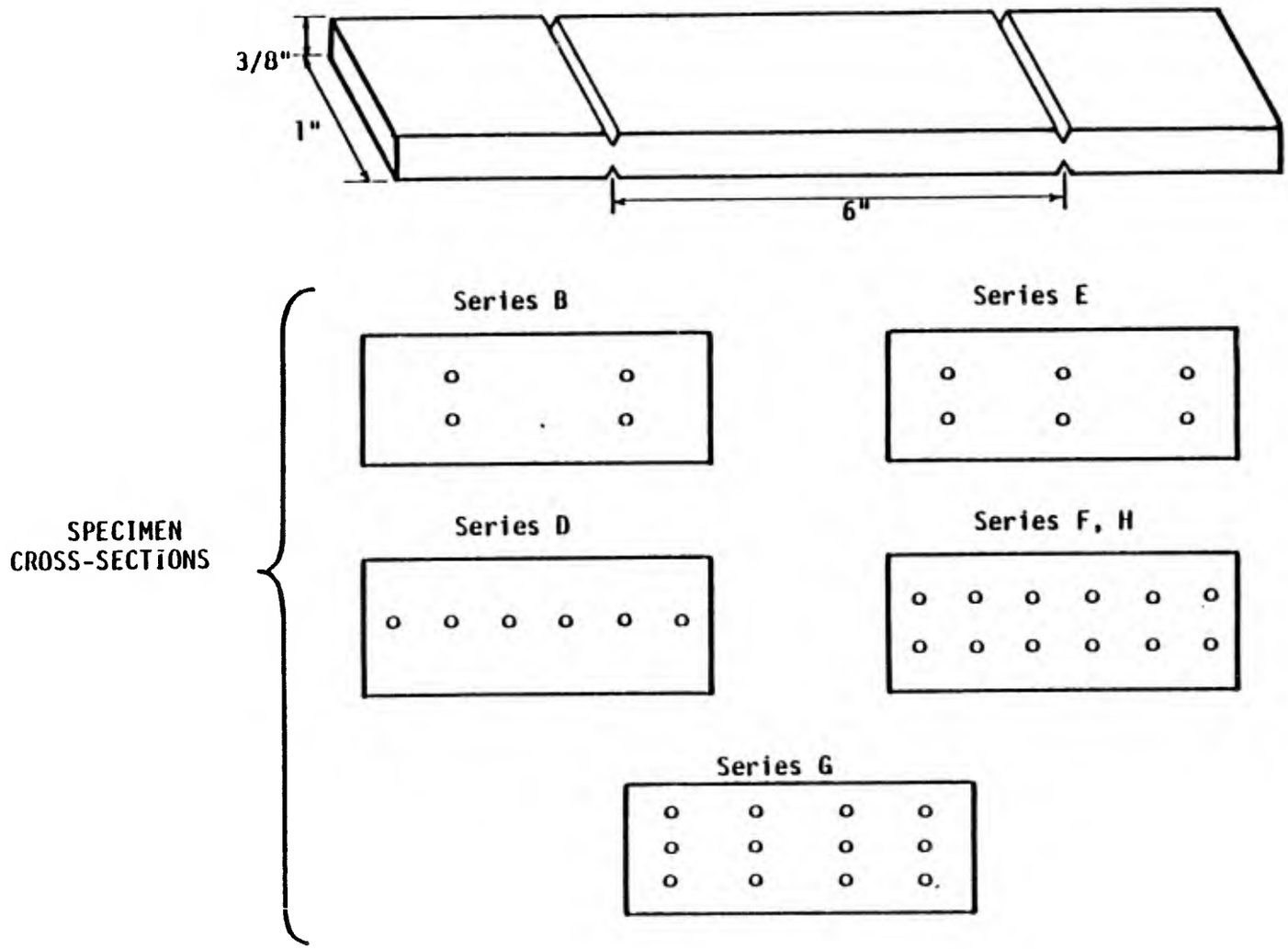


Figure 3.17. Specimen geometry.

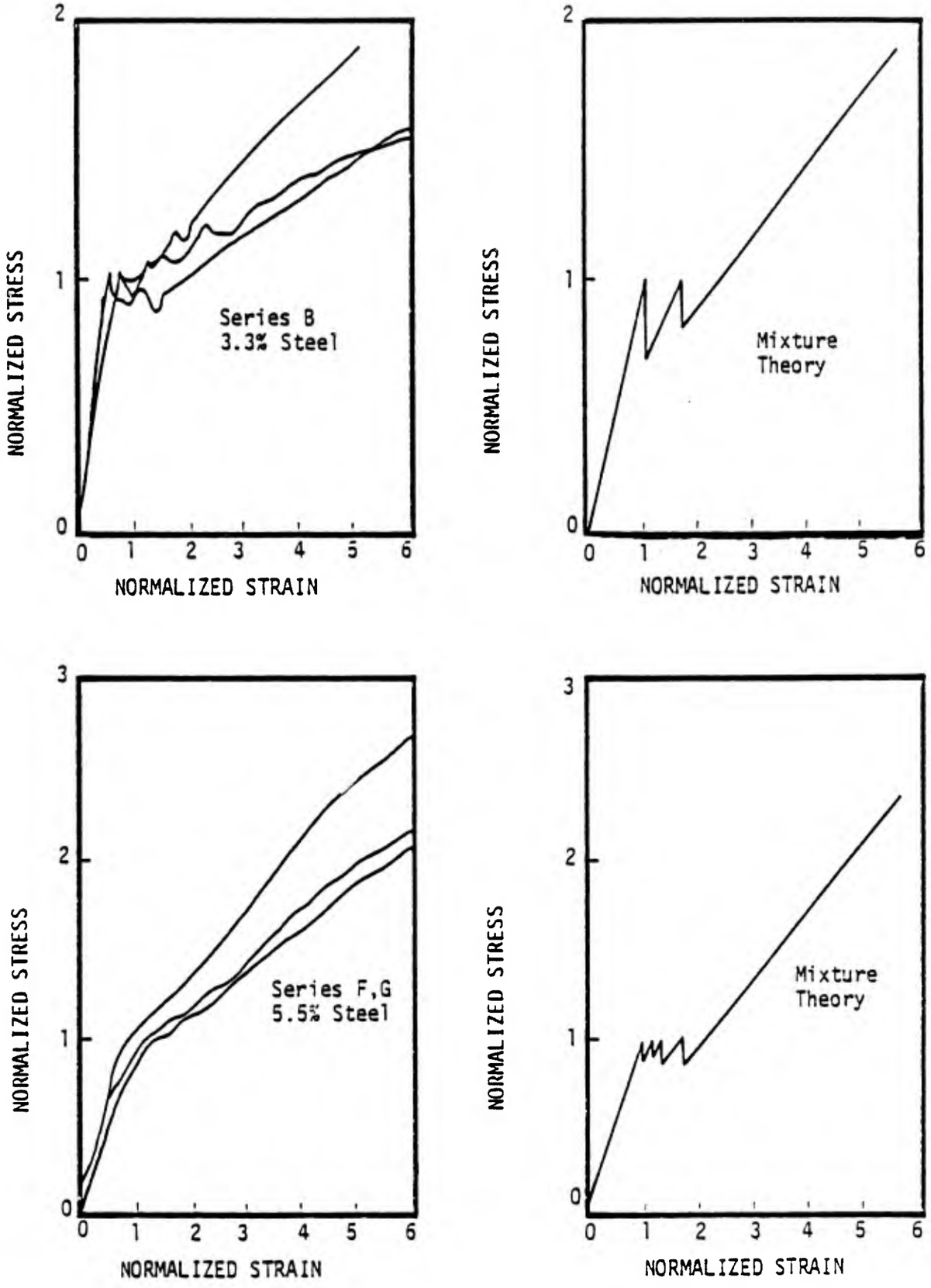


Figure 3.18. Comparisons of experiment and theory.

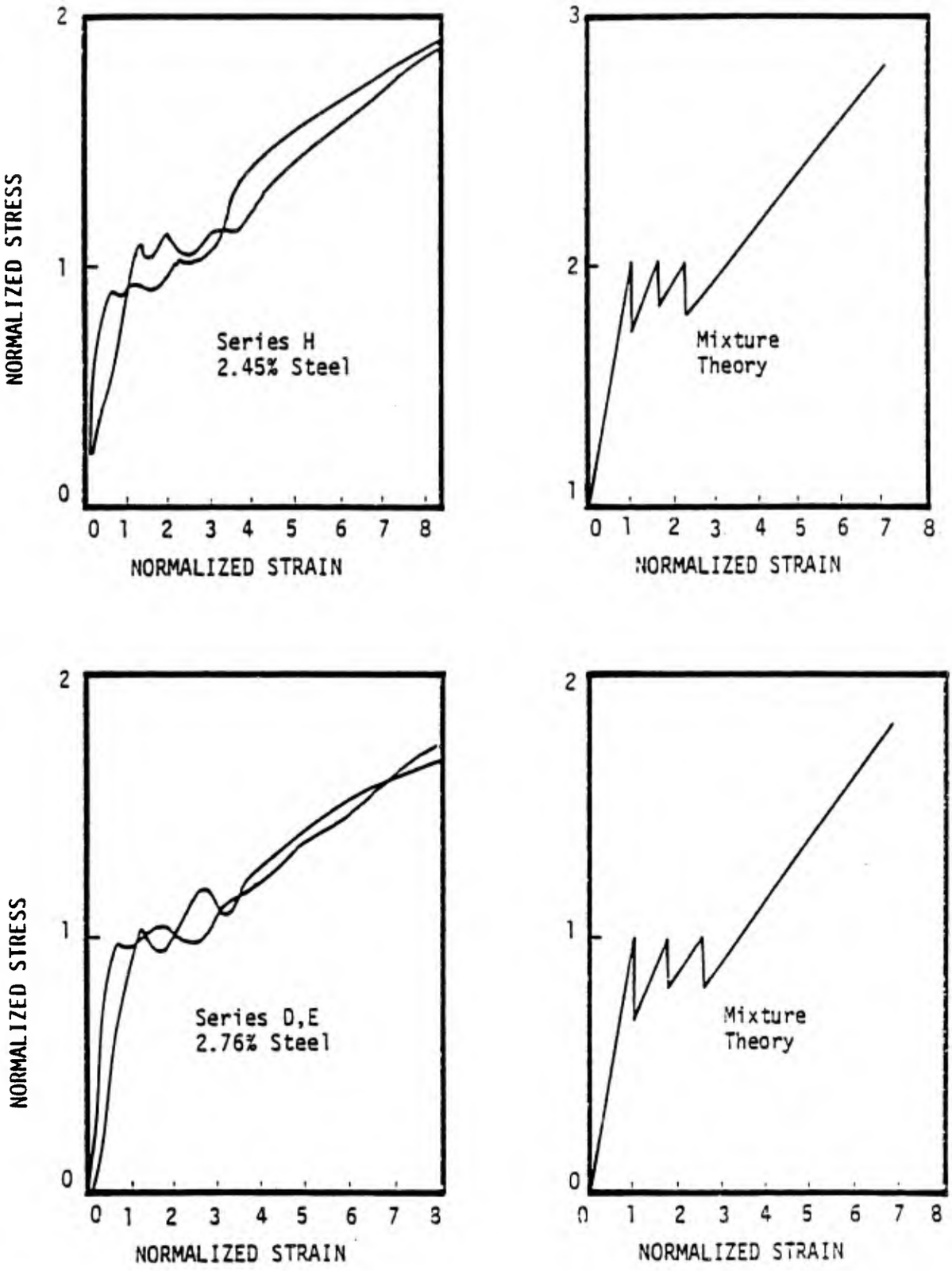


Figure 3.19. Comparisons of experiment and theory.

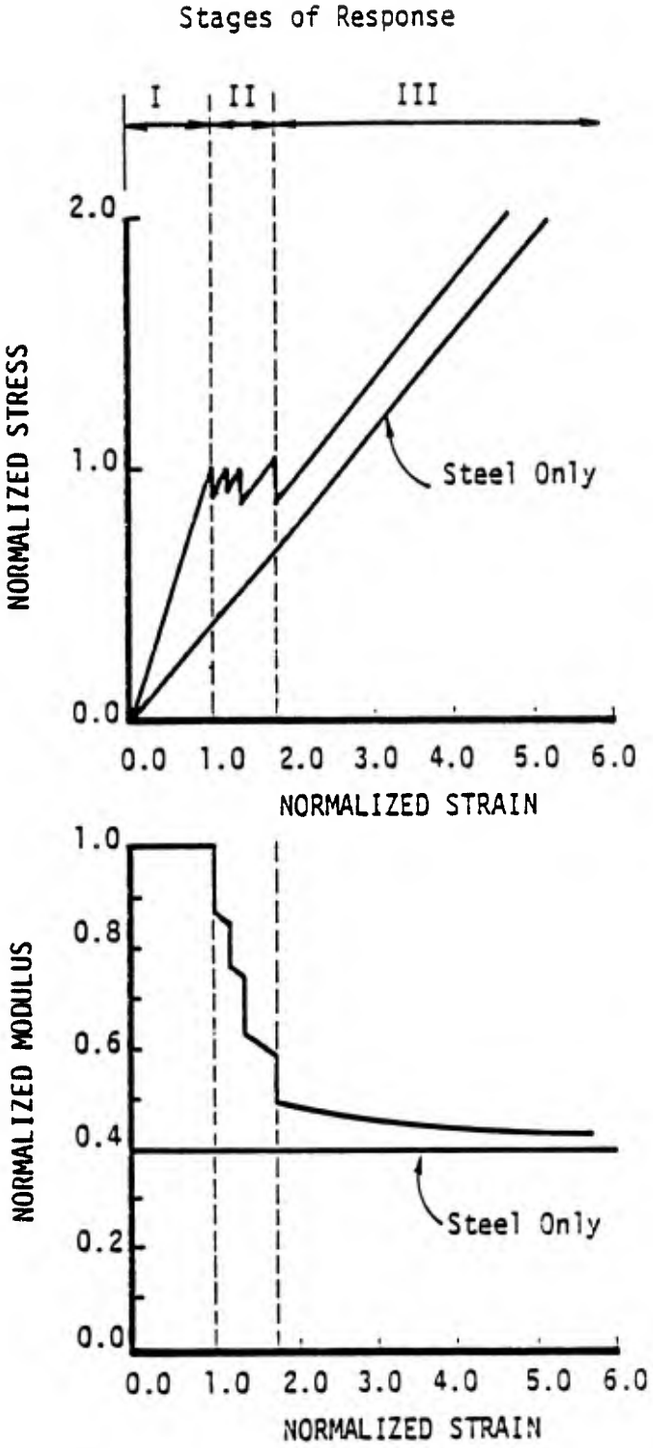


Figure 3.20. Stages of response predicted theoretically.

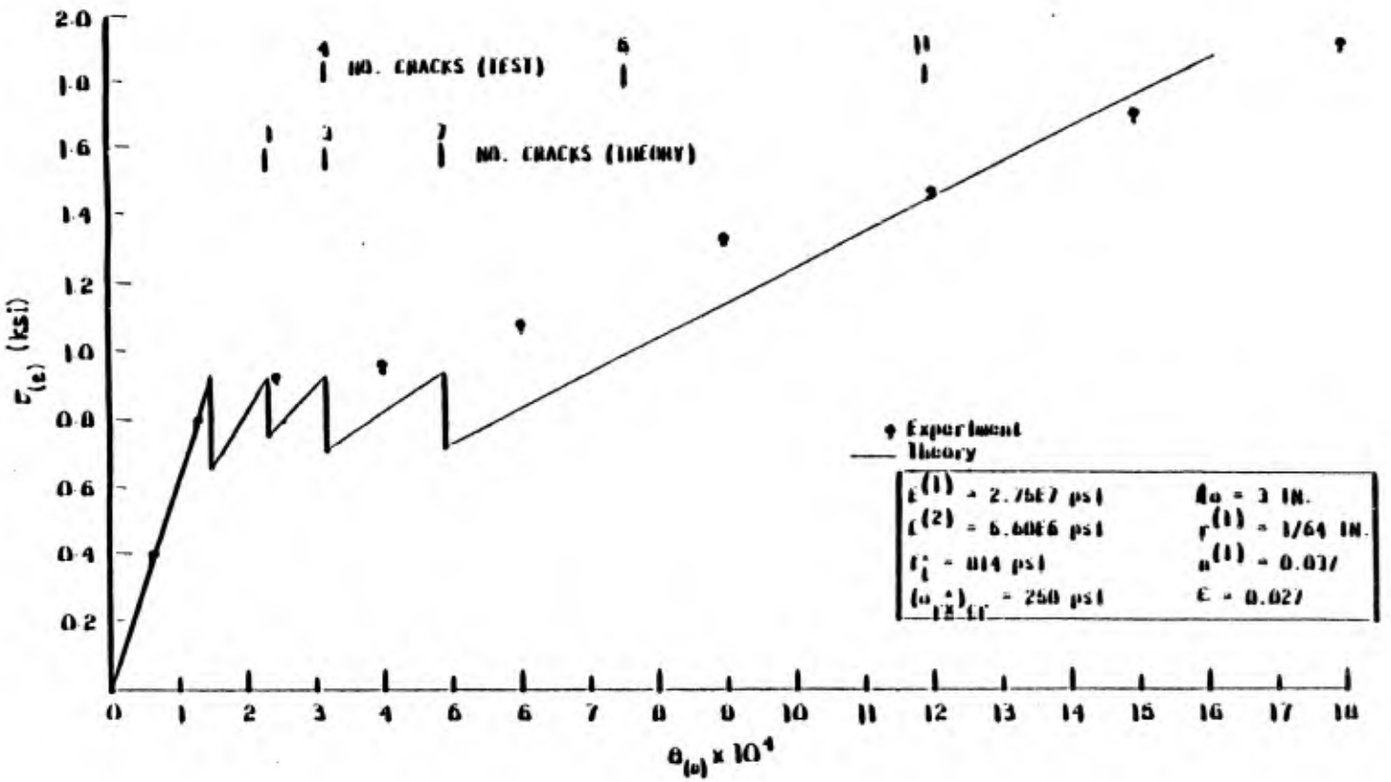


Figure 3.21. Theory versus experiment for monotonic extension.

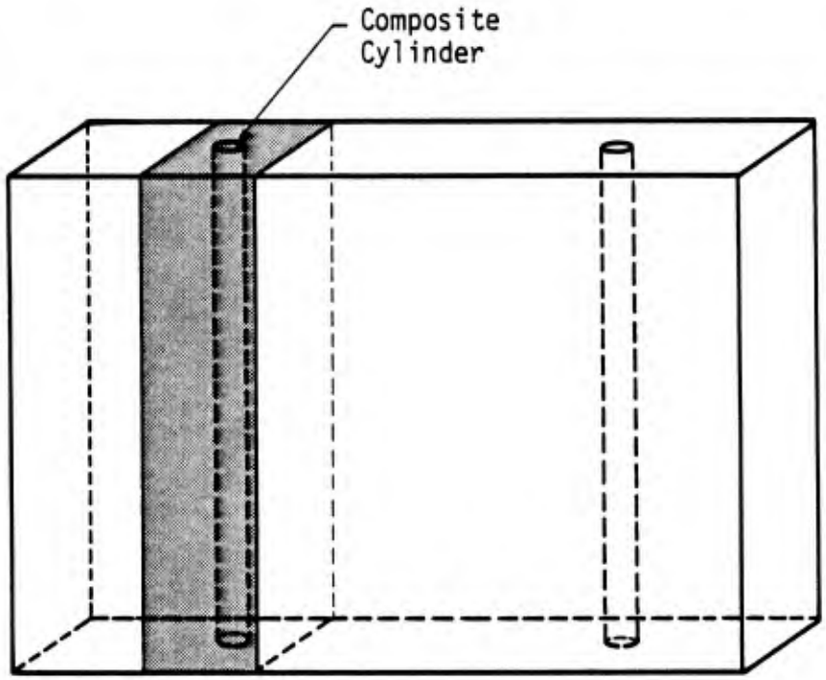


Figure 3.22. Sparsely reinforced concrete.

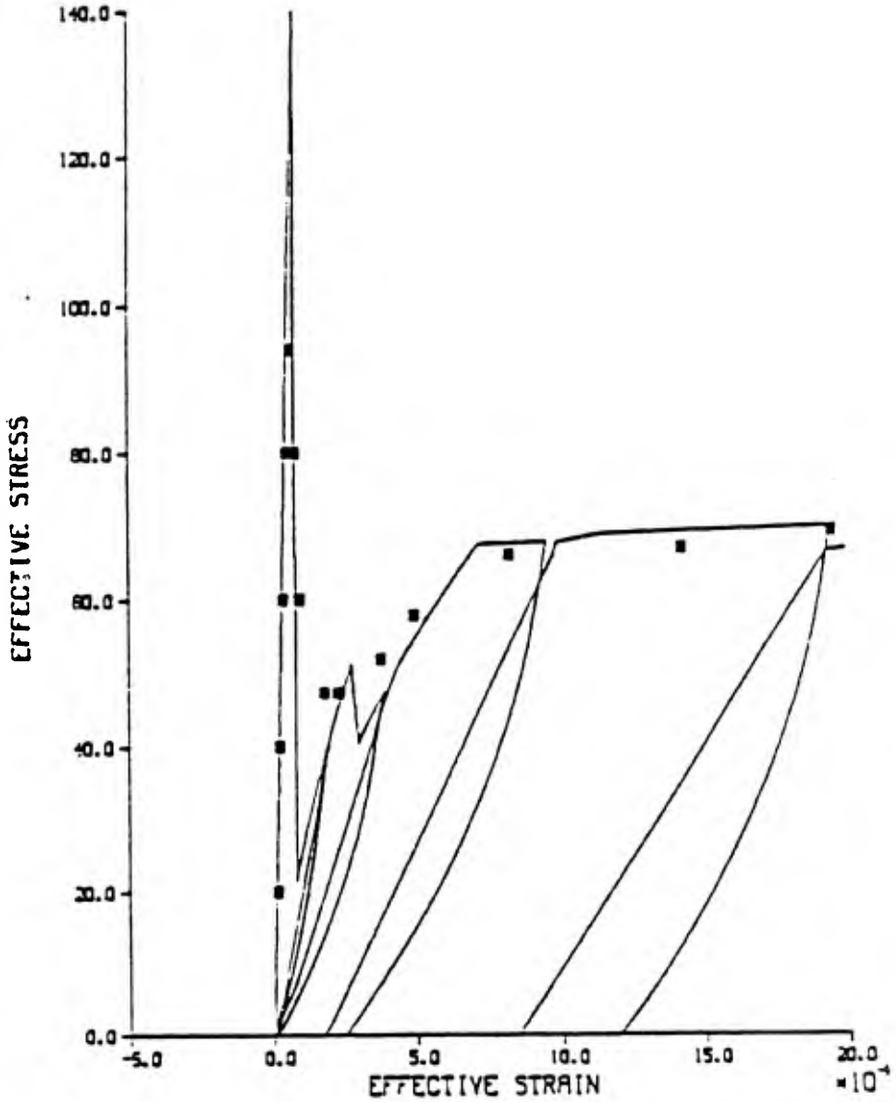


Figure 3.23. Comparison of experiment (squares) and theory (curves) effective stress versus effective strain envelope.

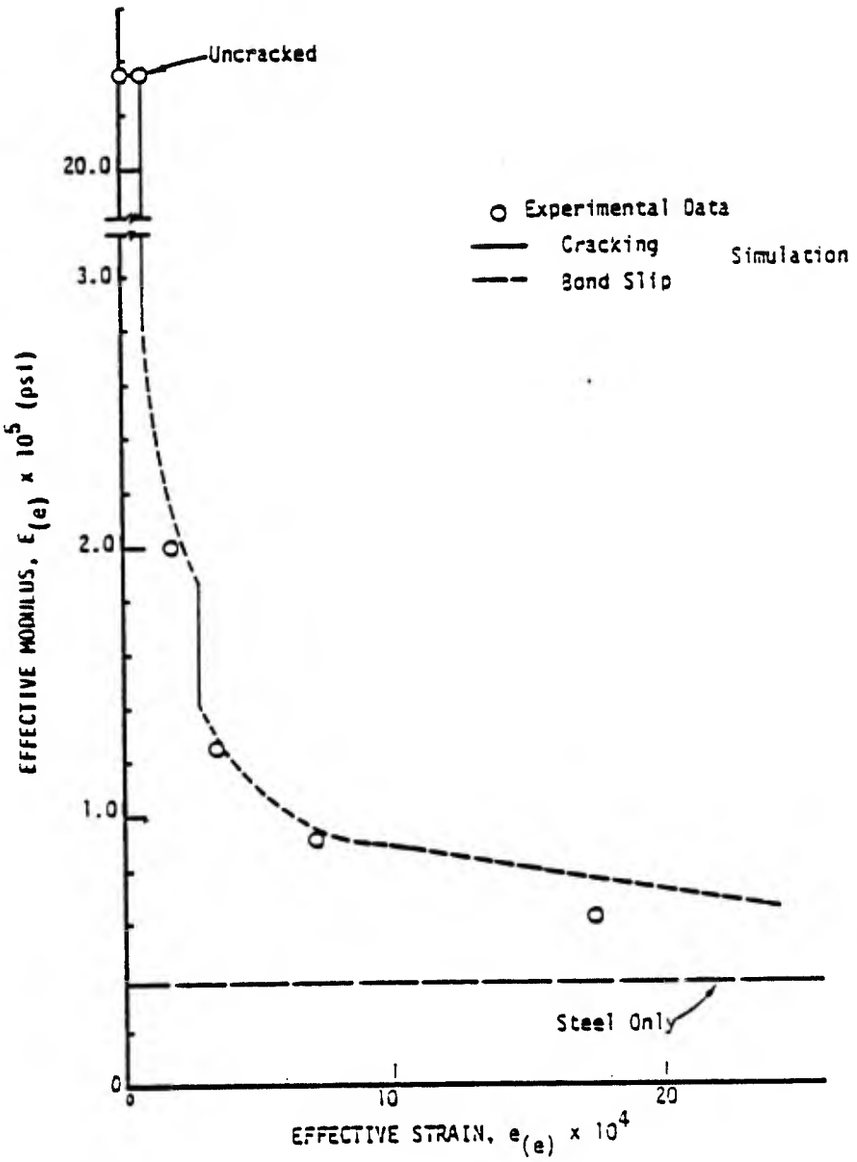


Figure 3.24. Comparison of experimental and theoretical stiffness degradation due to cracking and debonding.

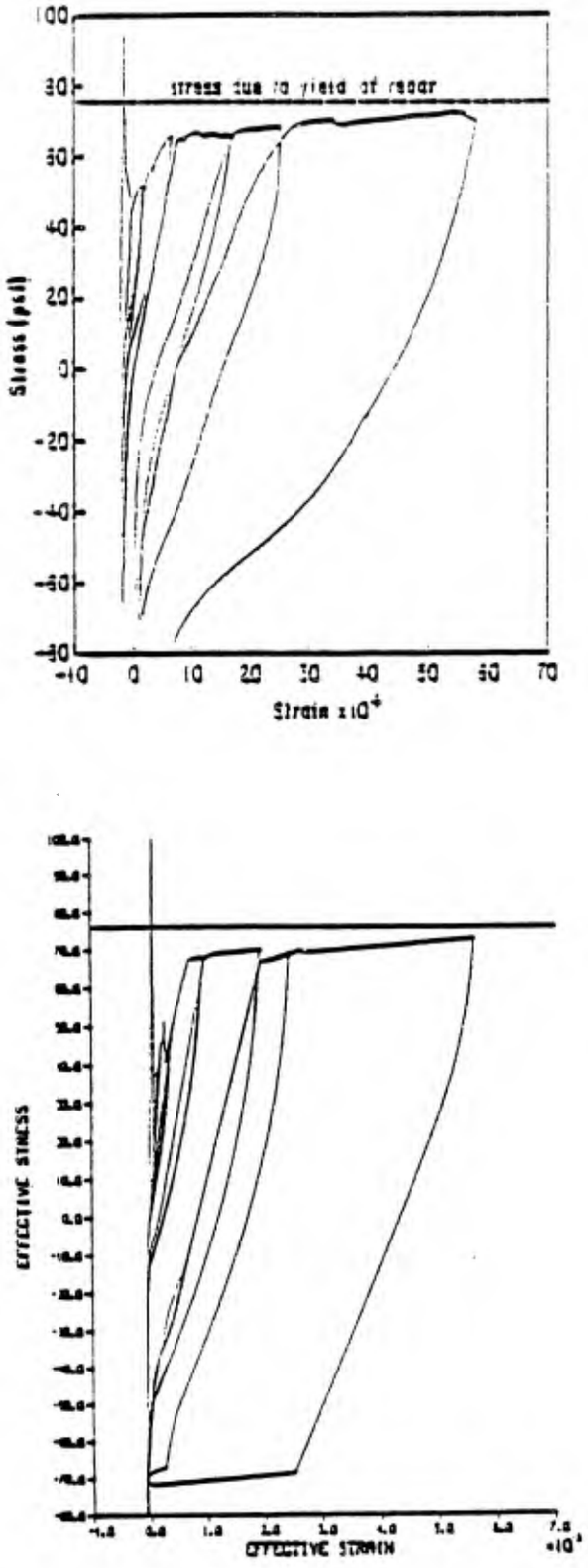


Figure 3.25. Effective stress versus effective strain for cyclic deformation of reinforced concrete (masonry) (a) test data, (b) numerical simulation.

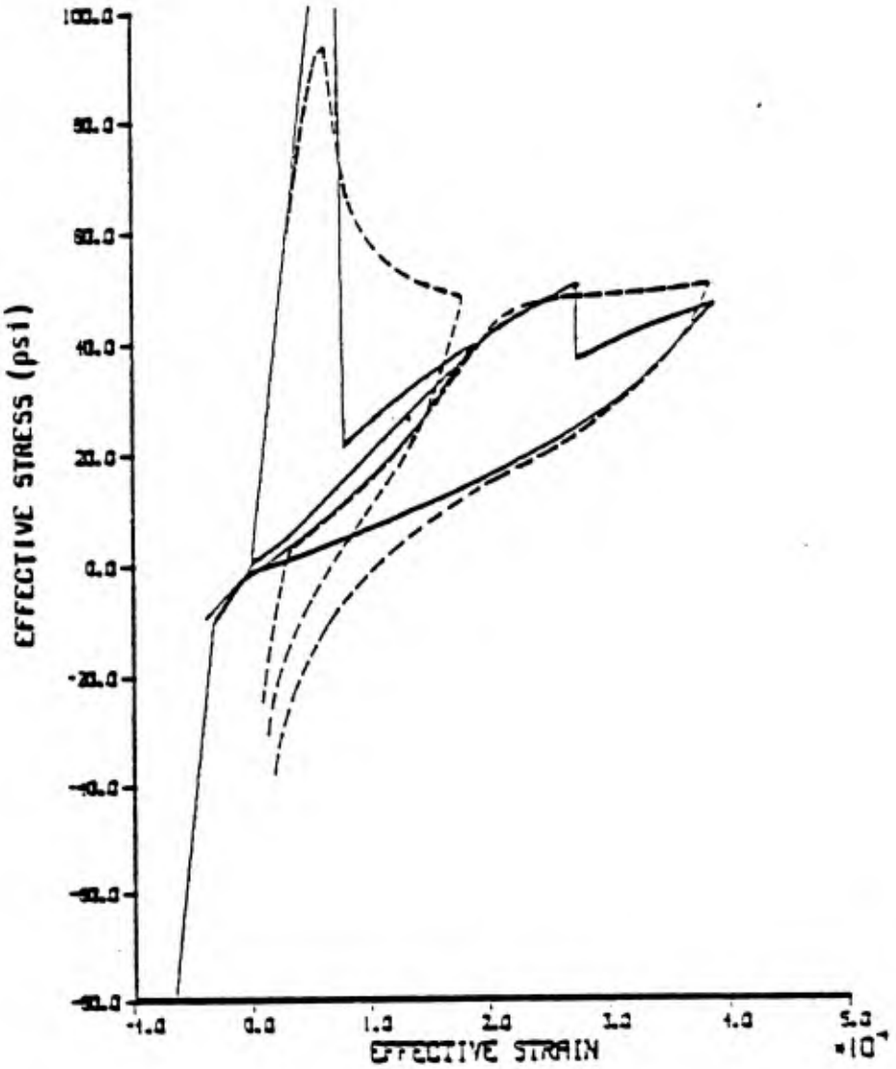


Figure 3.26 Comparison of experiment (dashed lines) and theory (solid lines) effective stress versus effective strain curves for the first two deformation cycles.

shear transfer across this plane. The shear plane itself is a crack in the concrete. In addition to dowel action (DA) the shear transfer is influenced by interface shear transfer (IST) and adhesion. IST refers to friction and aggregate interlock. DA and IST are interconnected in that DA can influence IST significantly by changing the effective normal stress on the shear plane and hence the frictional effects. Consequently, it is important to check this element of the mixture model in order to properly validate its simulation capability.

In what follows, two problems are explored. The first is a linearized dowel problem, which is convenient from an analytical viewpoint since a closed-form solution is available. The second is a nonlinear version of the first. The latter more closely simulates the actual physical problem.

## The Linearized Problem

For illustrative purposes the dowel problem depicted in Figure 3.27 will be considered. In this example, the planar transverse deformation of a reinforced element with a sparse layout and a pre-existing crack is to be examined. Consequently, within the context of the weighting functions (3-108) and the constraint (3-109), one has

$$U_1^{(\alpha)} = U_3^{(\alpha)} = S_1^3 = S_3^2 = S_3^3 \equiv 0 \quad . \tag{3-150}$$

This, in turn, implies

$$\delta U_1^{(\alpha)} = \delta U_3^{(\alpha)} = \delta S_1^3 = \delta S_2^3 = \delta S_3^2 \equiv 0 \quad . \tag{3-151}$$

In addition, the example dowel problem shall be selected such that $U_2^{(2)}$ and $S_1^2$ are specified (the boundary displacement of the concrete elements are to be specified such that each piece suffers opposite uniform transverse displacement as shown in Figure 3.27). Thus,

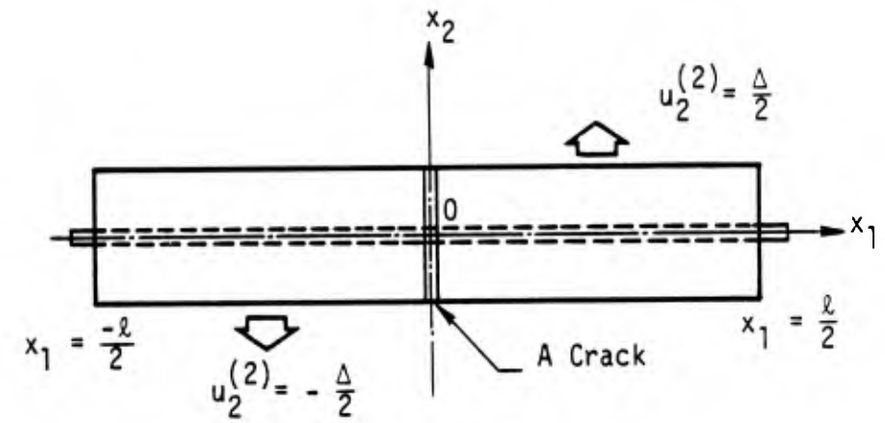


(a) Before Deformation

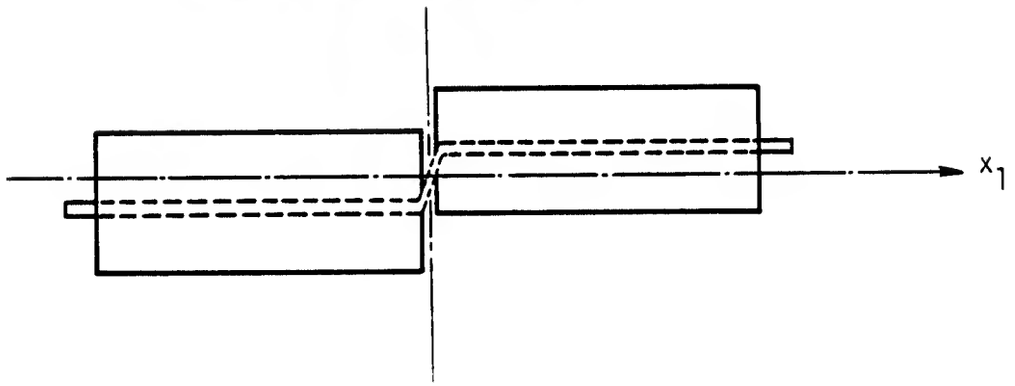


(b) After Deformation

Figure 3.27. A dowel action test simulation

$$\delta U_2^{(2)} = \delta S_1^2 = 0 \quad . \tag{3-152}$$

Upon combining equations (3-150), (3-152), (3-198a) and (3-110), one finds that, in the absence of body forces, the only mixture equilibrium equation that must be satisfied is

$$N_{12,1}^{(1)} + P_2 = 0 \quad . \tag{3-153}$$

Now, for illustrative purposes the example dowel problem will be restricted to elastic response. The appropriate mixture constitutive and interaction relations for this response are

$$N_{12}^{(1)} = \mu^{(1)} n^{(1)} U_{2,1}^{(1)} \quad , \tag{3-154}$$

$$P_2 = \beta_2 (U_2^{(2)} - U_2^{(1)}) \quad , \tag{3-155}$$

where $\beta_2$ = constant (determined from a separate elastic analysis).

The dowel problem boundary conditions on the lateral surfaces are selected as

$$U_2^{(2)} = \pm \Delta/2 \text{ for } x_1 \gtrless 0 \quad . \tag{3-156}$$

The boundary conditions at the cell termini are prescribed, from Equations (3-117), as

$$N_{12}^{(1)} = 0 \text{ at } x_1 = \pm \ell/2 \quad . \tag{3-157}$$

Further, symmetry of the problem requires

$$U_2^{(1)} = 0 \text{ at } x_1 = 0 \quad . \tag{3-158}$$

The symmetry condition allows one to examine only $0 < x_1 < \ell/2$.

Substitution of Equations (3-154), (3-155) into Equation (3-153) furnishes

$$\mu^{(1)}n^{(1)}U_{2,11}^{(1)} - \beta_2 U_2^{(1)} = -\beta_2 \Delta/2 \quad . \tag{3-159}$$

Solution of Equation (3-159) with the boundary conditions (3-157) and (3-158) yields

$$\frac{U_2}{\Delta} = \frac{1}{2}\left[1 - \cosh\left(\frac{\beta_2}{\mu^{(1)}n^{(1)}}\right)^{1/2} x_1 + \tanh\left(\frac{\beta_{2\ell}^2}{4\mu^{(1)}n^{(1)}}\right)^{1/2} \sinh\left(\frac{\beta_2}{\mu^{(1)}n^{(1)}}\right)^{1/2} x_1\right]. \tag{1-160}$$

This, from Equation (3-154), provides the following stress field:

$$N_{12}^{(1)} = \Delta\left(\frac{\beta_2 n^{(1)}\mu^{(1)}}{2}\right)^{1/2}\left[-\sinh\left(\frac{\beta_2}{n^{(1)}\mu^{(1)}}\right)^{1/2} x_1 + \tanh\left(\frac{\beta_{2\ell}^2}{4n^{(1)}\mu^{(1)}}\right)^{1/2} \cosh\left(\frac{\beta_2}{n^{(1)}\mu^{(1)}}\right)^{1/2} x_1\right] . \tag{3-161}$$

Equations (3-160) and (3-161) are the steel transverse displacement ($U_2^{(1)}$) and shear (partial) stress ($N_{12}^{(1)}$) fields. These are graphed in Figures 3.28 and 3.29 respectively.

The significance of Equation (3-161) is evident. Given a displacement $\Delta$, the maximum average shear stress in the steel can be evaluated and a failure analysis can be conducted.

Based upon experimental observations, the forms of (3-160) and (3-161) appear to be qualititatively correct for sufficiently small $\Delta$. It is evident that the dowel problem leads to a "boundary layer" phenomena wherein the steel deformation is confined to a narrow region adjacent to the crack.

## The Nonlinear Problem

As the dowel offset $\Delta$ increases, a point is reached when the above linear formulation is no longer valid. For larger offsets, a nonlinear theory is needed. Such a theory must account for finite

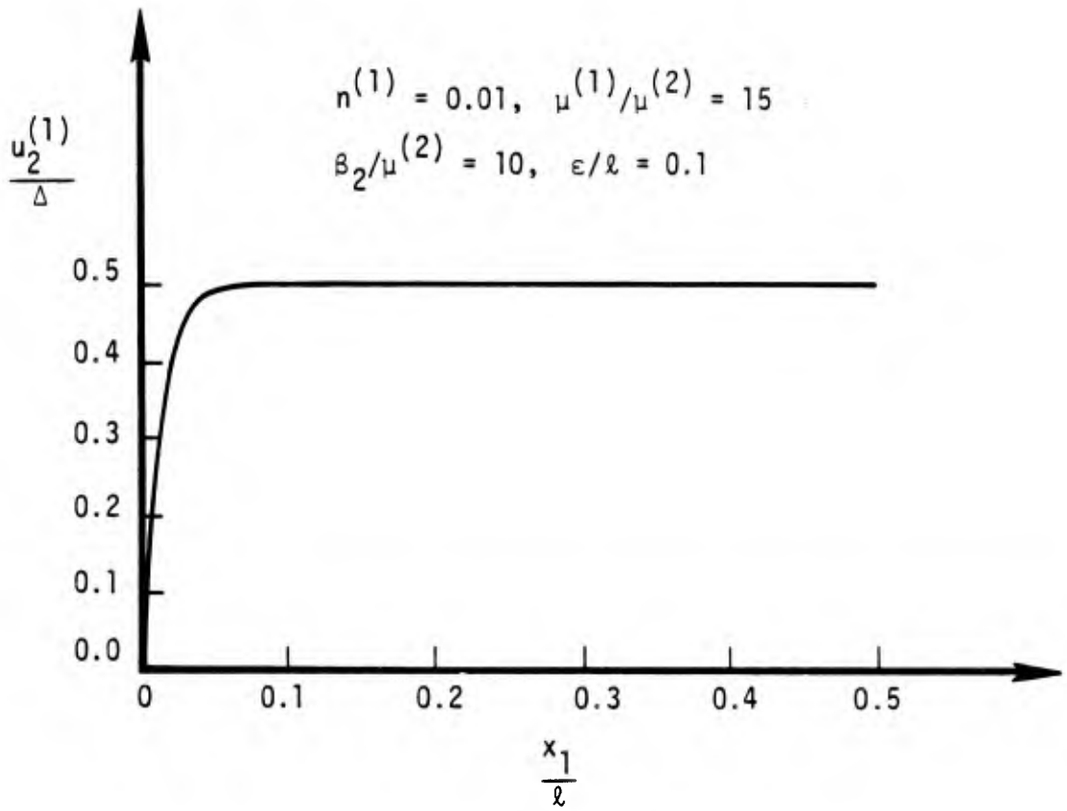


Figure 3.28. Displacement profile of steel.

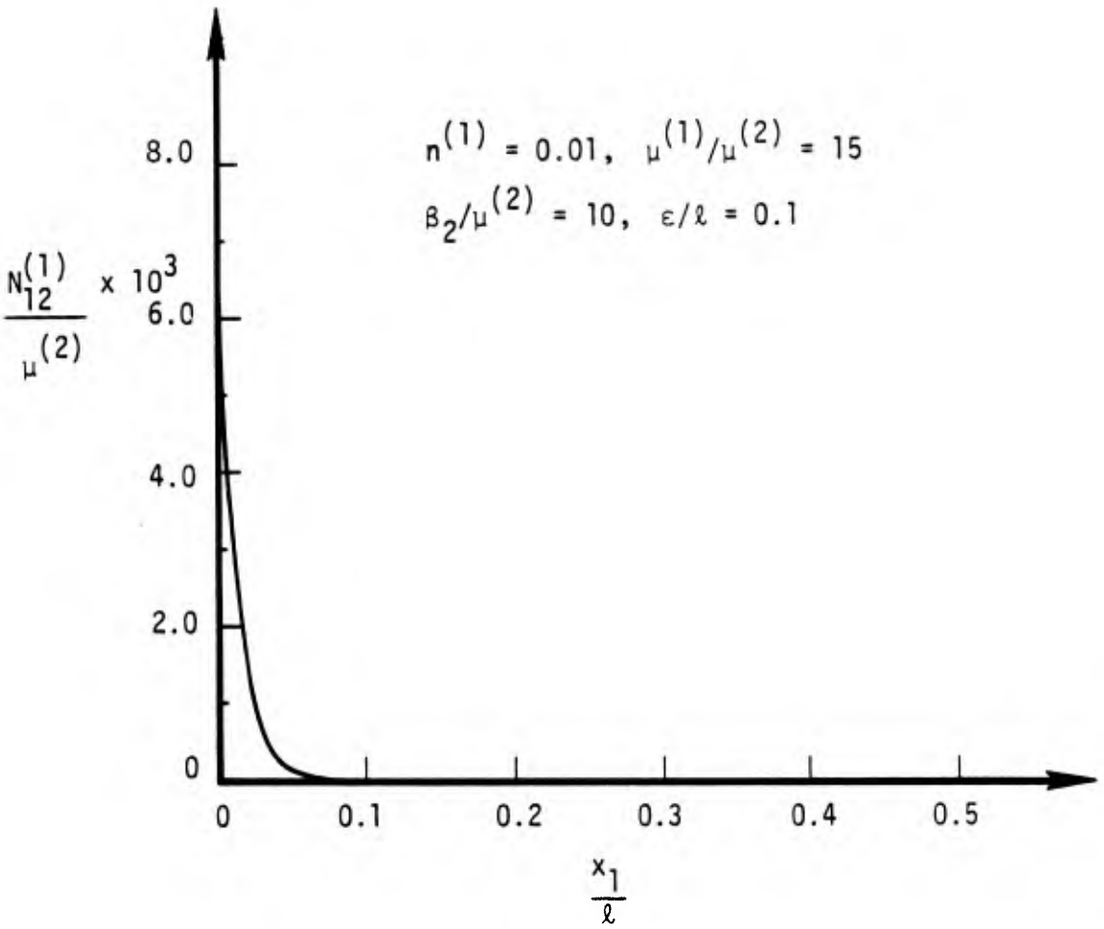


Figure 3.29 Shear stress in steel.

rotations of the steel, crushing of the concrete, and bond degeneration and slip. In what follows, therefore, the foregoing dowel problem is re-examined within the context of a nonlinear mixture theory.

The governing equilibrium equations to be used in the nonlinear analysis are given by (3-143a,b).

In contrast to the linear analysis, separate directors $S_1^{2(\alpha)}$ will be adopted for each material. The latter furnish the capability to adequately model the reinforcing steel bending mode. Consequently, the constraint (3-109) is replaced by

$$S_1^{3(1)} = S_1^{3(2)} \ , \ S_2^{K(1)} = S_2^{K(2)} \ , \ S_3^{K(1)} = S_3^{K(2)} \ . \qquad (3\text{-}162)$$

If the average deformation is confined to the $X_1,X_2$-plane, then

$$U_3^{(\alpha)} \equiv 0 \ , \ S_3^{K(\alpha)} \equiv 0 \ ; \ \delta U_3^{(\alpha)} \equiv 0 \ , \ \delta S_3^{K(\alpha)} \equiv 0 \ . \qquad (3\text{-}163)$$

If, in addition, the lateral boundary displacement of the concrete is prescribed, then

$$\delta U_2^{(2)} \equiv 0 \ , \ \delta S_2^{K(2)} \equiv 0 \ . \qquad (3\text{-}164)$$

Equations (3-164b) and (3-162b) furnish

$$\delta S_2^{K(1)} \equiv 0 \ . \qquad (3\text{-}165)$$

Thus, $\delta U_1^{(2)}$, $\delta U_1^{(1)}$, $\delta U_2^{(1)}$, $\delta S_1^{2(1)}$, $\delta S_1^{2(2)}$ are the remaining arbitrary variations.

Finally, if the von Karman approximation is now invoked wherein only nonlinear terms involving the transverse displacements are retained in the equilibrium equations, then one obtains from (3-143a,b) and (3-162) - (3-165) the following steel equilibrium equations:

$$N^{(1)}_{11,1} + P_1 = 0 \quad ,$$

$$(N^{(1)}_{12} + N^{(1)}_{11}U^{(1)}_{2,1})_{,1} + P_2 = 0 \quad , \tag{3-166}$$

$$M^{2(1)}_{11,1} - N^{(1)}_{12} + Q^2_1 = 0$$

where

$$P_1 = P_1(U^{(2)}_1 - U^{(1)}_1) \quad ,$$

$$P_2 = P_2(U^{(2)}_2 - U^{(1)}_2) \quad , \tag{3-167}$$

$$Q^{(2)}_1 = Q^{(2)}_1(S^{2(1)}_1) \quad .$$

The above steel relations are to be supplemented by appropriate steel constitutive relations. If the effect of the transverse stresses on the normal stress $\tau_{11}$ are neglected, then one obtains for <u>elastic</u> steel and a <u>circular</u> cell:

$$N^{(1)}_{11} = n^{(1)}\varepsilon^2 E^{(1)}(U^{(1)}_{1,1} + \frac{U^{(1)2}_{2,1}}{2}) \quad ,$$

$$N^{(1)}_{21} = n^{(1)}\varepsilon^2\mu^{(1)}(U^{(1)}_{2,1} + S^{2(1)}_1) \quad , \tag{3-168}$$

$$M^{2(1)}_{11} = E^{(1)}I^{(1)}S^{2(1)}_{1,1} \quad , \quad I^{(1)} \equiv n^{(1)2}\varepsilon^4/4\pi \quad ,$$

where $n^{(1)}$, $E^{(1)}$, $\mu^{(1)}$ denote volume fraction, Young's Modulus, and the shear modulus, respectively, for the steel. Equations (3-168) were obtained by (1) assuming small strains (but moderate rotations), (2) relating the Kirchhoff stress $\tau_{ij}$ and the Green's strain $E_{ij}$ via Hooke's law, and (3) averaging according to

$$(N^{(1)}_{11}, N^{(1)}_{21}, M^{2(1)}_{11}) \equiv \int_{A^{(1)}_o} (\tau^{(1)}_{11}, \tau^{(1)}_{21}, \tau^{(1)}_{11}g^{2(1)})dA_o \tag{3-169}$$

In the case of elastic-plastic steel behavior, equations (3-168) are replaced by the incremental relations

$$\dot{N}_{11}^{(1)} = n^{(1)}\varepsilon^{2}\bar{E}^{(1)}(\dot{U}_{1,1}^{(1)} + U_{2,1}\,\dot{U}_{2,1}) \quad ,$$

$$\dot{N}_{21}^{(1)} = n^{(1)}\varepsilon^{2}\bar{\mu}^{(1)}(\dot{U}_{2,1} + \dot{S}_{1}^{2(1)}) \quad , \tag{3-170}$$

$$\dot{M}_{11}^{2(1)} = \tilde{E}^{(1)}I^{(1)}\dot{S}_{1,1}^{2(1)}$$

where $\bar{E}^{(1)}, \bar{\mu}^{(1)}$, $\tilde{E}^{(1)}$ are elastic-plastic tangent moduli.

For the dowel problem posed, the interaction terms are selected as follows:

$$\dot{P}_{1} = K_{1}(\dot{U}_{1}^{(2)} - \dot{U}_{1}^{(1)}) \quad , \quad K_{1} = \text{constant}$$

$$\dot{P}_{2} = K_{2}(\dot{U}_{2}^{(2)} - \dot{U}_{2}^{(1)}) \quad , \quad K_{2} = \text{tangent modulus} \tag{3-171}$$

$$Q_{1}^{(2)} \equiv 0 \quad .$$

The forms (3-171) are motivated by independent linearly elastic solutions and experimental data.

The boundary conditions of the nonlinear dowel problem are specified as follows:

$$U_{1}^{(1)}(0) = 0 \quad , \quad U_{2}^{(1)}(0) = 0 \quad , \quad M_{11}^{2(1)}(0) = 0$$

$$U_{1}^{(1)}(L) = 0 \quad , \quad U_{2}^{(1)}(L) = \Delta \quad , \quad M_{11}^{2(1)}(L) = 0 \quad . \tag{3-171}$$

The conditions (3-171) are based, in part, on asymmetry with respect to $X_1 = 0$.

A numerical program was constructed to solve Equations (3-166), (3-170), (3-171) and (3-171) in the region $0 < X_1 < L$. A solution for $-L < X_1 < 0$ was obtained by asymmetry conditions.

Typical resultant transverse force (dowel force) versus offset displacement, $\Delta$, behavior, via the mixture model, is shown in Figure 3.30a,b for monotonic and hysteretic $\Delta$-displacement histories. When one compares this response with experimental data,[26,27] such as that shown in Figure 3.31a,b, it is evident that the mixture model is simulating the basic features of the complex dowel response. Details concerning the experimental setup are provided in Figure 3.32.

A search is presently in progress for dowel experimental data suitable for quantitative comparisons. Since dowel data is known to be sparse, it may be necessary to generate the appropriate experimental information.

## 3.5 CLOSURE

It has been observed by many researchers that the nonlinear response of reinforced concrete is largely dominated by complex interactions between the steel and the concrete. In an effort to simulate these interactions, a mixture theory approach was adopted as a basis for the construction of a new model for reinforced concrete. In a further effort to minimize the number and type of tests necessary to define the parameters of the model, a microstructural, in contrast to a phenomenological, approach was selected.

Based upon the microstructural mixture methodology, two nonlinear models for reinforced concrete have been constructed to-date: one for a dense steel layout, the other for a sparse steel layout. These theories allow finite deformations and include a wide class of component and component interface descriptions. Further, they include curvilinear steel layouts. At this time, however, the latter are restricted to unidirectional geometries.

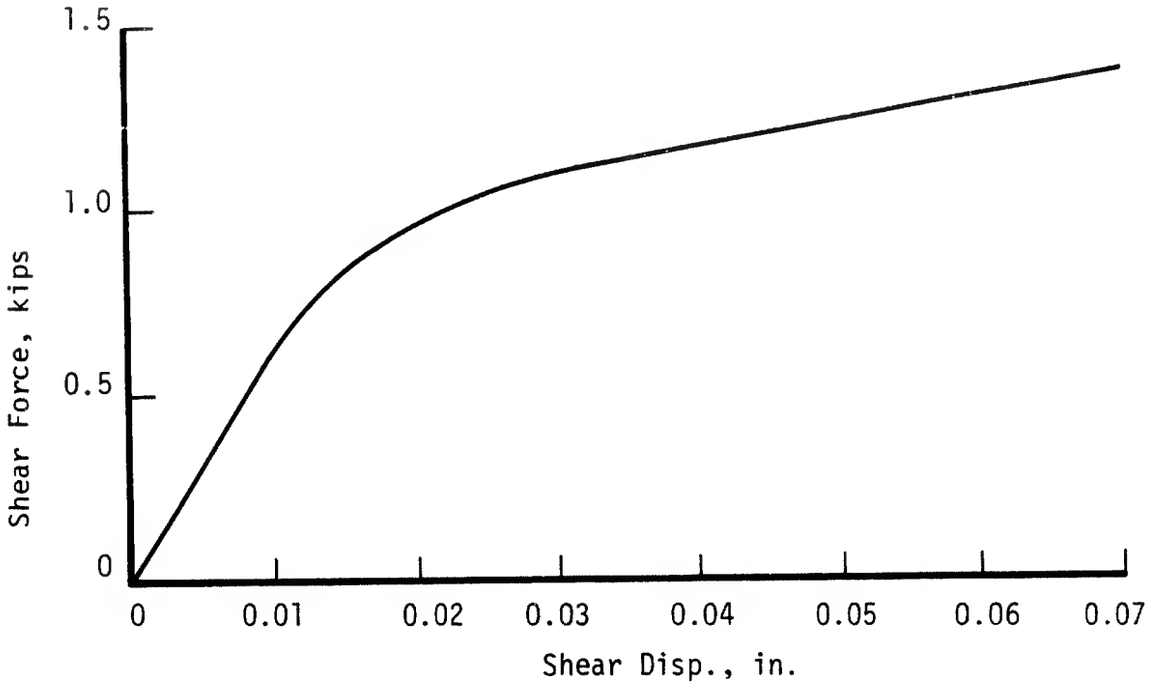


(a) Monotonic deformation.

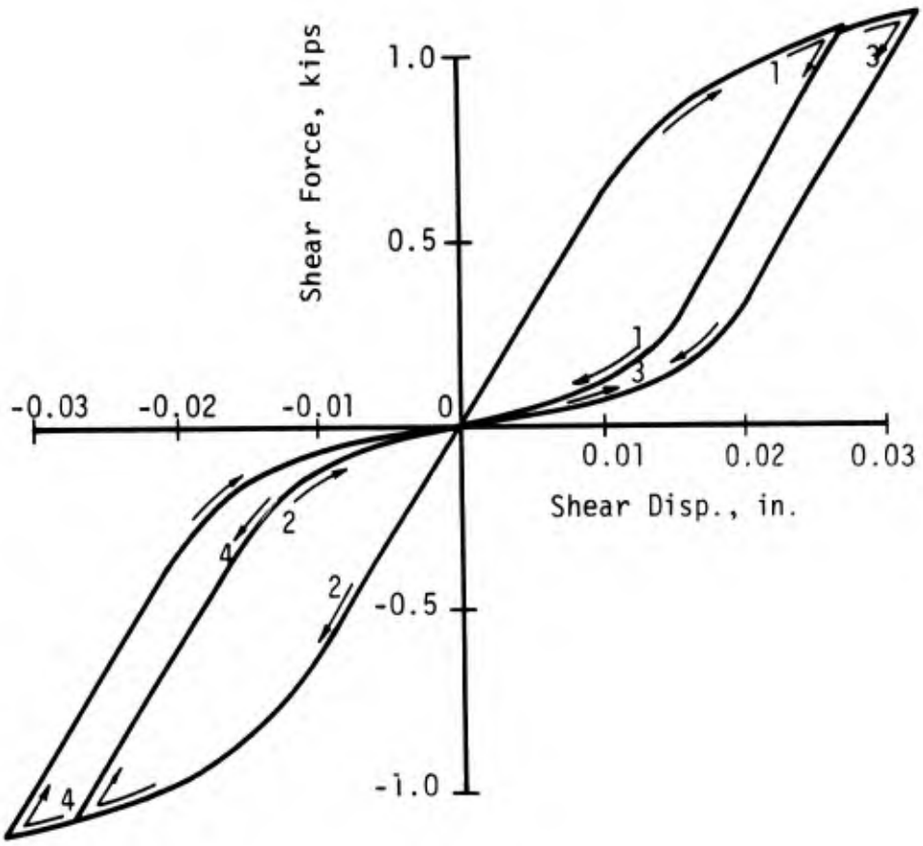


(b) Hysteretic deformation

Figure 3.30a,b. Response of mixture model in dowel mode.

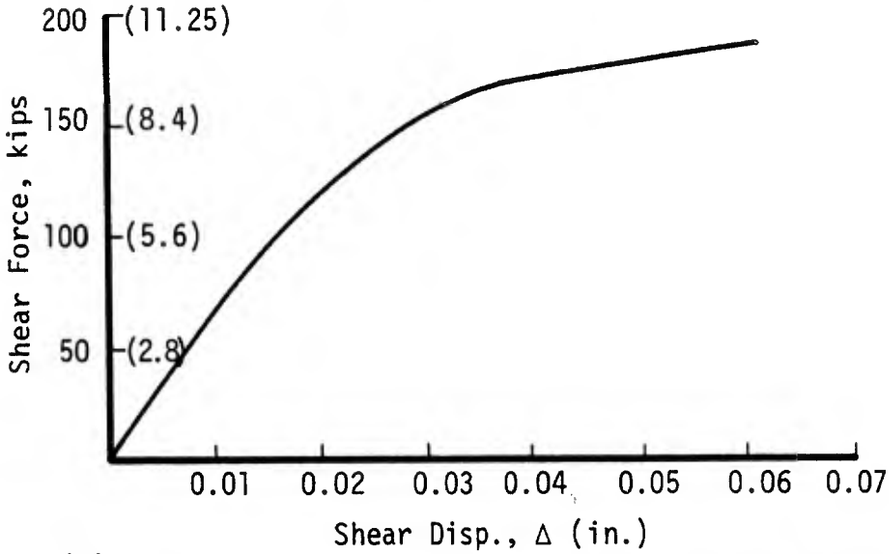


(a) Test De - 9A

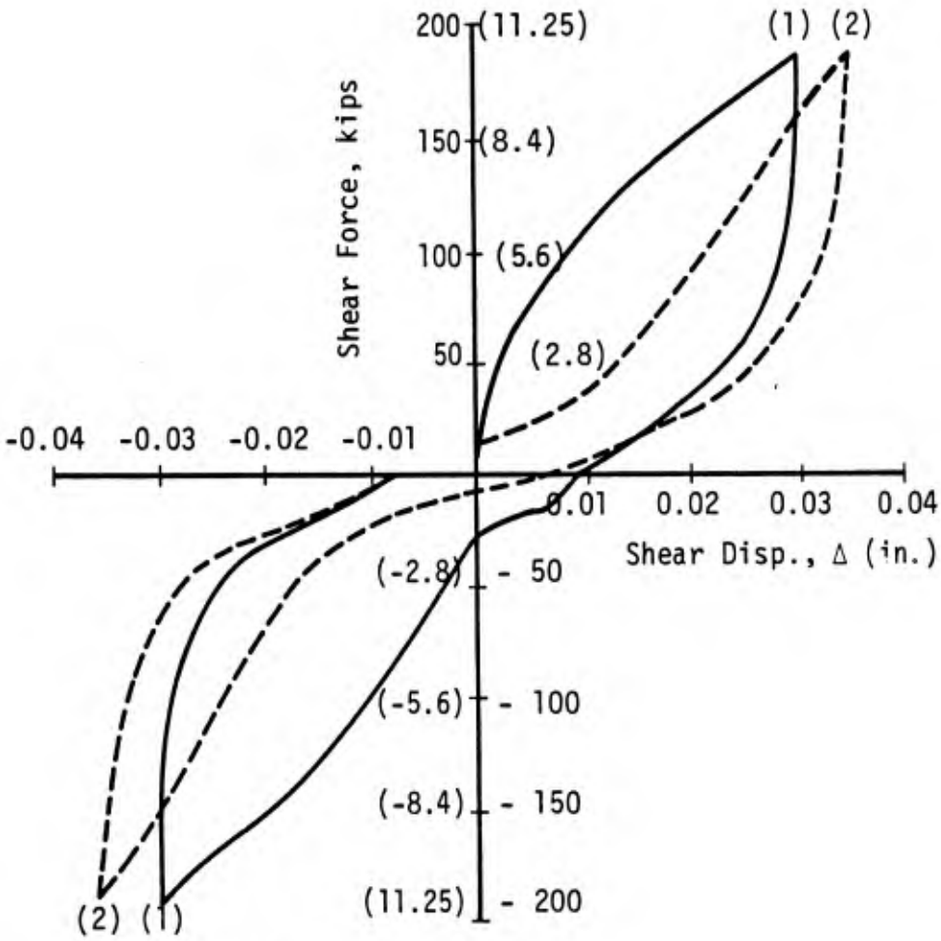


(b) Test D4 - 9B

Figure 3.31 Experimental load displacement curves (Test Series D) (From Ref. 26).

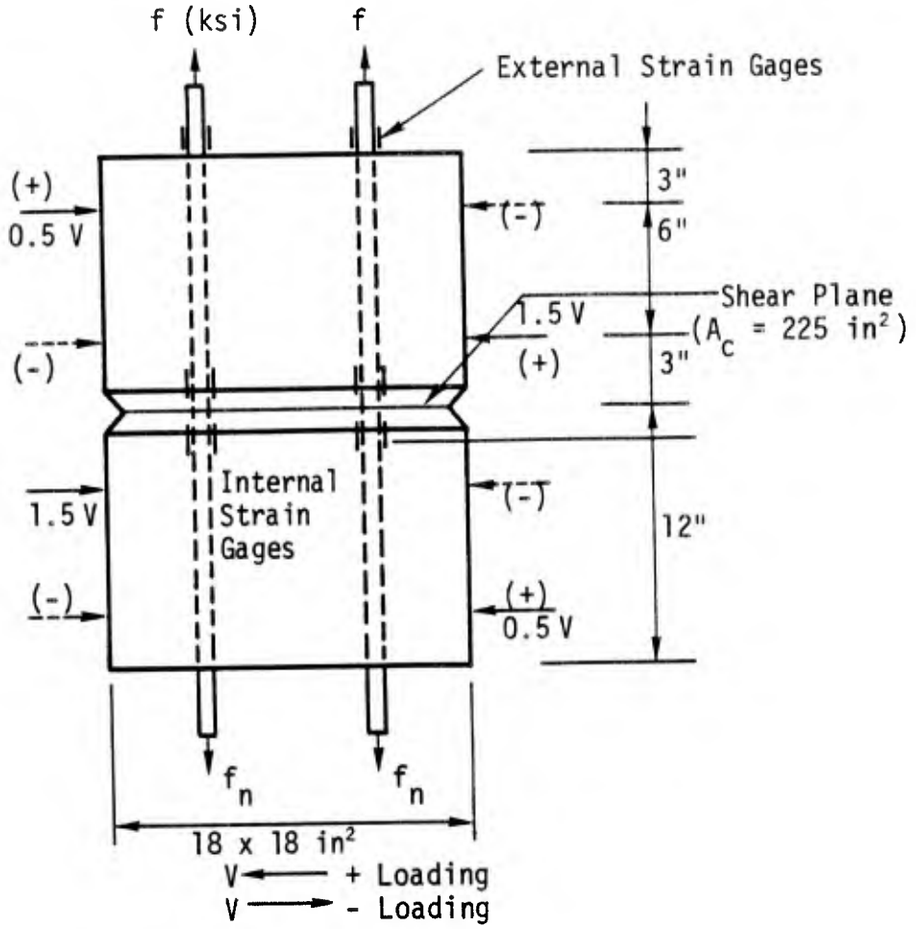


V = shear force at shear plane.

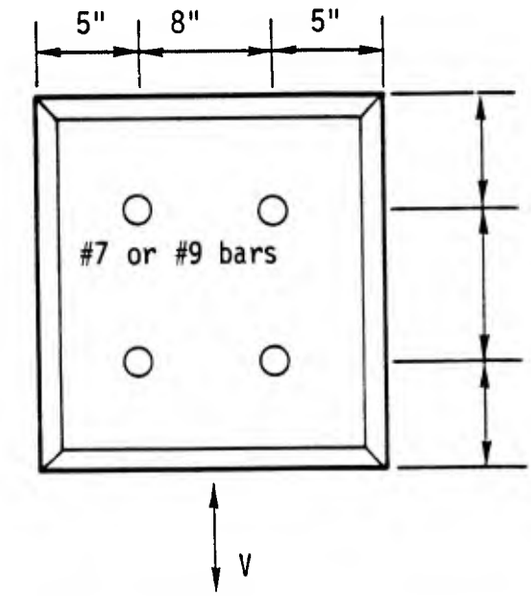


Tests: C4-7A, C4-9A and
C4-9B.
D4-9A to D4-9C

Figure 3.32. Experimental setup (Ref. 26).

The validation studies conducted thus far are of two types: (1) The Steel-Concrete Bond Problem and (2) the Dowel Problem. These studies, which consist of comparisons of analytical/numerical simulations and actual test data, reveal that the mixing procedures used in model construction provide excellent simulation capability for the global response of reinforced concrete under both monotonic and hysteretic loading conditions.

Continued research is, of course, necessary in order to bring the modeling process to fruition. Included in the necessary research tasks is the generalization of the current model to include multi-directional steel layouts. Continued validation studies are also necessary. These should include additional dowel and dowel plus interface shear transfer simulations, and steel buckling -- concrete spallation simulations. Such studies will requies test data of a higher quality than is currently available. The generation of the necessary data could be part of a continued research effort.

This Page Left Blank

## IV. STRAIN SOFTENING IN CONCRETE, ROCK AND SOIL

There are a number of materials, such as rock, concrete and dense soils, which when compressed at constant axial strain rate under conditions of either uniaxial stress or triaxial compression exhibit a phenomenon called "strain softening." Materials which exhibit such softening are characterized by a constitutive response in the axial direction in which the stress first rises monotonically with strain to a peak, and then decreases with further increases in strain.

Under general states of deformation, a material element is said to undergo strain softening when its stress rate $\dot{\sigma}_{ij}$ and strain rate $\dot{\varepsilon}_{ij}$ satisfy the following condition:[28]

$$\dot{\sigma}_{ij}\,\dot{\varepsilon}_{ij} < 0 \quad . \tag{4-1}$$

For those materials whose constitutive behavior can be described by an incrementally linear relation of the form:

$$\dot{\sigma}_{ij} = C_{ijk\ell}\dot{\varepsilon}_{k\ell}, \tag{4-2}$$

where $C_{ijk\ell}$ is the fourth order tangent stiffness tensor, it follows that the condition for strain softening reduces to the form:

$$C_{ijk\ell}\dot{\varepsilon}_{ij}\dot{\varepsilon}_{k\ell} < 0 \tag{4-3}$$

Thus, for the incrementally linear models, strain softening occurs when the matrix of the tangent stiffness components ceases to be positive definite. In almost all cases, the experimental data which show strain softening in concrete, rock and soils come from either uniaxial compression or triaxial compression tests. To observe strain softening in such tests, it is necessary that the displacement of the end platens be governed by a closed-loop servo-controlled system.* Softening is observed when the axial stress decreases with increases in the axial strain.

*If load control instead of displacement control is used, the test specimen will become unstable at the peak of the stress-strain curve and suddenly fail; the test will therefore terminate before the descending branch of the stress-strain curve can be established.

Until recently, strain softening was generally viewed as a true material property and routinely incorporated into constitutive models. As a result, the literature abounds with advanced, complex constitutive models for materials such as concrete, rock and soils which contain strain softening. The notion of a constitutive model, however, is fundamentally a continuum concept, and to include strain softening in a constitutive model implies that strain softening can occur in a homogeneous material element at the continuum level, i.e., it's a material property. Most of the data from which the notion of strain softening in rocks, concrete and soils developed has come from unconfined compression and triaxial compression tests conducted with displacement control in the axial direction. Since the unconfined compression test is the simplest to discuss and is sufficient for illustrating the major issues of concern here, attention will be restricted to this type of test in the discussion below.

Let us recall that the type of data generated by the unconfined compression test consists of the variation of the axial force F with the servo-controlled axial displacement u, i.e., F = F(u). It is common practice to transform this type of data to obtain the stress-strain relationship through the following equations:

$$\sigma = \frac{F}{A_0} \quad , \quad \varepsilon = \frac{u}{L_0} \tag{4-4}$$

where $\sigma$, $\varepsilon$ denote, respectively, the stress and strain, and $A_0$, $L_0$ are the original cross-sectional area and length of the unstrained specimen.

The validity of using the above equations to determine the stress and strain depends, however, on the following conditions being satisfied:[29]

- The specimen must be homogeneous
- A homogeneous state of stress must exist in the specimen at all times
- No significant changes in the geometry of the specimen can occur during a test.

If these conditions are not met, the constitutive relationship for the material cannot be inferred from the force-displacement data. As increasing deviations from the above conditions arise in a test, the use of Eqs. (4-4) to determine the stress-strain relationship becomes increasingly in error. Consequently, strain-softening models that are based on the descending branch of the force-displacement curve, without consideration of the physical condition of the specimen, must be viewed with considerable caution.

In the sections which follow, the above issues are explored in some further detail. The results from previous experimental studies that bear on these questions will be discussed. Pertinent and related theoretical concepts and studies are also reviewed.

## 4.1 EXPERIMENTAL OBSERVATIONS

### 4.1.1 Rocks.

While there are numerous laboratory studies which reveal strain softening in rocks, there are three studies, in particular, that provide important insight into the nature of the strain softening in these materials. One of these studies, conducted by Hudson, Brown and Fairhurst,[30] examines the unconfined compression response of marble. Another study, by Hallbauer, Wagner and Cook,[31] investigates the triaxial compression behavior of jacketed specimens of quartzite. Finally, Brady, Duvall and Horino[32] attempt to establish the true stress-strain relationship for six different rocks, compressed under uniaxial stress conditions, by using both experimental and theoretical methods to determine the variation of the true load bearing area with strain in the post-failure regime. From these three studies it is evident that the strain softening which appears in the force-displacement

curves does not reflect a true property of these materials, but is instead due to non-homogeneous deformation of the test specimens past the peak of the force-displacement curve. Further details of these studies are given below.

In the series of unconfined compression tests reported in Reference 30, cylindrical specimens of Georgia Cherokee marble, of various sizes and L/D ratios, were examined in a testing machine having axial displacement control. The tests were conducted at a constant strain rate of $1.5 \times 10^{-6}$ sec.* The purpose of these tests was to establish if the descending branch of the stress-strain curve for uniaxial compression is a true material property -- and thus independent of specimen size and geometry -- or the result of non-homogeneous deformation and therefore dependent upon specimen geometry.

A total of 45 tests was performed, and the results are summarized in Figure 4.1, where the effects of both specimen geometry and size on the complete stress-strain curve are shown. Each test was repeated twice so that the curves shown actually represent the average of three tests. The curves in Figure 4.1 were scaled from the measured force-displacement (F-u) curves by using Equation (4-1) given earlier, and in that which follows we shall refer to these as "apparent" stress-strain curves. It is evident from the figure that the portions of the apparent stress-strain curves up to near the peak are virtually unaffected by variations in specimen geometry and size, while the peak values and the descending branches are strongly dependent upon them.

In the experiments, it was found that progressive structural breakdown of the specimens began at about 50 percent of the ultimate strength. The inhomogeneous and anisotropic nature of the material

*The authors failed to note in their paper whether or not there was lubrication between the end plates and the test specimens.

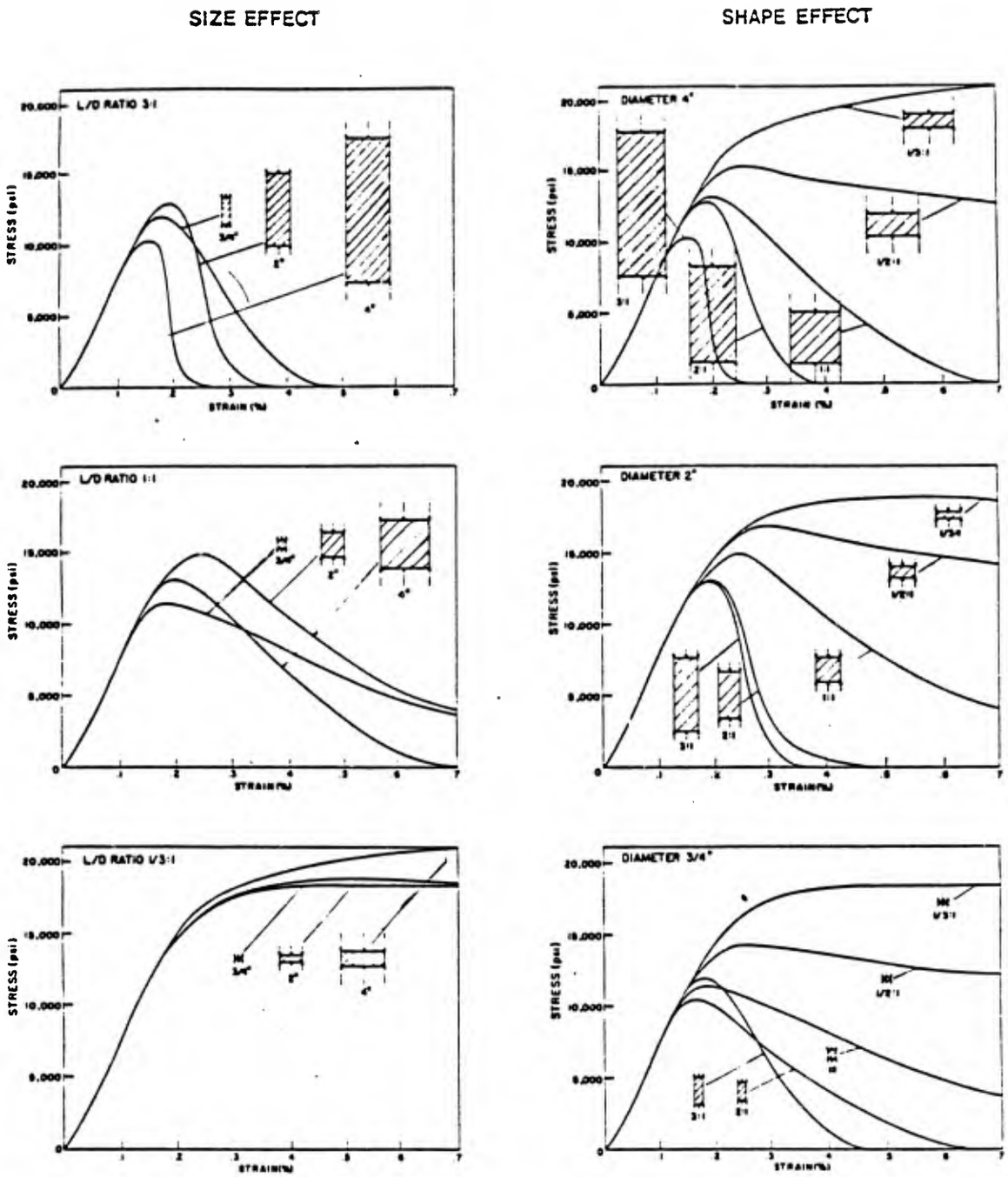


Figure 4.1. Influence of specimen size and shape on the complete stress-strain curve for marble loaded in uniaxial compression. (From Reference 30).

on the microlevel induces local tensile stresses which produce microcracks that grow and become aligned with the loading axis.* As the loading increases, the density of microcracks rapidly proliferates, leading to vertically aligned macrocracks which result in gross slabbing of material from the specimens' lateral surfaces. Illustrations of such slabbing in specimens are given in Figures 4.2 and 4.3. In general, the axial cracks are concentrated in the central portions of a specimen's length because lateral restraint at the specimen ends, due to friction, inhibits their growth near the specimen-platen interface. This is particularly true of the longer specimens. For the short specimens (L/D = 1/3), however, the axial cracks appeared to be uniformly distributed over the entire length. These differences in crack patterns no doubt cause the variations in the shapes of the stress-strain curves shown in Figure 4.1.

As noted above, the apparent stress-strain curves shown in Figure 4.1 were obtained by scaling the measured force-displacement curves according to Equations (4-1). The gross slabbing of material on the lateral surfaces of the specimens during testing, however, continuously reduces the cross-sectional area of the remaining intact material and, to determine the true stress at some cross-section, the current (true) area of the intact material at that cross-section should be used in Eq. (4-4), instead of the original area. The true (load bearing) cross-sectional area of a specimen, which will be denoted by A, will diminish during a test due to the slabbing (axial fracturing) of material at or near the free lateral surface. The true cross-sectional area A will thus decrease as the axial compressive strain $\varepsilon$ increases with the result that

*A recent paper by Horii and Nemat-Nasser[33] provides an interesting discussion of axial splitting of rocks in terms of out-of-plane crack growth.

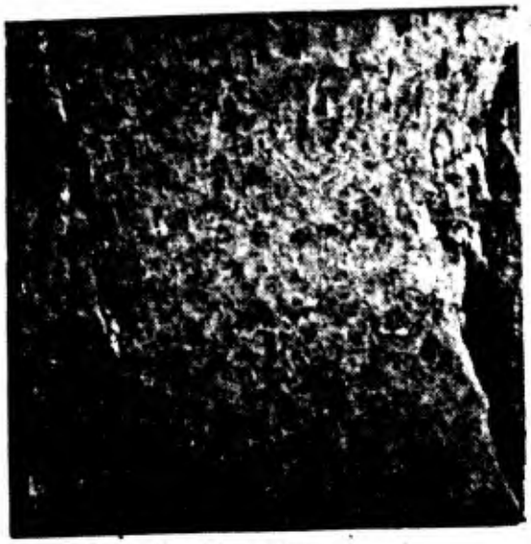

2-inch diameter

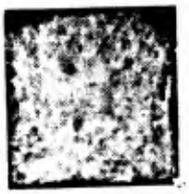

3/4-inch diameter

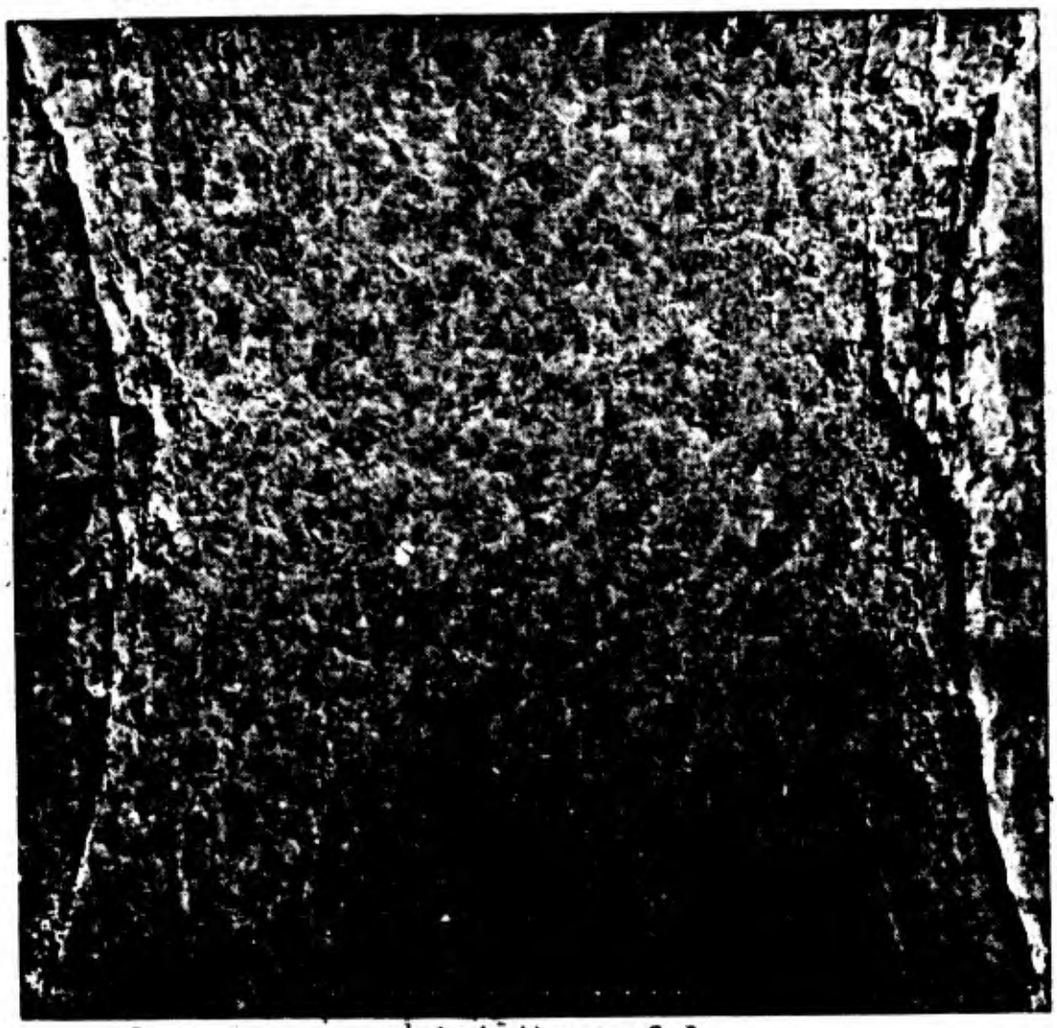

4-inch diameter

Figure 4.2. Cross-section of 1:1 specimens at an advanced state of failure. (Georgia Cherokee marble) (From Reference 30).

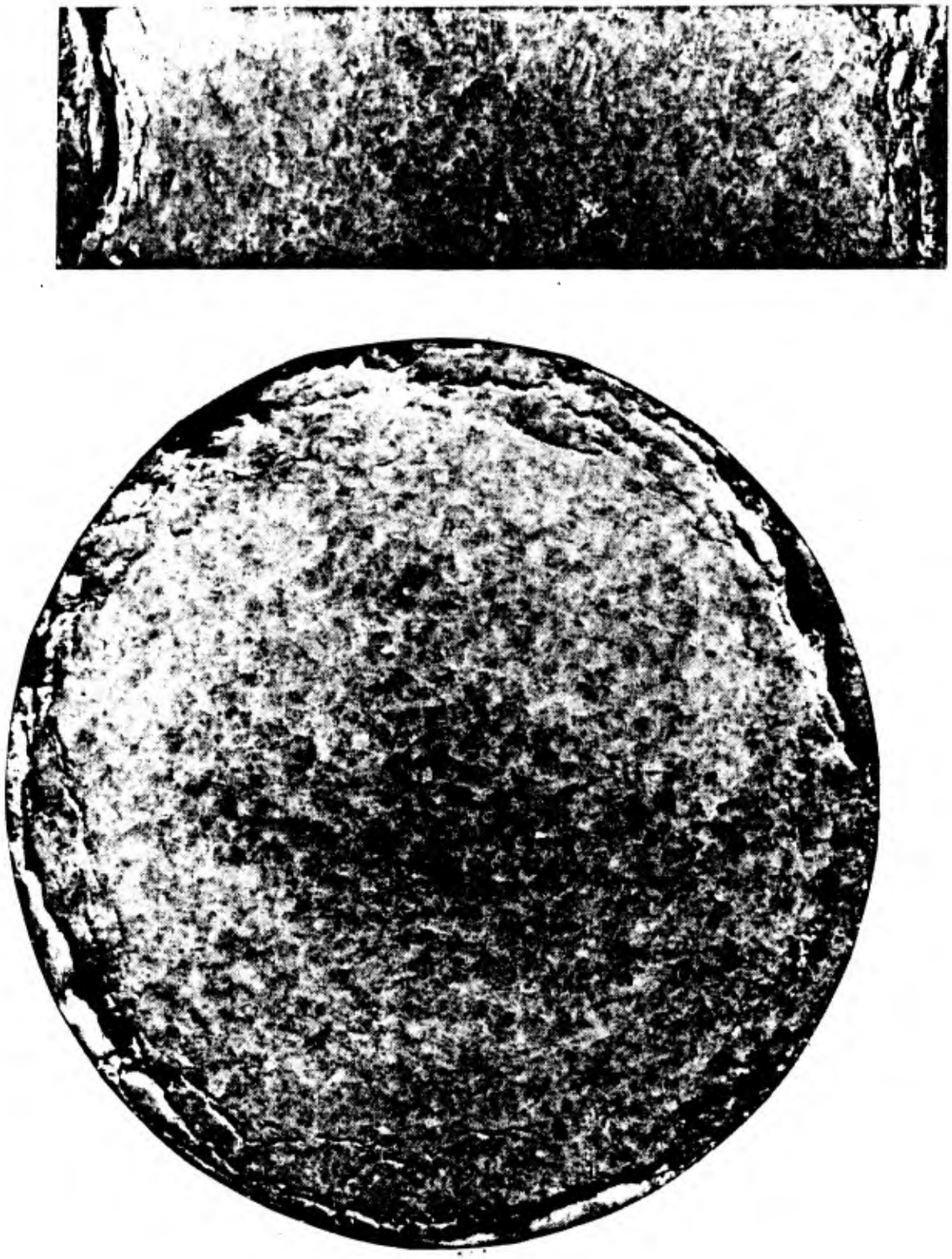

Figure 4.3. Cross-section and end view of 1/3:1 specimen (4-inch diameter) at advanced state of failure. (Georgia Cherokee marble) (From Reference 30).

$$A(\varepsilon) \leq A_0 \tag{4-5}$$

Consider now Figure 4.4 which depicts two test specimens, one of which has a large L/D ratio and the other a small one. For small L/D specimens, the slabbing of material from the lateral surface does not significantly reduce the effective load bearing cross-sectional area and, in this case, one can write $A(\varepsilon) \approx A_0$. If, in addition, it can be assumed that the state of stress in the short specimen is reasonably homogeneous, then it can be concluded that the true stress-strain curve is described quite closely by the apparent stress-strain curve, as shown in the figure. Now note from Figure 4.1 that the apparent stress-strain curves for the shortest specimens (L/D = 1/3) do not show any strain softening. On this basis then it may be concluded that the true stress-strain curve also does not exhibit strain softening; the validity of this conclusion will be further substantiated by the work of Brady, Wagner and Horino[32] to be discussed in the sequel.

For the tall specimens, the true cross-sectional area A can be drastically reduced as the test proceeds, with the result that the applied force F may drop while the true stress continues to increase. In this case, $A < A_0$ and the apparent stress-strain curve provides a poor representation of the true stress-strain curve. Thus, it follows that the extent to which the apparent and true stress-strain curves differ depends upon the L/D ratio of the specimen. Parenthetically, it should also be noted that the material near the axes appears to experience more confinement in the case of specimens with small L/D ratios than for those with large ones; this enhanced confinement results from friction between the specimens and the load platen and tends to reach a maximum at the axis.

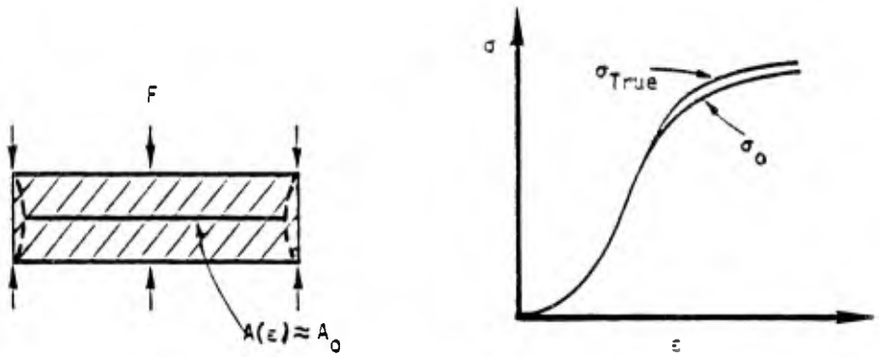


(a) Specimens with small L/D ratios.

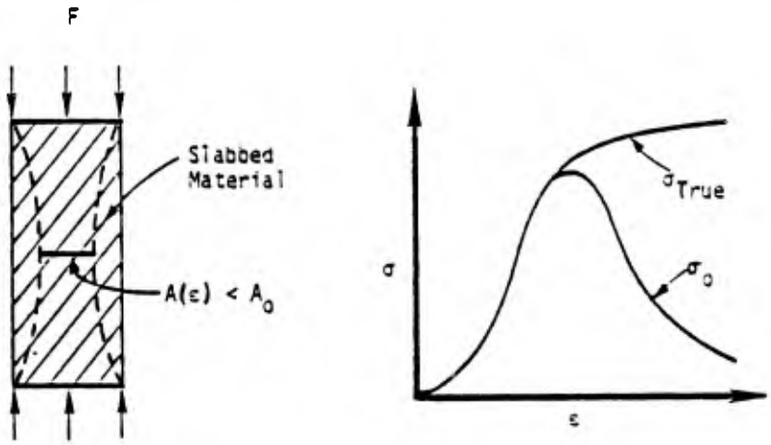


(b) Specimens with large L/D ratios.

Figure 4.4. Effect of L/D ratio on the difference between the true and apparent stress-strain curves.

Hallbauer, Wagner and Cook reported a series of triaxial compression tests on quartzite.[31] The tests were done on cylindrical specimens (L/D = 3) which were jacketed in thin copper tubes so that their lateral expansion would be resisted by the increasing confinement. The rate of axial strain was kept constant at $10^{-3}$/min during the tests. The purpose of these tests was to determine the microstructural changes that progressively take place in the rock as it is compressed to failure. Particular emphasis was given to the structural changes that occur in the vicinity of the peak of the stress-strain curve. To accomplish this, the tests were stopped at various predetermined points along the strain path; the specimens were unloaded and removed for sectioning and microscopic examination.

Figure 4.5 shows the nominal stress-strain curve obtained from the tests, and photographs of specimen sections at the various points along this curve. Little damage is evident until the stress reaches about 80 percent of the ultimate stress. As the stress is increased from 80 to 90 percent of ultimate, a rapid proliferation of microcracks occurs, with the number of microcracks increasing about seven-fold.

A very important observation which resulted from this study is that, at the ultimate stress, a macroscopic fracture plane first appears in the central portion of the specimen. With further compressive straining, the fracture plane grows toward one or both of the ends, eventually leading to complete splitting of the specimen. The rapid drop in the load carrying capacity after the peak of the stress-strain curve was attributed to the complete failure of existing partially fractured material ahead of the macroscopic failure plane. Thus, on the basis of this evidence, it is concluded that the falling branch of the stress-strain curve in Figure 4.5 is actually not a material property, but the result of the propagation of a macroscopic fracture plane through the specimen. Beyond the peak of the stress-strain curve, the specimens were in the process of splitting and therefore could not be treated as a homogeneous

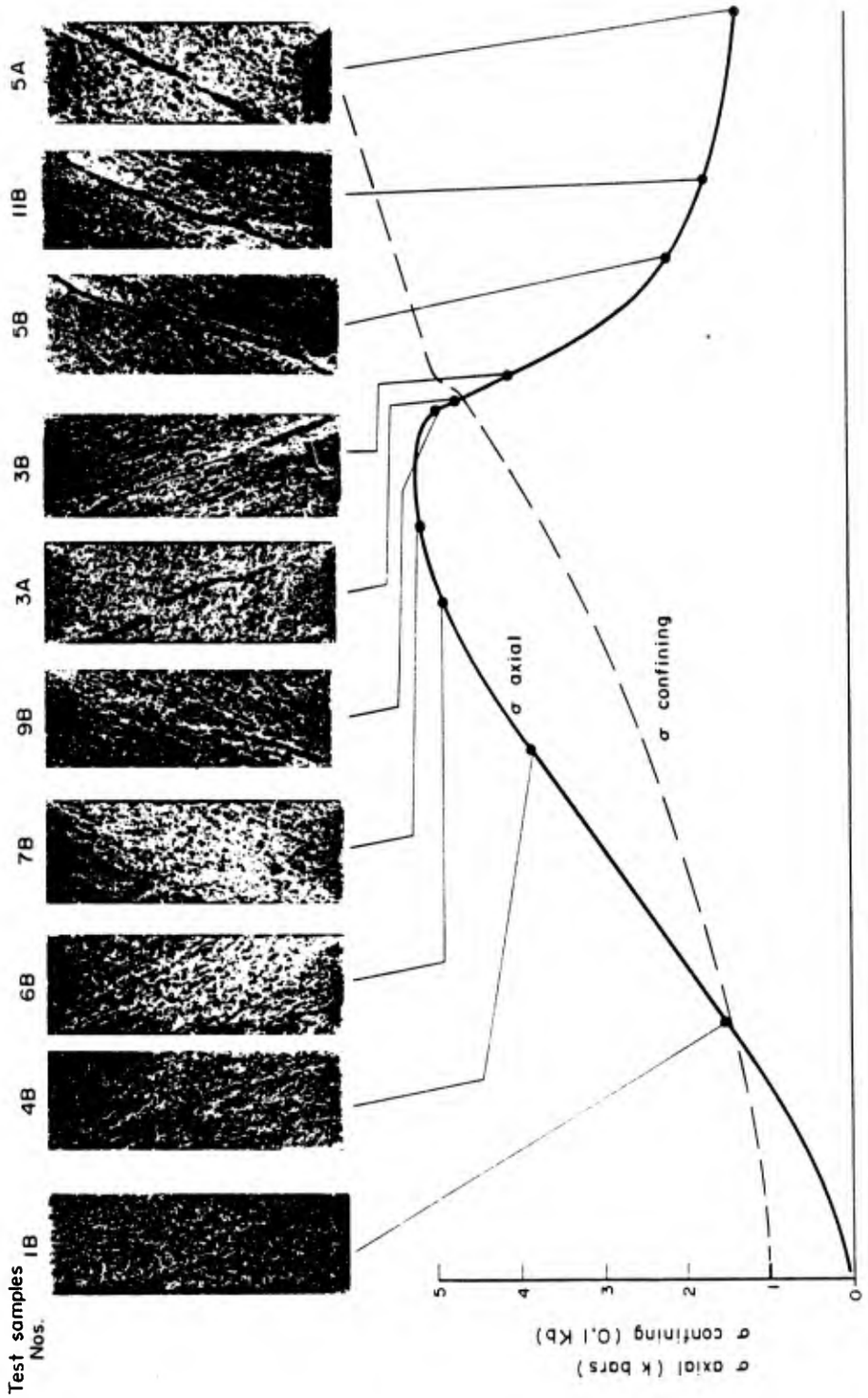


Figure 4.5. Stress-strain curve and photograph of test specimens at different stress levels. (From Reference 31)

continua. It is therefore concluded that the observed strain-softening is the result of inhomogeneous deformation and fracturing, and is not a material property phenomenon.

Finally, Brady, Duvall and Horino[32] conducted an interesting study of the unconfined compression behavior of rocks which offers considerable insight into the true nature of strain softening. Six different rock types were studied, including marble, two types of granite, sandstone, limestone and a schist. Tests were conducted on five specimens from each of the rock types; the tests were done in a conventional testing device which was artificially stiffened by placing high-strength steel columns in parallel with the specimens. The axial deformation of a specimen was measured by three LVDT devices connected in series. A small load cell in series with the specimen measured the applied load. The test specimens were 2.125 inches in diameter and 4.295 inches in length.

Each specimen was loaded to a preselected position along the post-failure curve, unloaded and then cast in hydrostone. It was then sectioned at one-half inch intervals normal to the specimen axis, and the resulting disks were ground smooth. The disks were impregnated with fluorescent dye to reveal the cracked portions of the cross-sections. By assuming that the load was carried essentially by the uncracked cross-section, the true stress acting upon the specimen can be found. In this manner, the true stress-strain curve under uniaxial compression was determined for the six rock types, and it was found that (a) there is a maximum true stress that the solid (intact) rock can sustain without extensive inelastic deformation and (b) the maximum true stress does not change with axial strain. Figure 4.6, from Reference 32, shows the general shapes of the true and apparent (nominal) stress-strain curves obtained from this study. While the nominal stress-strain curve shows the usual strain-softening, the true stress-strain curve does not; the true curve has the form of an elastic-perfectly plastic material. This study, therefore, clearly reveals that strain

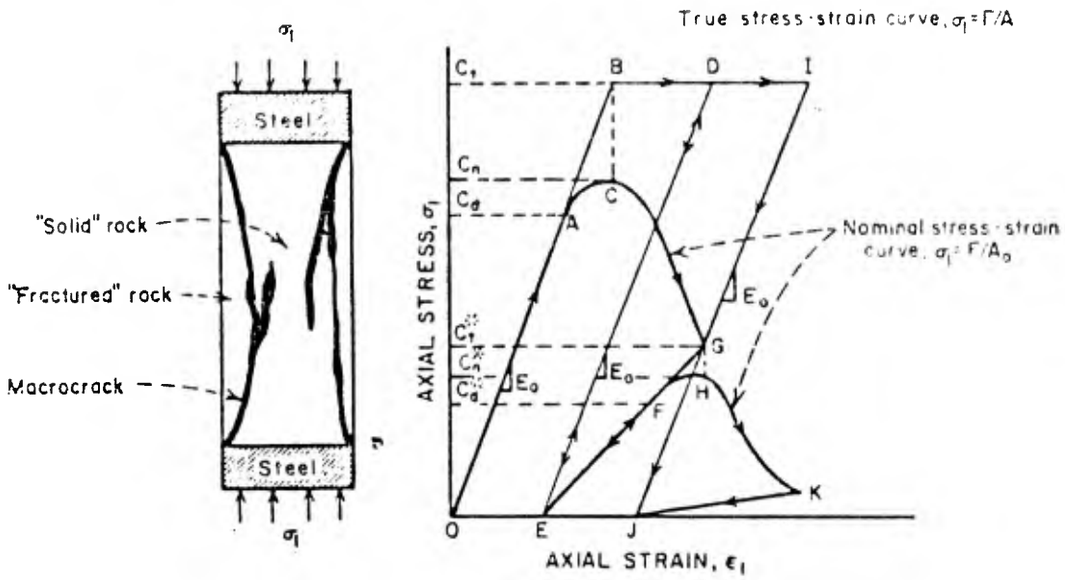


Figure 4.6. Idealized axial stress-strain behavior of solid rock in pre- and post-failure region (from Ref. 32)

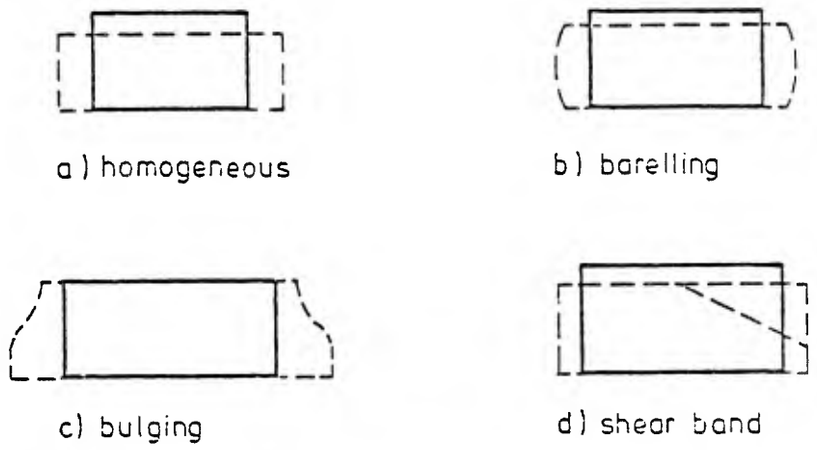


Figure 4.7. Homogeneous and nonhomogeneous modes of deformation (from Ref. 34).

softening is not a true material property of the six rocks considered, but is the result of scaling the force-displacement data by the original cross-sectional area, instead of the true cross-sectional area of the unfractured material.

4.1.2 Soils

The evidence of strain softening in soils comes essentially from standard triaxial compression tests on dense specimens. It is well-known that, because of friction between end plates and specimen and the possible development of modes of bifurcation (instabilities), it is difficult in such tests to maintain a state of homogeneous deformation within the specimen as the deformation progresses. Furthermore, as pointed out by Hettler and Vardoulakis,[34] experiments with "perfect" boundary conditions (ideally lubricated) and "perfectly" homogeneous material cannot insure, in general, homogeneous deformation, since various modes of bifurcation are possible and do actually develop. Examples of such modes of instability are barreling, bulging, necking and shear banding, some of which are depicted in Figure 4.7; these instability modes can occur in tests with lubricated as well as non-lubricated ends.

There is a growing body of evidence which supports the viewpoint that the observed strain softening in soils is not a true material property but mainly the result of non-homogeneous deformation of the test specimens during the experiments. To illustrate the point, several recent laboratory studies of the triaxial compression behavior of dense soils, in which special precautions were taken to produce homogeneous deformations, are described and discussed below. In these studies, it was found that when the deformations are homogeneous, or nearly so, the soils exhibit very little or no strain softening.

Deman[35] used X-ray techniques to investigate strain fields inside cylindrical specimens of dry dense sand produced by triaxial compression. In these tests, small metal spheres were carefully positioned in the material in a vertical plane which was parallel to and passed through the specimen axis. By measuring the movement of

the spheres with X-rays as the tests progressed, the deformation field inside the specimens was determined. Tests were performed with and without lubrication.

Figure 4.8 shows typical stress ratio versus strain curves obtained by Deman for specimens having L/D ratios of about 1:3 and tested with lubricated and non-lubricated end platens. As this figure reveals, both curves show a peak, but the softening is much more pronounced in the case of the non-lubricated platens. An inspection of the corresponding internal strain fields, shown in Figure 4.8, reveals that the non-lubricated end platens resulted in a non-homogeneous mode of deformation (barrelling) in which rigid cores of material developed adjacent to the end plates. The greatest deformation occurred near the central portion of the specimen. On the other hand, when the end platens were lubricated, the deformation was very nearly homogeneous, as shown in the figure. Thus, from these tests, it appears that the apparent strain-softening observed in these tests was essentially due to non-homogeneous deformation caused by the friction on the end plates and is therefore not a true property of the material; when the deformation was homogeneous or nearly so, very little softening was evident.

More recently, Hettler[36] performed a series of triaxial compression tests on relatively short cylindrical specimens of the same dry dense sand studied by Deman. The dimensions of the specimens (L/D = 0.35) were chosen, on the basis of theoretical work by Vardoulakis,[37] so that disturbances in homogeneity of deformation due to bulging instability or due to imperfections in the specimen height should not arise. The end plates were lubricated to prevent friction. Typical results from these tests are depicted in Figure 4.9, where stress ratio versus strain curves are shown for several confining pressures. Notice that for the range of strains studied (0 - 10 percent), no significant strain softening was apparent, while the test results for taller specimens of the same material, shown in Figure 4.8a, show various degrees of softening by

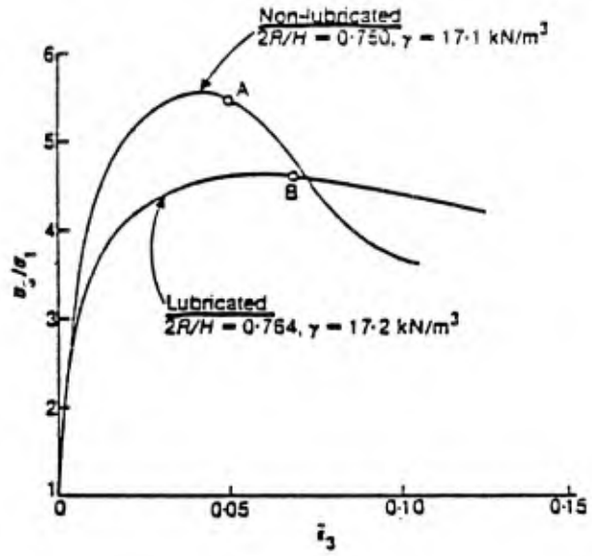


(a) Stress ratio versus axial strain.

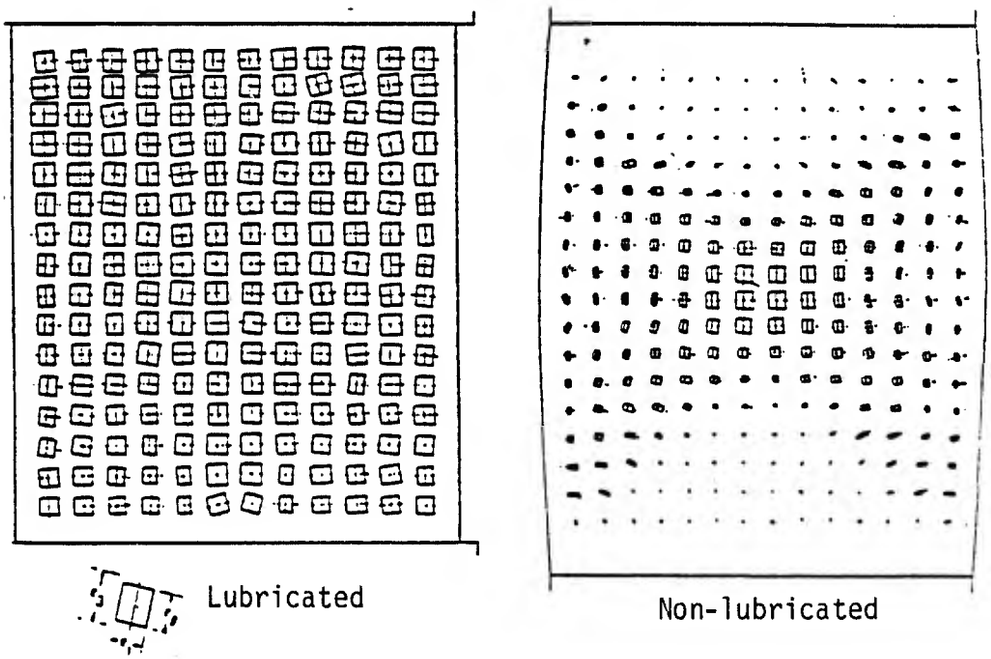


(b) Internal deformation field for lubricated and non-lubricated end platens.

Figure 4.8. Results from triaxial compression tests on dense sand with lubricated and non-lubricated end platens (from Ref. 35).

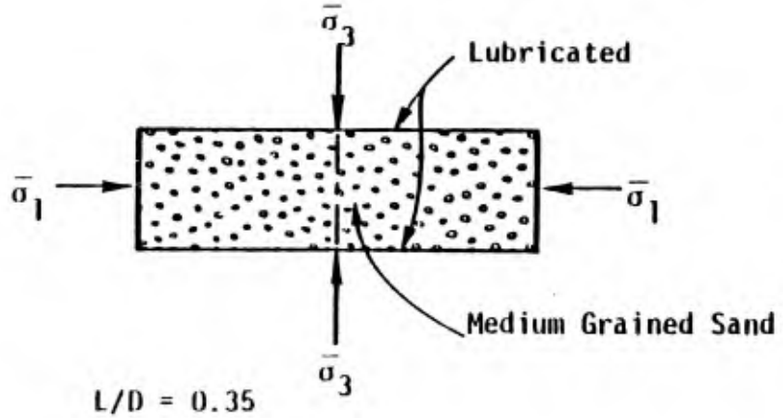


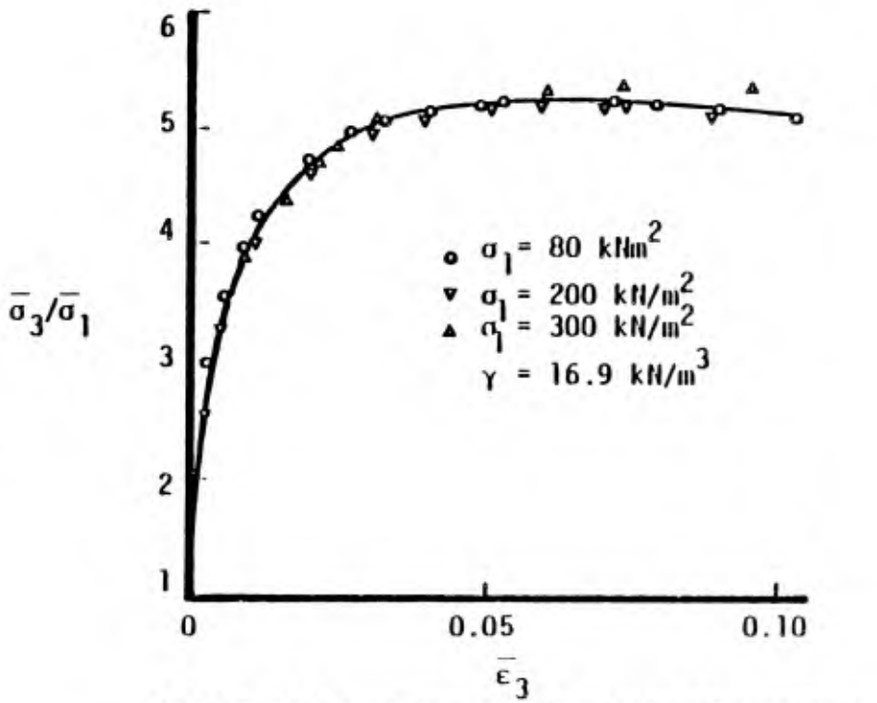


Stress ratio versus axial strain for various confining pressures.

Figure 4.9. Triaxial compression tests on flat, well lubricated specimens of dense medium grained sand (from Reference 36).

10 percent strain. Thus, as Dresher and Vardoulakis concluded[38] "These (Hettler's) results mean that true material softening is very slow and can be neglected for relatively large strains after the limiting state has been reached."

Further testing of the sand investigated by Deman[35] and Hettler[36] was done by Hettler and Vardoulakis,[34] using a newly developed triaxial device designed specifically to accommodate short cylindrical specimens and to virtually eliminate friction at the specimen-platen interfaces. Specimens with an L/D ratio of 0.36, sufficient to prohibit bulging instability, were tested. The specimens had different initial porosities ranging from the minimum porosity (0.36) to the maximum porosity (0.45). The confining pressure was 50 $kN/m^2$ in all tests. Figure 4.10 shows the stress ratio versus axial strain curves for these tests. For axial strains out to at least 10 percent, the specimens deformed with near-perfect homogeneity. The three lower curves show no softening while the upper two curves exhibit a small amount of softening, which for practical purpose can be reasonably neglected. These tests therefore confirm the earlier results of Deman[35] and Hettler[36], and demonstrate that very little or no softening arises in homogeneously strained samples of this sand, at least for axial strains of at least 10 percent. For larger strains, say 14 percent, it was found[34] that shear banding (instability) occurs and further deformation becomes non-homogeneous and exhibits strain softening.

The careful studies by Deman,[35], Hettler[36] and Hettler-Vardoulakis[34] clearly establish that, when sand is deformed homogeneously in triaxial compression, very little or no softening occurs for axial strains of at least 10 percent. For larger strains, bifurcation (instability) modes inevitably develop, producing subsequent non-homogeneous deformation accompanied by pronounced strain softening. Unfortunately, it is impossible to avoid such instabilities even if it were possible to achieve "perfect" boundary conditions and "perfectly" homogeneous material.

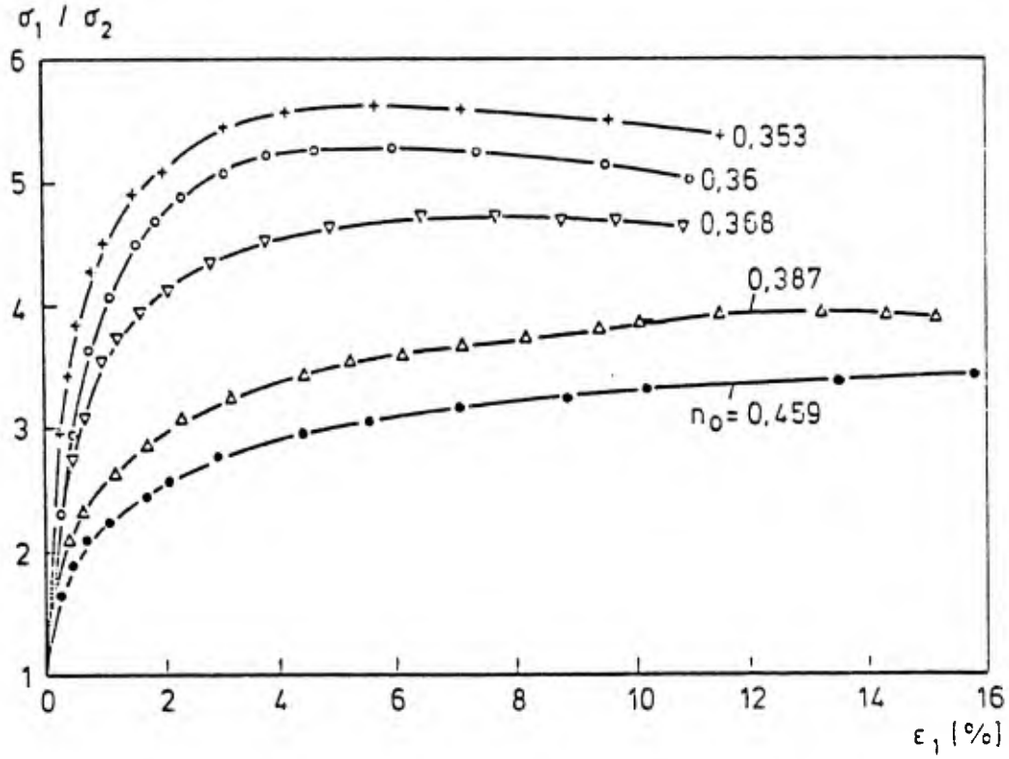


Figure 4.10 Test series with constant confining pressure ($\sigma_2$ = 50 kN/m$^2$) and varying initial density for specimens with L/D ratio of 0.36 (From Reference 34).

These studies therefore demonstrate that the strain softening observed in the conventional triaxial tests on dense sands is not a true material property, but the result of inhomogeneous deformation due to either end friction or instability modes.

### 4.1.3 Plain Concrete

Despite the effort that has been devoted in the past to measuring and mathematically modeling the descending branch of the stress-strain curve for plain concrete, very little has been reported regarding the corresponding conditions of the test specimens during such tests. Figure 4.11, for example, shows recently reported[39] stress-strain data at several different strain rates for a plain concrete loaded in unconfined compression. The stress denoted in the figure was determined by dividing the measured axial force by the original cross-sectional area of the specimen. Unfortunately, no information was given concerning the conditions of the specimens during the tests, except that " ... the plain concrete had virtually disintegrated" by a strain of 1 percent. As a result, it is not known at what point on the stress-strain curve macroscopic cracking first appeared, although it is very likely that it occurred near the peak of the stress-strain curve, as was the case for rock considered earlier.

Because of the similarities between the deformation mechanisms of rock and concrete, however, it is expected that concrete will behave much like rock, and therefore experience the onset of macroscopic cracking near the peak of the stress-strain curve. There are several studies that provide insight into the relationship between the macroscopically observed behavior of plain concrete and the internal microstructural changes that take place during deformation. The first to directly relate the shape of the stress-strain curve of plain concrete to the type and extent of internal microcracking were Hsu, Slate, Sturman and Winter.[40] These investigators made direct observations of microcracking in

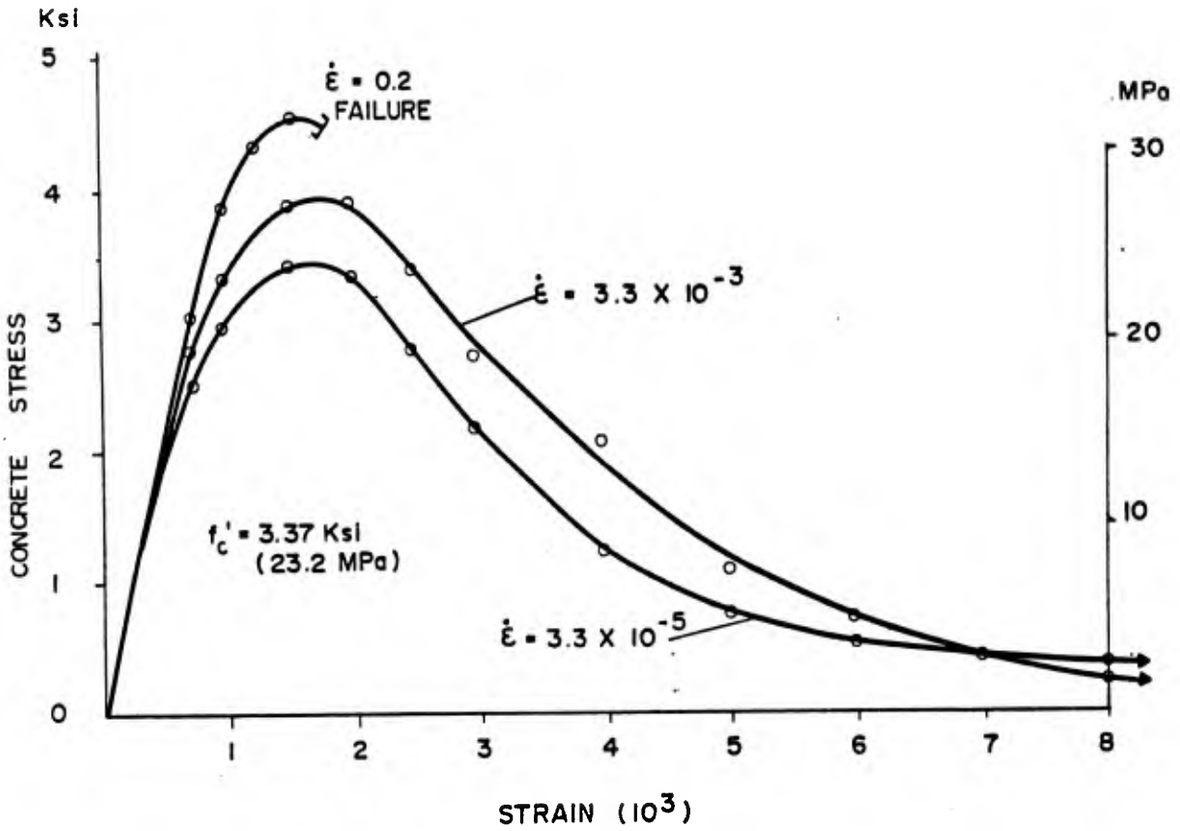


Figure 4.11. Stress-strain relationship for plain concrete under different strain rates (from Reference 39).

plain concrete cylinders axially compressed over a range of strains from 0 to 0.003. The ends of the cylinders were lightly greased to minimize frictional effects; this treatment promoted a vertical splitting mode of failure, in contrast to the "hour-glass" failure mode. The direct observation of microcracks in the strained concrete was achieved by two methods. In one, the specimen was cut and the cracks filled with colored dye; it was then examined under a microscope. In the other method, a thin slice was removed from the strained cross-section and then X-rayed. In this manner, the shape of the stress-strain curve was correlated with the nature of the internal microcracking.

It is well-known that microcracks can be divided into three types, e.g., cracks at the interface between aggregate and mortar (bond cracks), cracks through the mortar, and cracks through the aggregate. Bond cracks exist before concrete is subjected to any load, while the mortar cracks remain negligible until a later loading stage. Moreover, the bond cracks are the weakest link in the heterogeneous concrete system. At all stages of straining, the total extent of mortar cracking is considerably less than that of bond cracking. The authors note that "at about 70 percent of the ultimate load, the stress-strain curve begins to curve more sharply toward the horizontal, indicating the beginning of the breakdown of internal structure." They go on to state "On the descending branch of the stress-strain curve, concrete is extensively cracked. The amount of cracking is greater when the slope of the stress-strain curve is steeper. The descending branch of uniformaly compressed plain concrete represents a disintegration of internal structure, as is shown by the extensive interconnecting of mortar and bond cracks." (Underscores added.) An example of this is shown in Figure 4.12 which is taken from the work of Shah and Slate.[41] Here, the cross-sectional cracking patterns are shown for two different positions on the post-failure curve. Figure 4.12(a) shows the cracking pattern near the peak of the stress-strain curve while Figure 4.12(b) gives the pattern well into the post-failure region.

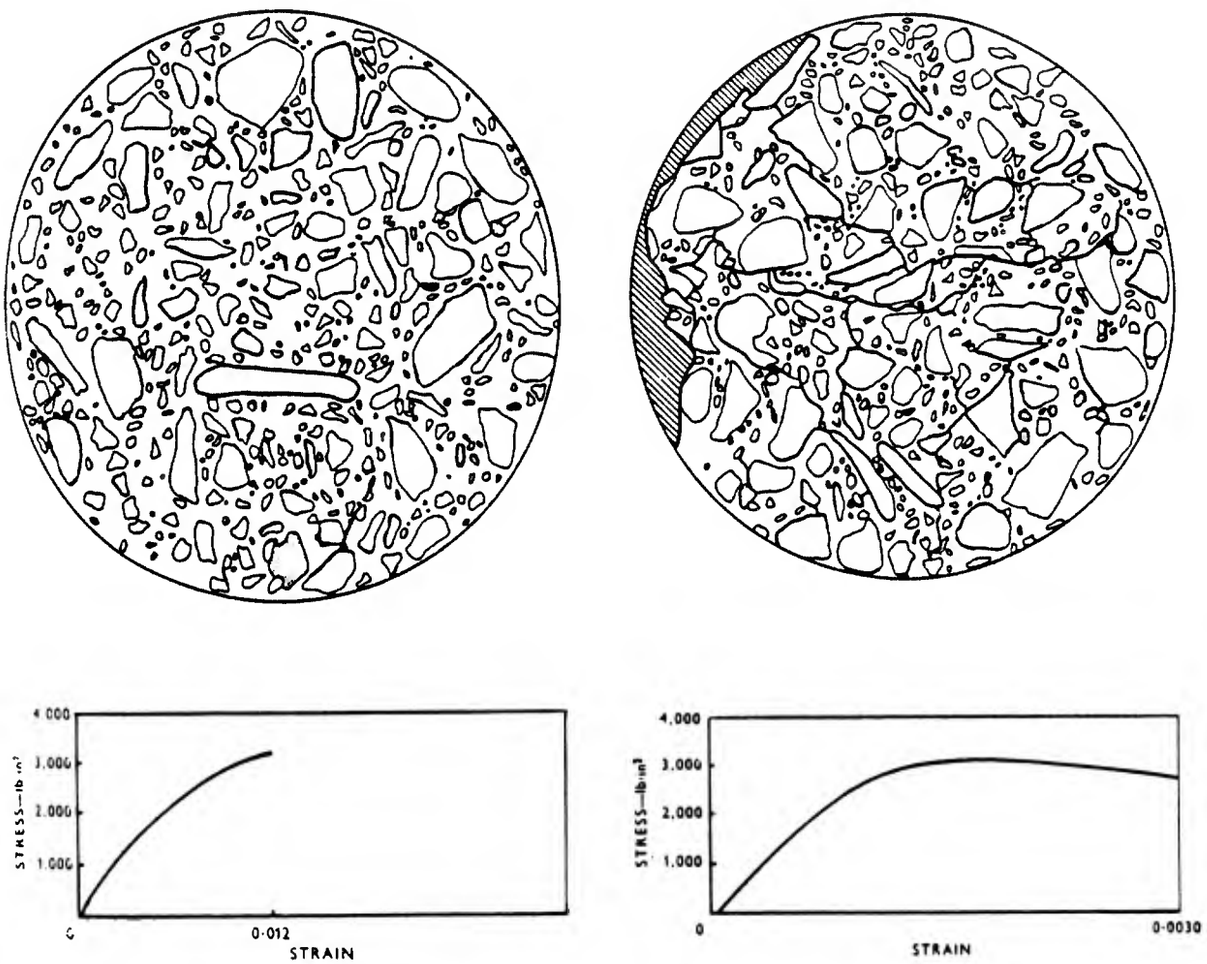


(a) Specimen 111 W 11-12
Strain: 0.0012

(b) Specimen 111 W 3-30
Strain: 0.0030

Figure 4.12. Cracking maps and stress-strain curves for concrete specimens compressed uniaxially into the post-failure region (from Reference 41).

Notice that very little mortar cracking is evident near the peak of the stress-strain curve, while extensive interconnecting cracks are present in Figure 4.12(b). From this study, Shah and Slate concluded[41] "... when a continuous crack pattern has developed extensively, the carrying capacity of concrete decreases and the stress-strain curve begins to descend."

From the results reported in References 40 and 41, it therefore appears that plain concrete, like rocks, experiences the beginning of extensive macro-crack development at or slightly beyond the peak of the stress-strain curve, and that further straining is simply accompanied by increasing disintegration of the material and increasing inhomogeneity of deformation.

Further experimental evidence in support of this position has recently been reported by Maher and Darwin,[42] who conducted unconfined compression tests at constant strain rate with a servo-controlled testing device on plain concrete specimens. They reported that "Hairline cracks begin to appear in the specimens shortly after crossing the peak of the stress-strain curve. As the strain increases, the size and length of these cracks increase, accompanied by a large increase in the lateral strain. At larger strains, sliding of material in the cracked zone is observed. This sliding appears to be the major component of both the longitudinal and lateral strains in the descending branch of the stress-strain curve." (Underscores added.)

On the basis of the work reported in References 40 to 42, it appears that the descending branch of the stress-strain curve for plain concrete is due essentially to inhomogeneous deformation, consisting of progressively increasing macroscopic fracture and material sliding, similar to that observed in rock. Further studies, of the type reported in Reference 32 for rock, are clearly needed on plain concrete to further confirm the validity of this conclusion. In the future, it is also suggested that investigators take additional care to monitor and report on the condition of the

specimens during tests so that the validity of scaling the measured force by the original cross-sectional area to obtain the stress can be assessed. On the basis of the evidence presented here, it is concluded that strain-softening of plain concrete is not a real material property but simply a manifestation of inhomogeneous deformation and macroscopic cracking.

Before leaving the subject of concrete, a few comments regarding strain softening in reinforced concrete are appropriate. The effect of confinement on the response of reinforced concrete has been examined in the past by a number of investigators.[43-45] A recent study by Dilger, Koch and Kowalczyk[39] is of particular interest, however, inasmuch as it considers the effects of both strain rate and confinement on the response of concrete. In this study, uniaxial compression tests were performed at various strain rates from $3 \times 10^{-5}$ $sec^{-1}$ to 0.2 $sec^{-1}$ on concrete prisms with square cross-sections and transverse reinforcement. The reinforcement consisted of discrete square ties and continuous square spirals, which were spaced at distances of 1, 2, and 4 inches in the test specimens.

Typical results from Reference 39 are shown in Figure 4.13, where the uniaxial compression responses of specimens having different amounts of transverse displacement and at two different strain rates are depicted. At the high strain rate, the plain concrete virtually exploded at the peak stress, causing termination of the stress-strain curve, as shown. It was found that although the ultimate strength of the specimens did not increase as a result of the addition of the transverse reinforcement, the shape of the stress-strain curve was very significantly affected by the presence of the transverse steel. As the spacing of the reinforcements is decreased, the concrete experiences greater confinement and shows less tendency toward softening. As Figure 4.13 shows, the strain softening that occurs in the specimens having reinforcements with 1 inch spacing is small and could reasonably be neglected for practical purposes. Again, there is no information given in

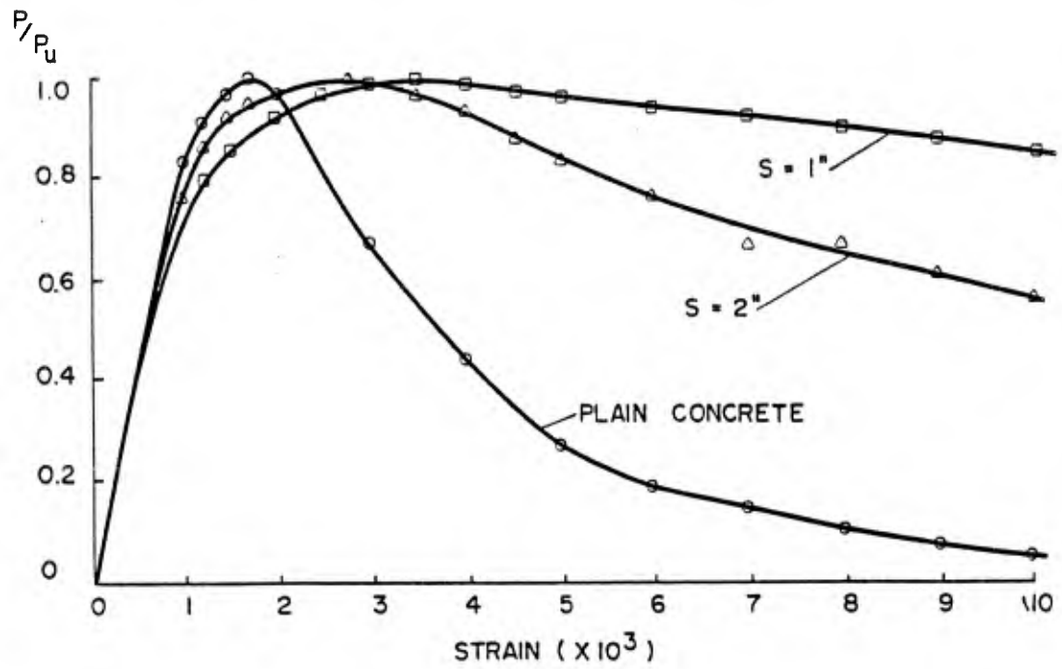


(a) Strain rate of $3.3 \times 10^{-3}$ $sec^{-1}$.

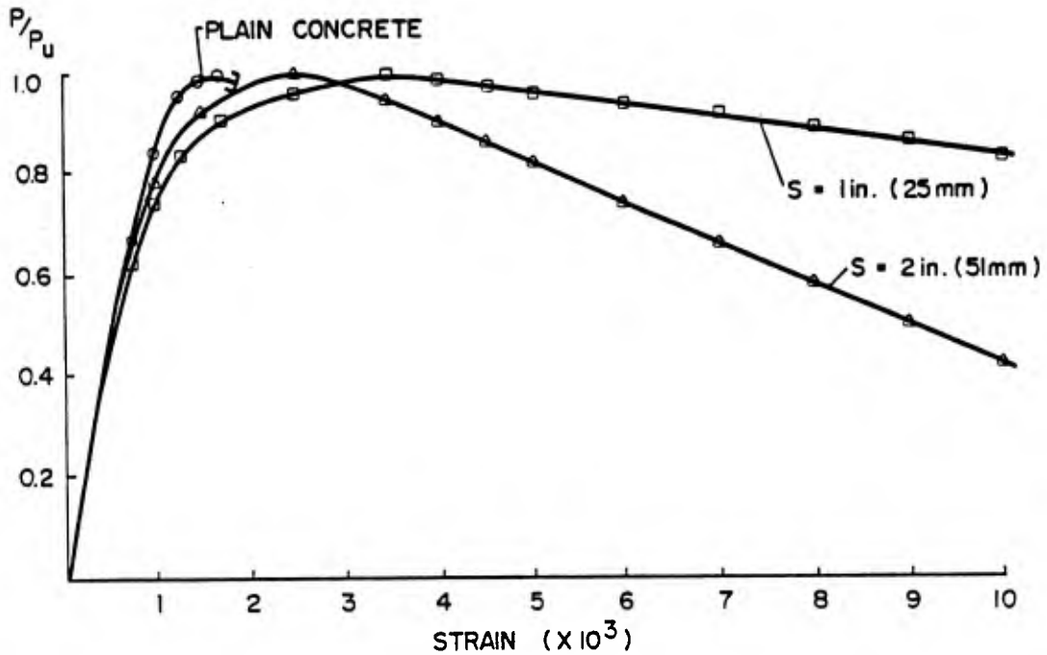


(b) Strain rate of 0.2 $sec^{-1}$

Figure 4.13. Uniaxial compression response of concrete with different amounts of transverse reinforcement and at two different strain rates. The letter S denotes the spacing between reinforcements. (From Reference 39).

Reference 39 regarding the conditions of the specimens after the ultimate strength had been reached, so little is known regarding the homogeneity of the specimens during the strain softening stage. Most likely, however, there was increasing inhomogeneity, since it was noted that, by a strain of 1 percent, the specimens had "virtually disintegrated."

### 4.1.4 Closure

In the preceding sections, an attempt has been made to identify and review relevant experimental studies that shed some light on the physical nature of strain softening in soils, rock and plain concrete. In all cases examined, the reported strain softening appears to be the result of inhomogeneous deformation of specimens during testing, and is not attributable to the inherent properties of homogeneous material. In fact, in reviewing the literature, we did not uncover any instance where strain softening was observed in materials that were homogeneously deformed. On the basis of this review, it is therefore concluded that strain softening is not a real property of such materials and, as a result, should not be incorporated into constitutive theories intended for the continuum representation of their response.

## 4.2 IMPLICATIONS OF STRAIN SOFTENING IN STRESS WAVE PROPAGATION

In the preceding section, it was concluded, on the basis of what is generally accepted as accurate, credible experimental evidence, that strain softening does not appear to be a true material property of soils, rocks or concrete. In the present section, however, we will assume that strain softening is a true material property and explore the consequences of this assumption, theoretically and numerically, on stress wave propagation. To keep the following discussion relatively simple, attention is restricted in the remainder of this section to wave propagation in one-dimension.

The system of equations which govern the transient one-dimensional nonlinear response of isotropic media that strain soften will be examined using the method of characteristics; this will include both rate-independent and viscous materials. Then, a recent theoretical study[46] of "deformation-trapping" in strain softening materials, aimed at increasing the understanding of slip band formation in metals, will be reviewed. Finally, the results from a recent numerical study[19] of one-dimensional wave propagation in a strain softening material will be discussed, and it will be shown that the insight provided by Reference 46 allows a theoretical explanation of the numerical results reported in Reference 19.

### 4.2.1 On The Nature of the Governing Systems of Equations for Several Different Constitutive Models

Consider the one-dimensional motion of a semi-infinite material which strain softens after reaching some critical strain. Letting $\sigma$ and $\varepsilon$ denote, respectively, the stress and strain*, the equations of momentum balance and continuity for small strains have the form:

$$\frac{\partial \sigma}{\partial x} + \rho_o \frac{\partial v}{\partial t} = 0 \tag{4-6}$$

$$\frac{\partial v}{\partial x} + \frac{\partial \varepsilon}{\partial t} = 0 \tag{4-7}$$

where $\rho_o$ is the unstrained density, v is the velocity, and x is a coordinate along a line normal to the surface of the half-space which is measured positively in a direction into the material from the surface. In addition to Eqs. (4-6) and (4-7), the constitutive equation for the material must be specified and, in that which follows, several different constitutive models with strain softening are considered, including both inviscid and viscous models.

*Here, stress and strain are assumed to be positive in compression.

Simple Rate-Independent Model

Consider a simple, rate-independent constitutive model with strain softening whose limiting curve in compressive loading is of the general form:

$$\sigma = F(\varepsilon) \tag{4-8}$$

where F has a continuous derivative. If $\varepsilon_0$ denotes the strain at the peak of the stress-strain curve, then the function $F(\varepsilon)$ satisfies the conditions:

$$\begin{aligned} &F'(\varepsilon) \geq 0, \quad \text{for } 0 < \varepsilon \leq \varepsilon_0 \\ &F'(e) < 0, \text{ for } \varepsilon > \varepsilon_0 \end{aligned} \tag{4-9}$$

where the superposed prime denotes differentiation with respect to $\varepsilon$. Upon combining Eqs. (4-6), (4-7) and (4-8), the following system of quasi-linear first order partial differential equations result:

$$\begin{aligned} F'(\varepsilon)\frac{\partial \varepsilon}{\partial x} - \rho_0 \frac{\partial v}{\partial t} &= 0 \\ \frac{\partial v}{\partial x} - \frac{\partial \varepsilon}{\partial t} &= 0 \end{aligned} \tag{4-10}$$

which has the characteristic determinant:

$$\begin{vmatrix} F'(\varepsilon) & 0 & 0 & -\rho_0 \\ 0 & -1 & +1 & 0 \\ dx & dt & 0 & 0 \\ 0 & 0 & dx & dt \end{vmatrix} = 0 \tag{4-11}$$

It follows from this that the characteristics are given by

$$\frac{dx}{dt} = \pm \sqrt{\frac{F'(\varepsilon)}{\rho_0}} \tag{4-12}$$

When $F'(\varepsilon) > 0$, which corresponds to the hardening range of behavior, the characteristics are real and distinct; in this case,

the system is hyperbolic and the solution to the initial value problem is unique. When $F'(\varepsilon) < 0$, which corresponds to the strain softening regime, the characteristics are complex and the system of equations is elliptic. Well known mathematical theorems[47] lead to the conclusion that, if a set of quasi-linear first order partial differential equations has complex characteristics, it is ill-posed as an initial value problem. Lack of well-posedness caused by the existence of complex characteristics implies growth of disturbances of all wave lengths*, which of course leads to numerical instabilities when these equations are treated by finite difference or finite element techniques. Finally, the case $F'(\varepsilon) = 0$, which can only occur at a point, $\varepsilon = \varepsilon_0$, results in the system of equations being parabolic. Therefore, in view of the above considerations, mathematical and numerical difficulties are expected to occur in one-dimensional wave propagation problems as soon as the material enters the strain softening range, making the subsequent solution non-physical.

Simple Rate-Dependent Model

Perhaps the simplest one-dimensional model which exhibits both rate-sensitivity and strain softening during loading is given by the expression

$$\sigma = F(\varepsilon) + m \frac{\partial \varepsilon}{\partial t} \tag{4-13}$$

where $F(\varepsilon)$ has the properties given in Eq. (4-9) and m is a material constant. Upon combining Eqs. (4-6), (4-7) and (4-13), the following system of semi-linear first order partial differential equations results:

$$\begin{aligned} \frac{\partial \sigma}{\partial X} - \rho_0 \frac{\partial V}{\partial t} &= 0 \\ m \frac{\partial V}{\partial X} &= \sigma - F(\varepsilon) \end{aligned} \tag{4-14}$$

*For an excellent discussion of this, see pages 62 and 63 of Reference 48.

The corresponding characteristic determinant is:

$$\begin{vmatrix} 1 & 0 & 0 & -\rho_o \\ 0 & 0 & m & 0 \\ dx & dt & 0 & 0 \\ 0 & 0 & dx & dt \end{vmatrix} = 0 \quad , \tag{4-15}$$

from which it follows that the system (4-14) is parabolic, regardless of the specific form of $F(\varepsilon)$. One therefore concludes from this that no unusual mathematical or numerical difficulties are to be expected in using such a model, even when strain softening is reflected in the quasi-static loading curve, $F(\varepsilon)$.

Malvern's Rate-Dependent Model

A one-dimensional rate-dependent model which has received considerable attention is that proposed by Malvern.[49] This model is described by the expression:

$$E_o \frac{\partial \varepsilon}{\partial t} = \frac{\partial \sigma}{\partial t} + K\{\sigma - F(\varepsilon)\} \quad , \tag{4-16}$$

where $E_o$ is the elastic modulus, K is a positive material constant which reflects the strain rate sensitivity, and $F(\varepsilon)$ is the quasi-static loading curve. Since the function $F(\varepsilon)$ is quite general, it can have the properties given by Eq. (4-9) and thereby provide the model with the capability to describe strain softening under quasi-static deformation. When Eqs. (4-6), (4-7) and (4-16) are combined, the following set of semi-linear first order partial differential equations results:

$$\begin{aligned} &\frac{\partial \sigma}{\partial x} - \rho_o \frac{\partial v}{\partial t} = 0 \\ &-\frac{\partial \sigma}{\partial t} + E_o \frac{\partial v}{\partial x} = K\{\sigma - F(\varepsilon)\} \end{aligned} \tag{4-17}$$

The corresponding characteristic determinant is:

$$\begin{vmatrix} 1 & 0 & 0 & -\rho_0 \\ 0 & -1 & E_0 & 0 \\ dx & dt & 0 & 0 \\ 0 & 0 & dx & dt \end{vmatrix} = 0 \quad , \tag{4-18}$$

which leads to the following expression for the characteristic directions:

$$\frac{dx}{dt} = \pm \sqrt{\frac{E_0}{\rho_0}} \tag{4-19}$$

From this equation it follows that, since both $E_0$ and $\rho_0$ are positive, the characteristics are real and distinct. The system of equations is therefore hyperbolic, irrespective of the nature of the rate dependence and of the form of the quasi-static loading curve, $F(\varepsilon)$. Consequently, $F(\varepsilon)$ can exhibit strain softening without destroying the hyperbolicity of the system of governing equations.

Parenthetically, let us note that Valanis, in a more general context, recently derived[28] the condition under which rate-dependent, strain-softening materials, whose constitutive relations are derivable through internal variable theory, possess unique solutions to initial value problems. He considers the general class of materials whose free energy density $\psi$ depends upon the strain $\varepsilon$ and n internal variables $\underset{\sim}{q}^{(r)}$, i.e.,

$$\psi = \psi(\underset{\sim}{\varepsilon}, \underset{\sim}{q}^{(n)}) \tag{4-20}$$

The stress $\sigma$ is therefore given by the expression:

$$\underset{\sim}{\sigma} = \frac{\partial \psi}{\partial \underset{\sim}{\varepsilon}} \tag{4-21}$$

and the internal variables follow evolutionary equations of the form:

$$\dot{\underset{\sim}{q}}^{(r)} = \underset{\sim}{f}^{(r)}(\underset{\sim}{\varepsilon}, \underset{\sim}{q}^{(n)}) \tag{4-22}$$

To insure a positive rate of irreversible entropy production, it is necessary that

$$\frac{\partial \psi}{\partial \underset{\sim}{q}^{(r)}} \underset{\sim}{f}^{(r)} < 0 \tag{4-23}$$

Within the context of the above constitutive framework, Valanis found that the fourth order tensor, $\partial^2\psi/\partial\underset{\sim}{\varepsilon}^2$, must be positive definite to insure uniqueness of the initial value problem. Interestingly, this condition is independent of the forms of the functions $\underset{\sim}{f}^{(r)}$ and $\psi$, and holds irrespective of whether the thermodynamic inequality (4-23) is satisfied or not. Because of this, the question of uniqueness of the initial value problem does not depend on a positive rate of irreversible entropy production. Work is presently underway by Valanis to explore the full implications of the condition $\partial^2\psi/\partial\underset{\sim}{\varepsilon}^2 \geq 0$ with the specific goal of identifying the particular class of rate-independent, strain-softening materials which satisfy it.

In this section, the nature of the system of equations which govern the one-dimensional behavior of several types of materials which exhibit strain softening has been examined via the method of characteristics. When the materials are rate-independent, we showed that the equations are hyperbolic and therefore have a unique solution, so long as the material is hardening; when softening occurs, however, the equations become elliptic. Since initial value problems for elliptic equations are notoriously ill posed, analytical and numerical difficulties arise and, as a result, numerical instabilities develop in the governing equations if they are treated by either finite-difference or finite-element methods. On the other hand, we showed that for several rate-dependent strain softening materials the governing system of equations were either hyperbolic or parabolic, depending upon the exact form of the rate-dependence.

In these cases, unique solutions to the initial value problem can be obtained regardless of whether or not the quasi-static loading curve exhibits strain softening. More general studies by Valanis[50] are presently underway to determine the general class of rate-dependent, strain softening materials which provide unique solutions to initial value problems. Without rate-dependence, initial value problems become ill-posed as soon as the material begins to soften.

### 4.2.2 Deformation Trapping

The one-dimensional initial value problem mentioned in the preceding section is considered further below to illustrate the concept of deformation trapping and to expand somewhat on the notion of well-posedness. The basic mathematical approach adopted below is closely modeled on that given recently by Wu and Freund[46], who considered a somewhat different physical problem, namely, shear wave propagation in a half space of strain softening material.* Despite the physical differences, however, the mathematical formulation of both problems leads to identical systems of equations.

Consider a half-space or semi-infinite rod, $x > 0$, occupied by a nonlinear rate-independent strain softening material described by the constitutive relation:

$$\sigma = F(\varepsilon) \tag{4-24}$$

where $\sigma,\varepsilon$ denote, as before, the stress and strain, respectively, in the x-direction, and F has a continuous derivative. The material is stress free and at rest for time up to $t = 0$ and, thereafter, the material is subject to the boundary velocity V(t) in the x-direction, that is:

$$v(0,t) = V(t) \quad , \qquad t > 0 \tag{4-25}$$



*See also, Reference 51.

where V(t) is a non-decreasing function of time. Upon combining Eqs. (4-6), (4-7) and (4-24), the following system of quasi-linear first order partial differential equations is obtained (see Eqs. (4-10) also):

$$F'(\varepsilon)\,\frac{\partial \varepsilon}{\partial x} - \rho_o\,\frac{\partial v}{\partial t} = 0$$

$$\frac{\partial v}{\partial x} - \frac{\partial \varepsilon}{\partial t} = 0 \qquad (4\text{-}26)$$

For $F' > 0$, the system (4-26) is hyperbolic, and the solution subject to quiescent initial conditions and the boundary condition (4-25) is unique, having the form of a simple wave. Accordingly, a given level of particle velocity propagates into the material from the boundary $x = 0$ along a straight line characteristic of slope $dt/dx$ in the x-t plane at a speed c, where

$$\frac{dt}{dx} = c^{-1}(\varepsilon) \qquad , \quad c(\varepsilon) = \sqrt{\frac{F'(\varepsilon)}{\rho_o}} \qquad (4\text{-}27)$$

Consider now the situation in which the boundary velocity V has increased to the point where the material at the boundary attains the condition $F'(\varepsilon) = 0$ at $\varepsilon = \varepsilon^*$ and $t = t^*$. Then, from Eq. (4-27b), the speed of propagation of this particular strain level is zero and the associated characteristic is aligned with the t-axis in the x-t plane (see Figure 4.14a). When this occurs, the boundary itself becomes a characteristic and it is therefore no longer possible to transmit boundary information to interior points in the material. As V increases further for $t > t^*$, a discontinuity in the velocity field develops at $x = 0$; this discontinuity can only exist, however, if the above characteristic remains aligned with the t-axis. Thus, for $t > t^*$ and for points in the neighborhood of the boundary, the fields v, $\sigma$ and $\varepsilon$ become uniform at levels $v^*$, $\sigma^*$ and $\varepsilon^*$, respectively, and there is accordingly a discontinuity of magnitude $V(t) - v^*$ across $x = 0$, where

$$v^* = \int_0^{\varepsilon^*} c(\varepsilon)d\varepsilon \tag{4-28}$$

Based on the above considerations, the development of the velocity profiles with time, and the velocity discontinuity at $x = 0$ for $t > t^*$, are depicted in Figure 4.14b.

The vanishing of the tangent modulus $F'(\varepsilon)$ at $\varepsilon = \varepsilon^*$ leads to the concept of "deformation trapping" in general, and shear banding for the particular problem considered by Wu and Freund.[46] Here, one argues that, since the speed of propagation of increasing strain levels vanishes at the critical strain $\varepsilon^*$, strains greater than $\varepsilon^*$ are trapped at the boundary and are accumulated into an infinitely thin deformation band. This, then results in an infinite strain rate at $x = 0$, and indicates that strain rate effects must become increasingly important as $F'(\varepsilon) > 0$. However, it must be noted that an infinite strain rate is not consistent with the assumption of small strains implicit in the deveopment of the governing equations, since such a strain rate will lead to finite strain for any small finite time.

Physically, the velocity discontinuity noted above cannot actually develop in a half-space since this would result in the volume of the material element at the boundary going to zero. From experience, we know that real materials resist such a condition through corresponding increases in hydrostatic pressure, a feature which is not reflected in the simple constitutive model, Eq. (4-8), being considered. Therefore, to avoid such difficulties, it appears that the limiting velocity at which the boundary can in a practical sense be driven is $V = v^*$. Consequently, since the prescribed form of $V$ is such that

$$V(t) > v^* \quad \text{for} \quad t > t^* \tag{4-29}$$

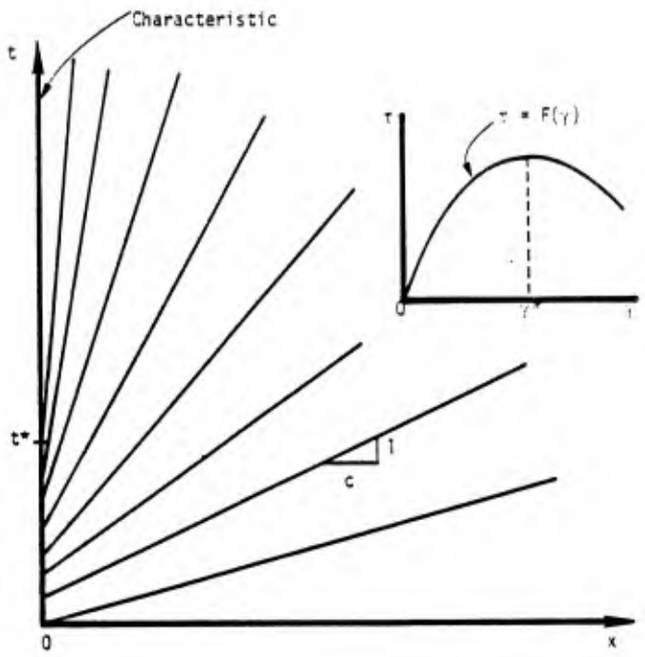


(a) Evolution of characteristics

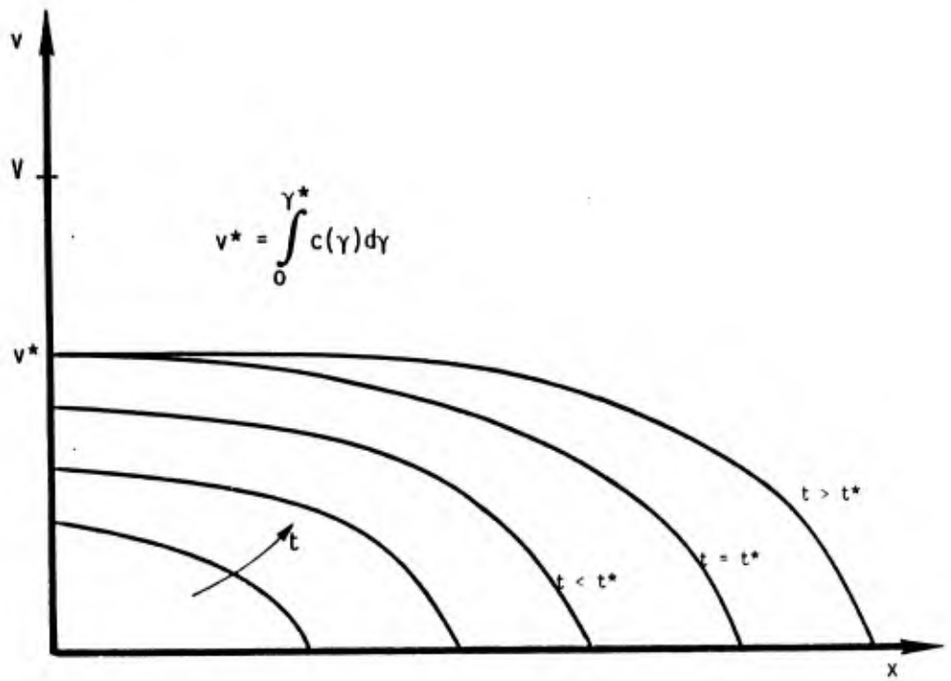


(b) Velocity profiles.

Figure 4.14. Wave propagation features for inviscid case treated by Wu and Freund (Ref. 46).

it follows that the problem as formulated is not compatible with the behavior of the physical system, and thus the problem is improperly posed for $t > t^*$.

How does the picture change if the material is rate-dependent? As shown by Wu and Freund,[46] the velocity profile near $x = 0$ for such a material will show a continuous drop from $V(t)$ at $x = 0$ to $v^*$ at some small distance $\delta$ into the material as shown in Figure 4.15; the distance $\delta$ may be thought of as a boundary layer thickness, and it is to be expected that this thickness will depend on the particular form of rate-dependence in the model.[46] As V increases beyond $v^*$ for $t > t^*$, the strain in the boundary layer will increase accordingly, with the result that the assumption of small strain implicit in the governing equations becomes increasingly in error. Therefore, while rate-dependence removes the discontinuity in velocity at $x = 0$, the solution to the problem can only be carried out to some small time slightly beyond $t^*$ before the small strain assumption implicit in the governing equations breaks down. For times greater than this, the problem is improperly posed.

In summary, we have examined in this section a one-dimensional initial value problem for a strain-softening material. The assumption of small strains was implicit in the governing equations. For the rate-independent model, we conclude:

1. The initial value problem is improperly posed for all times greater than that at which the material at the boundary $x = 0$ first reaches the peak of the stress-strain curve, say $t^*$. Meaningful analytic or numerical solutions cannot be obtained for $t > t^*$.

2. Information pertaining to the descending (strain softening) branch of the stress-strain curve cannot be communicated to interior points of the material.

For the rate-dependent model, we conclude:

1. The velocity field near the boundary $x = 0$ is continuous. For $t > t^*$, the drop in velocity from $V$ to $v^*$ is confined to a thin boundary layer.

2. Meaningful solutions can be obtained only for values of $t$ slightly greater than $t^*$ before the strains in the boundary layer become sufficiently large to violate the small strain assumption.

### 4.2.3 Numerical Solutions

The purpose of this section is to illustrate, via example, the difficulties that arise when one attempts to solve an initial value problem involving a rate-independent strain-softening material. For this purpose, we consider below a recent numerical study reported by Wright and Sandler,[19] in which the numerical aspects of such a problem were explored with a standard one-dimensional finite-difference method. It is shown that the results from this numerical study are completely consistent with the theoretical conclusions arrived at in the preceding section, namely, (a) that the problem is ill-posed whenever the material is strained past the peak of the stress-strain curve, and (b) that no information about the strain-softening branch of the curve can be communicated to the interior of the material.

Wright and Sandler[19] considered a rate-independent strain-softening material whose limiting stress-strain curve for loading is of the form:

$$\sigma = F(\varepsilon) \tag{4-30}$$

where

$$F(\varepsilon) = E_0 \varepsilon \exp(-\varepsilon/\varepsilon_0) \tag{4-31}$$

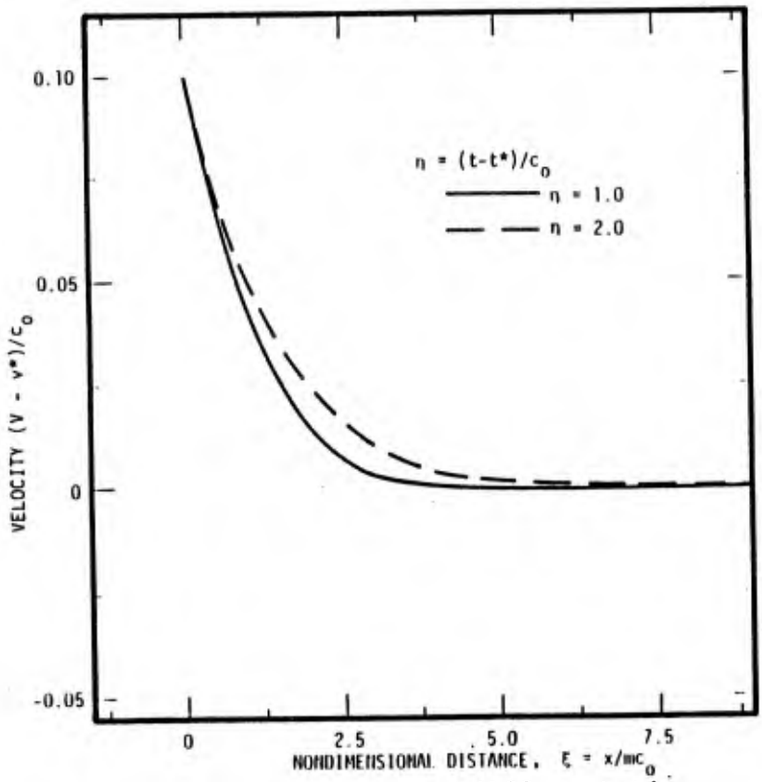


(a) Velocity profiles at two different times

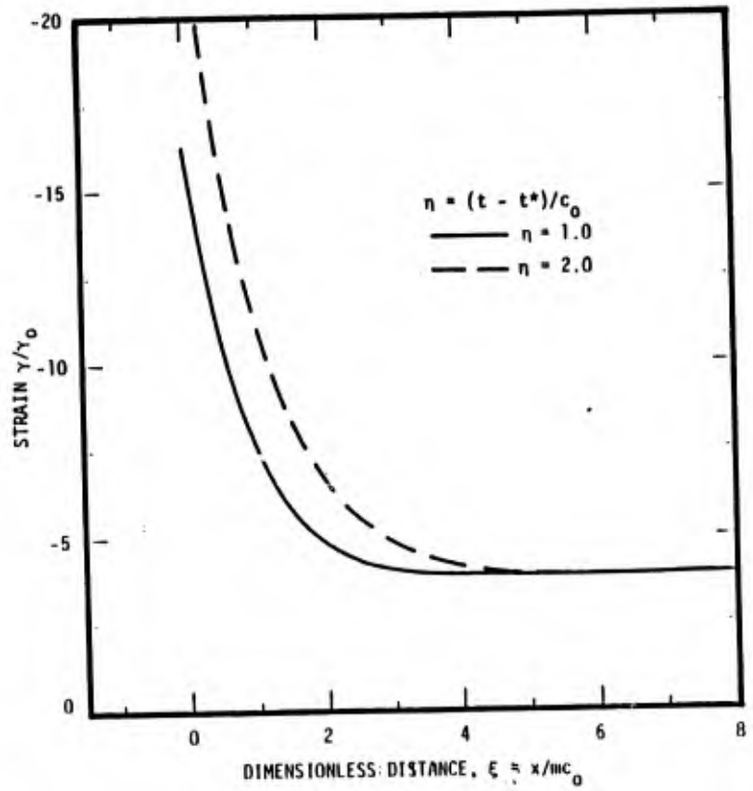


(b) Strain profiles at two different times

Figure 4.15. Velocity and strain profiles for rate-dependent models. (From Reference 46)

and $E_0$, $\varepsilon_0$ are material constants. The small strain assumption was adopted, with the strain $\varepsilon$ defined as in Eq. (4-7) given earlier. Compressive unloading and reloading beneath the limiting loading curve were taken to occur reversibly and parallel to the initial slope $E_0$, as illustrated in Figure 4.16a. Moreover, the material was not allowed to support tension. The velocity boundary condition at x = 0 was prescribed as follows:

$$V(t) = \begin{cases} V_0 \, [1 - \cos(\pi t/t_0)]/2 & , \text{ for } t \leq t_0 \\ V_0 & , \text{ for } t > t_0 \end{cases} \qquad (4\text{-}32)$$

where $t_0$ = 0.2 msec; the variation of V with time according to Eq. (4-32) is illustrated in Figure 4.16b. At t = 0, the material was assumed to be quiescent and stress free. The following values of the material parameters were adopted which are typical of plain concrete: $E_0 = 3 \times 10^6$ psi, $\varepsilon_0 = 0.002$ and $\rho_0 = 150$ lb/ft$^3$. The governing system of equations to be solved numerically therefore consists of Eqs. (4-10a), (4-10b), (4-30) and (4-31), subject to the boundary condition, Eq. (4-32).

Numerical solutions for the initial value problem described above were obtained by Wright and Sandler[19] for two different, but very close, values of the peak boundary velocity, $V_0$. In one case, the value $V_0$ = 127 in/sec was selected so that the material was driven very near to, but not over, the peak of the stress-strain curve. For this case, the tangent modulus, $F'(\varepsilon)$, is always positive and the equations remain hyperbolic. In the other case, the value $V_0$ = 128 in/sec was adopted, which was just large enough to drive the material into the strain-softening region; as noted in the preceding section, the problem becomes ill-posed as soon as material begins to strain-soften and, as demonstrated in Reference 19 and illustrated below, the corresponding numerical solution develops peculiar features when this occurs.

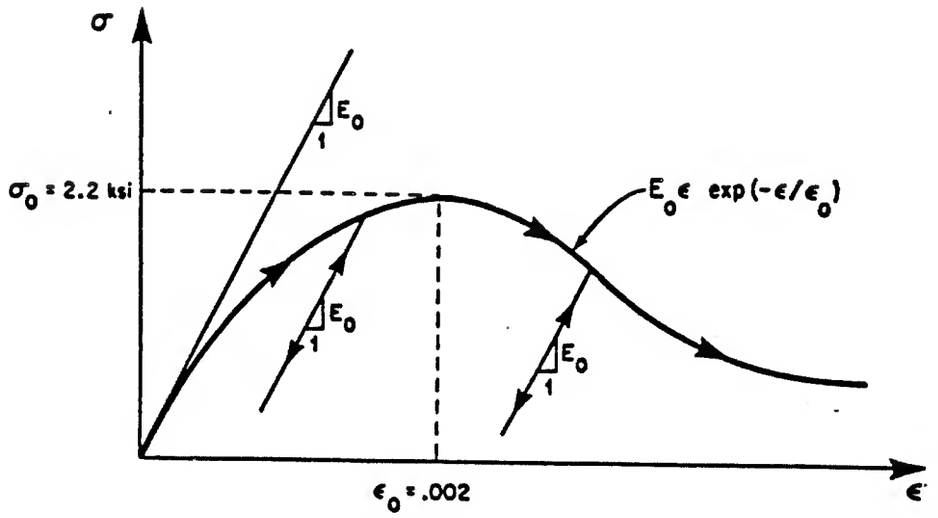


(a) Softening stress-strain model.

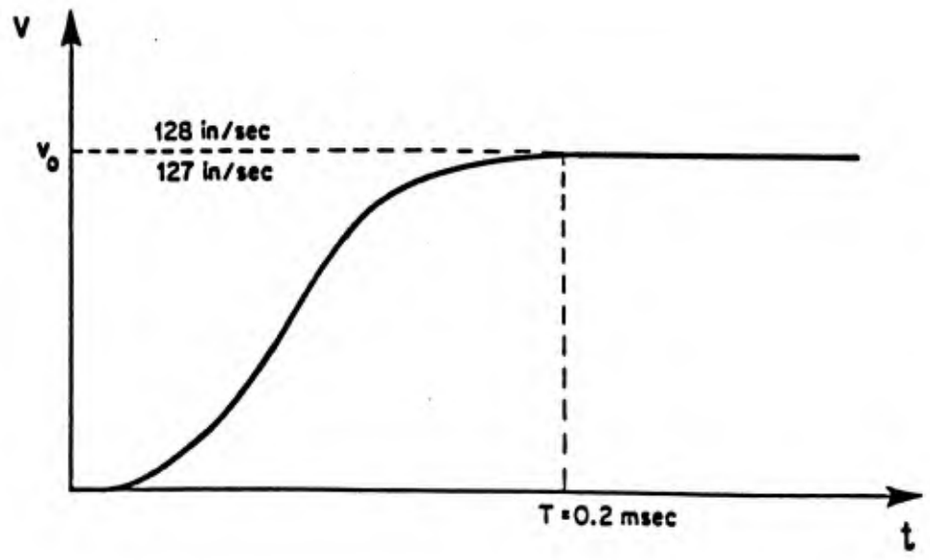


(b) Input boundary velocity history at x = 0.

Figure 4.16. Some features of the one-dimensional initial value problem considered numerically in Reference 19.

Figure 4.17(a) depicts the numerical results given in Reference 19 for the case $V_0 = 127$ in/sec.* Here, the calculated velocity histories at a depth of 12 inches for two different zone sizes are shown. As this figure reveals, such zoning was adequate, as evidenced by the fact that the two calculated velocity histories essentially overlay one another.

The numerical results for the case $V_0 = 128$ in/sec are given in Figure 4.17(b). Here, calculated velocity-time histories at $x = 12$ inches for three different zone sizes are shown. The prescribed boundary velocity drives the material into the softening region and, when this occurs, the problem becomes ill-posed; this is reflected in the numerical results in several ways.

1. Strain softening was confined, in all cases studied, to the zone adjacent to the boundary. Therefore, the amount of material that strain softens is actually dictated by the numerics (zone size) and not the physics. As a result, as the zone size is reduced toward zero, the amount of material that actually softens can be reduced to zero. Thus, the material can be prevented from exhibiting, under dynamic response conditions, the strain softening that is an integral part of its constitutive model. This is the way the numerical solution reflects the observations arrived at earlier on theoretical grounds that, as soon as the system is overdriven, the boundary information cannot be transmitted into the interior material.

2. The calculated velocity profiles depicted in Figure 4.17(b) show an extraordinary sensitivity to zone

*Numerical studies of the problems discussed in this section were also performed independently by the authors as part of the present study and the results were in complete agreement with those reported in Reference 19.

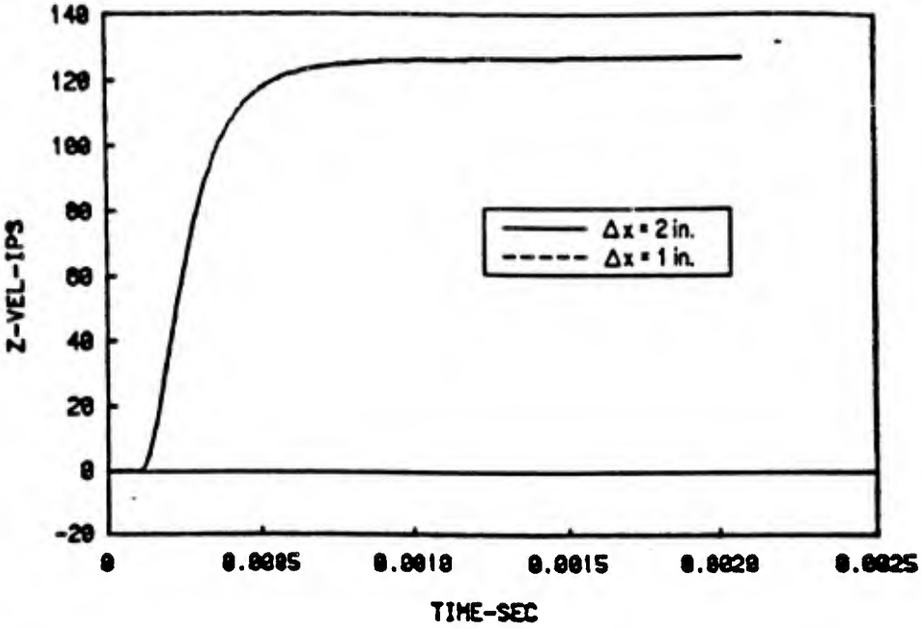


(a) $V_o$ = 127 in/sec

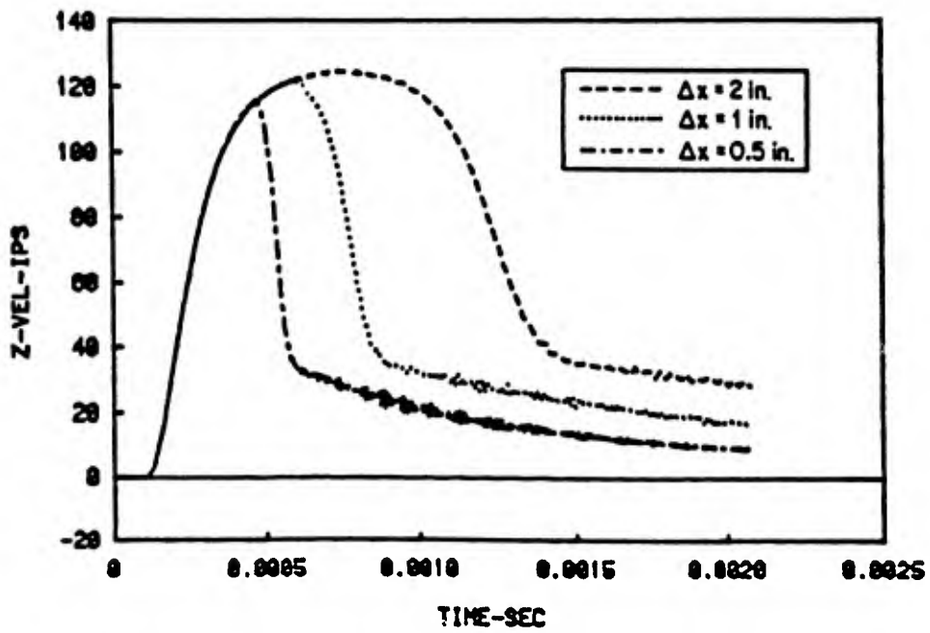


(b) $V_o$ = 128 in/sec

Figure 4.17. Velocity profiles at depth of 12 inches for various grid sizes and two different peak input velocities. (From Reference 19)

size that was not present in Figure 4.17(a). This evidently occurs because the softening is always confined to the first zone and the resulting response transmitted from this zone to the others depends on the size of the first zone.

3. The strain in the first zone grows very rapidly after the material begins to soften and quickly invalidates the assumption of small strains. The calculated strain-time history for the case $\Delta x = 1$ inch, shown in Figure 4.18, illustrates the point.

In spite of the fact that the problems became ill-posed, the corresponding numerical solutions were smooth and remained stable after the softening took place. Perhaps this is due to the fact that only the first zone experienced softening while the material in the remaining zones never got past the peak of the stress-strain curve and therefore the equations remained hyperbolic.

### 4.2.4 Summary

In the preceding sections, it was assumed for the sake of discussion that strain softening is a true material property, and the implications of this assumption for one-dimensional wave propagation problems were explored from both the theoretical and numerical standpoints. The major results that emerged from this examination are summarized below.

1. Theoretical analysis of the rate-independent, strain-softening material showed that whenever the tangent stiffness, $F'(\varepsilon)$, becomes negative (strain softening), the governing equations change from hyperbolic to elliptic, and the initial value problem then becomes ill-posed. Attempts to theoretically or numerically analyze the problem

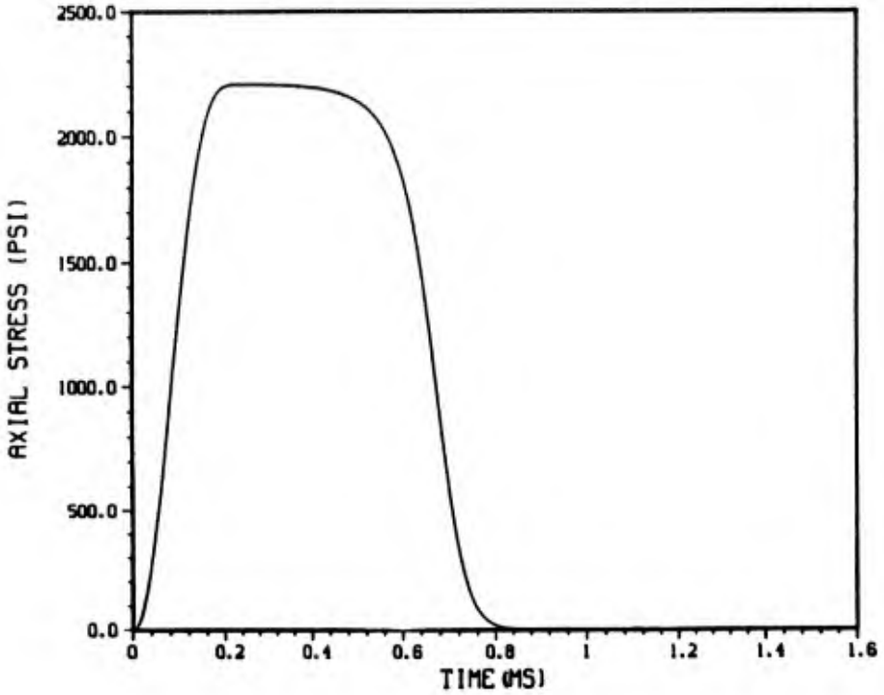


(a) Stress-time history

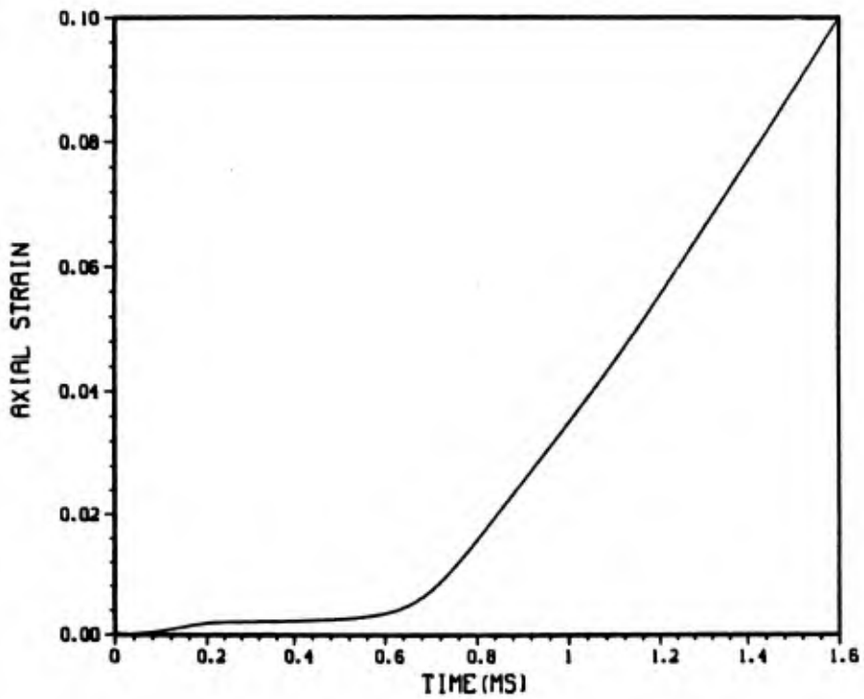


(b) Strain-time history

Figure 4.18. Calculated histories of stress and strain in zone adjacent to boundary for $\Delta x$ = 1 inch and $V_0$ = 128 in/sec (from present study).

beyond this point proves, of course, to be meaningless. Consequently, the problem becomes ill-posed before any material interior to the body can experience strain softening. Thus, despite the fact that the material model itself exhibits strain softening, the body can never experience strain softening under dynamic conditions; this appears to pose a physical contradiction.

2. The results from the numerical study by Wright and Sandler for the rate-independent, strain-softening material were independently confirmed in the present study and are fully consistent with the theoretical developments presented herein. In essence, both confirm the fact that material interior to the body never experiences softening. Furthermore, after the material at the boundary reaches a state of incipient softening, the numerical solution begins to exhibit a peculiar dependence on zone size, which evidently is its way of reflecting the ill-posedness of the problem. At no time, however, did the numerical solution show any evidence of instability.

3. The introduction of several forms of rate-dependence into the model kept the system of equations from becoming elliptic, and therefore ill-posed, even through the quasi-static loading curve exhibited strain-softening. It was shown that in the case of linear rate-dependence, the equations are parabolic (diffusive), while Malvern's rate-dependent model leads to a hyperbolic system of equations.

4. A rate-dependent, strain-softening model leads to "deformation trapping," i.e., a boundary layer

region in which the fields are highly nonhomogeneous. The strain softening which the body experiences is confined to this region, in which large strains develop.

Finally, it must be noted that the simple one-dimensional material models considered in this section only approximate, at best, the behavior of real materials under the conditions of dynamic deformation considered. If one considers the one-dimensional response to be that of a half-space (uniaxial strain), then increasingly large hydrostatic pressures will simultaneously occur with the increasing strain; this hydrostatic hardening, which is not reflected in the models, can be sufficient to counter the effect of deviatoric softening. On the other hand, if one considers the one-dimensional response to be that of a bar, the effect of radial inertia could prove to be important as the bar begins to soften, and this effect is not accounted for in the models considered. It would, therefore, be interesting to reexamine the problems considered herein with more realistic material models and with the assumption of small strains removed.

The above comments apply to the one-dimensional problems considered herein. The extent to which they can be applied also to multi-dimensional problems requires further study.

## 4.3 NUMERICAL ANALYSIS OF QAUSI-STATIC PROBLEMS INVOLVING STRAIN SOFTENING

The wave propagation problems considered above illustrate the difficulties that arise in the numerical analysis of such problems when the materials exhibit strain softening. Difficulties of a different type have been reported in numerical studies of the quasi-static loading of strain softening materials.[52-54] It has been found, for example, that if standard numerical approaches are used, the numerical solutions suffer from instability and mesh size sensitivity as soon as the material enters the strain softening range; the deformations tend to localize along thin bands whose width is sensitive to the selected mesh size.

A special finite element approach was recently proposed by Pietruszczak and Mroz for numerically analyzing the behavior of materials which soften through shear banding.[55] In this approach, a shear band of specified thickness and orientation is introduced into those finite elements which reach a prescribed shear band initiation criterion. The characteristic thickness of the shear band is supposed to be determinable from compression test data. The incremental stiffness matrix of the elements is accordingly modified to reflect the effect of the shear bands. To illustrate the advantages of the proposed approach, the authors considered the plane strain response of a strain softening material that was compressed between two rigid parallel plates; the material was assumed to be bonded to the plates at their common interface. In addition, the material was loaded by applying specified increments in vertical displacement to the rigid plates. Figure 4.19(a) depicts the problem geometry and the three finite element meshes considered. In the proposed approach, the thickness of the shear band is held fixed as the mesh size is changed. The load-displacement relationship calculated by the proposed approach is depicted in Figure 4.19(b). Here, it is seen that the results are nearly insensitive to the mesh size. In contrast, Figure 4.19(c) shows the corresponding load-displacement relationship calculated with the conventional finite element approach; it is seen that the resulting curves are very sensitive to the element mesh size. It has been pointed out by Ottosen,[56] however, that the two largest meshes considered in the study are probably too crude to provide a realistic description of a linear elastic stress field.

The above approach appears to be potentially useful in threating materials for which softening is known <u>a priori</u> to occur through shear banding. On the other hand, for brittle materials such as rocks and concrete which deform and macroscopically soften through microcracking, the usefulness of the above method is doubtful.

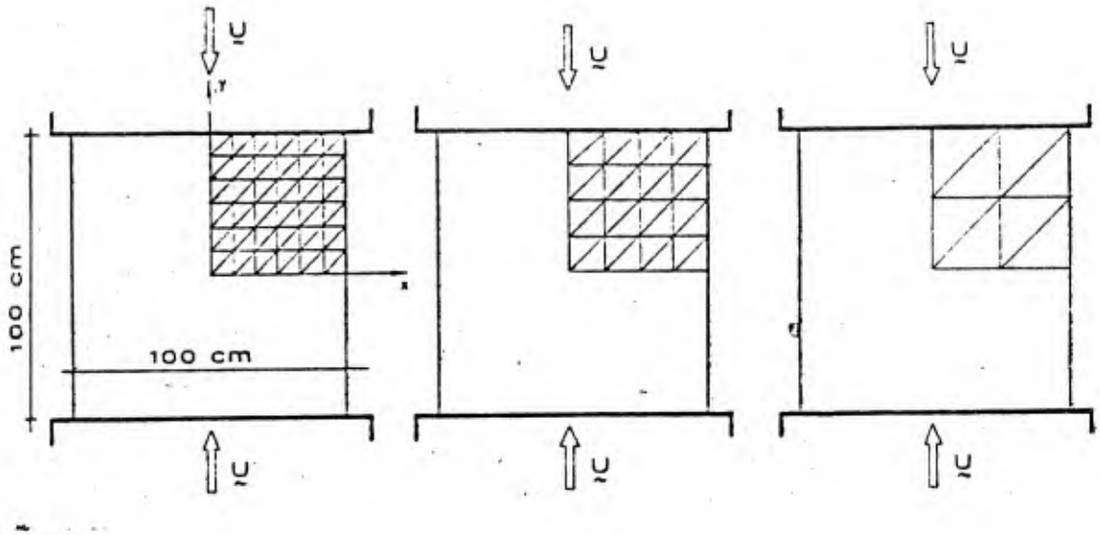


(a) Geometry of the problem and the three discretizations considered.

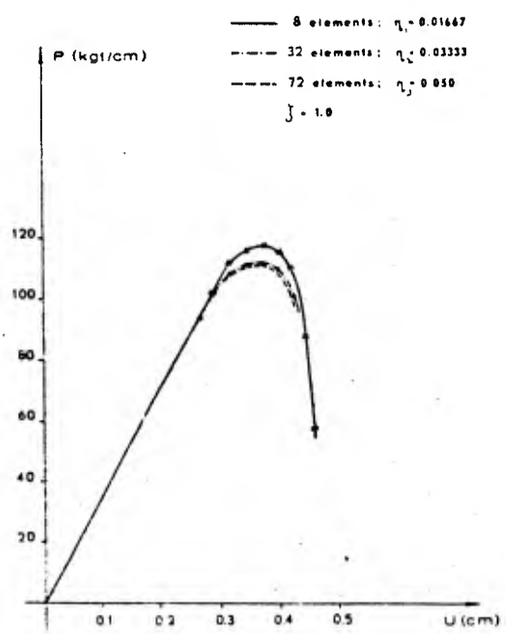


(b) Load-displacement relationship calculated with proposed approach.

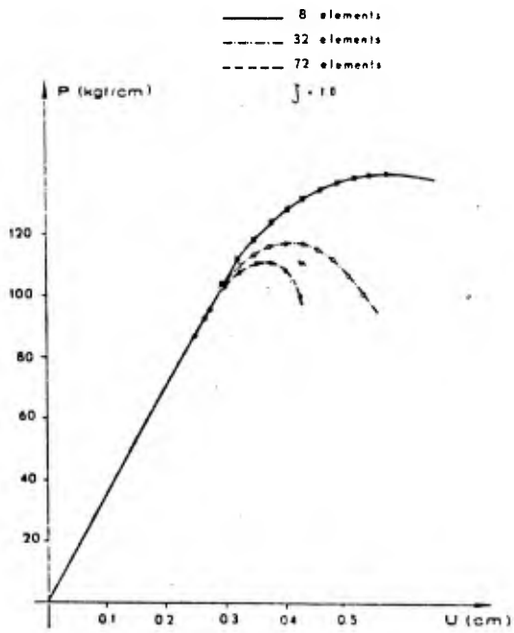


(c) Load-displacement relationship calculated with conventional finite element approach.

Figure 4.19. Plane strain compression problem considered by Pietruszczak and Mroz.(From Reference 55)

In a more recent study,[56] Ottosen employed a standard finite element method to analyze the unconfined concrete cylinder test. For this purpose, a relatively simple constitutive model, similar to the elastic-fracturing model, was used to describe the concrete behavior; the model accounted for strain hardening and strain softening in the pre- and post-failure regimes, respectively. The concrete cylinder was compressed between thick steel loading plates, and a perfect bond was assumed to exist between the cylinder and the loading plates. Numerical calculations were performed for several cylinders, with L/D ratios ranging from 1 to 3. Triangular finite elements were employed in the study, and the corresponding finite element meshes used for most of the calculations are depicted in Figure 4.20(a). To investigate the sensitivity of the results to mesh size, the case of the cylinder having L/D = 2 was recalculated, using twice as many zones as before. Interestingly, it was found that for variations of the mesh size within the limits otherwise required to obtain a realistic solution, the calculated results were virtually insensitive to mesh size; in fact, the predicted strength in both cases differed by only one percent. This insensitivity to mesh size for strain softening materials appears to be in conflict with the numerical studies reported earlier in References 52 to 54, where substantial sensitivity was found. Further work is needed to resolve this apparent discrepancy.

Despite the apparent success that Ottosen has reported in simulating the unconfined compression test for concrete with a finite element technique, it is the writers' opinion that Ottosen's work is not based on sound physical modeling of the material behavior. Based upon evidence presented in Section 4.1.3, we concluded that strain softening is not a true material property of concrete but results from (a) extensive macrocracking of material which eventually separates test specimens into a number of disconnected pieces and (b) using the original cross-sectional area to

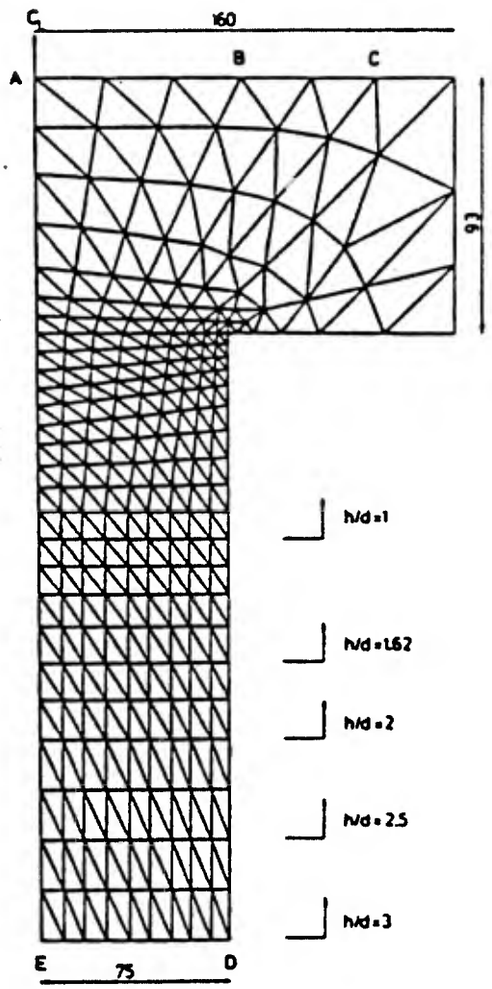


(a) Finite element meshes for different h/d ratios.

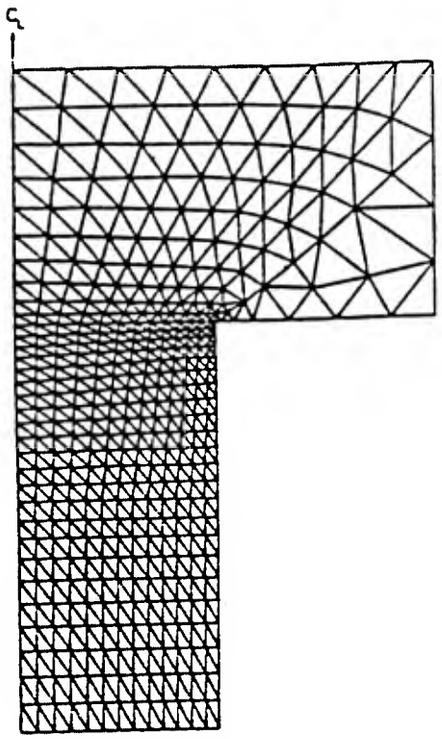

(b) Very fine mesh for h/d = 2.

Figure 4.20. Finite element meshes used in numerical study conducted by Ottosen. (From Reference 56)

determine the stress-strain relationship from the measured force-displacement curve. We seriously question the use of a homogeneous continuum model, such as Ottosen employed, to describe the behavior of inhomogeneous material having macrocracks whose size is on the order of the specimen dimensions.

## 4.4 DISCUSSION

In the preceding sections, a variety of evidence pertaining to strain softening in concrete, rock and soil has been presented and examined for the purpose of determining whether or not strain softening is a true property of these materials. The subject has been approached from the experimental, theoretical and numerical viewpoints. Without exception, the evidence presented supports the conclusion that strain softening is not a true property of these materials but is simply a manifestation of the effects of progressively increasng inhomogeneity of deformation. In tests on concrete and rock, the development of internal cracking of material caused by imperfect boundary conditions between the specimen and the loading plates was found to be the source of strain softening while, for soils, strain softening was found to arise from either stable inhomogeneous deformation caused also by imperfect boundary conditions or through unstable deformation modes which can occur irrespective of the nature of the boundary conditions. In all cases where strain softening was reported for these materials, the measured force-displacement data from laboratory tests was transformed to a stress-strain curve by simply using the original values of the length and cross-sectional area of the specimen; little or no attention was given to the physical condition of the specimen during the test. In some cases, the specimen had "virtually disintegrated" by the end of the test.[39]

Since the evidence presented here indicates that strain softening is not a true material property of concrete, rock or soil, it therefore follows that it is not legitimate to incorporate it into constitutive models for these materials intended for use within

a continuum mechanics framework. It should be emphasized that it is not simply the inhomogeneity of deformation, by itself, that makes the use of a constitutive model for treating strain softening invalid; it is the scale of the inhomogeneity that accompanies strain softening which is important. The deformation of a material may appear to be homogeneous on the macrolevel, but a sufficiently small scale can always be found for which the deformation, when viewed on this scale, is inhomogeneous. Metals, for example, can deform in a macroscopically homogeneous manner through the motion of dislocations along glide planes in the lattice and by twinning, both of which are locally inhomogeneous on a microscale. Soils deform through inhomogeneous sliding of granular particles. Reasonable continuum representations for the mechanical behavior of these materials can be constructed so long as the scales of inhomogeneity remain sufficiently small compared with the size of the material element under consideration. The difficulty with strain softening in concrete, rock and soils is that the scale of the inhomogeneities that accompany it are of the same order as the specimen size and, when this is the case, the use of a continuum representation is difficult to justify on physical grounds.

This Page Left Blank

## V. REFERENCES


1. Hegemier, G. A., "Evaluation of Material Models for MX Siting. Vol. II: Reinforced Concrete Models," S-CUBED Final Report to the Air Force BMO, SSS-R-80-4155, November 1979.

2. Cheverton, K. J., "Reinforced Concrete Models Evaluation for MX Nuclear Hardness and Survivability," S-CUBED Final Report to the Air Force BMO, SSS-R-81-4733, November 1980.

3. Hegemier, G. A., K. J. Cheverton, L. J. Hageman and P. V. Lade, "On the Development of Constitutive Relations for Plain and Reinforced Concrete," S-CUBED Final Report to the Defense Nuclear Agency, SSS-R-82-5495, April 1982.

4. Hegemier, G. A., L. J. Hageman, J. A. Trangenstein and H. E. Read, "Development of Advanced Constitutive Model for Reinforced Concrete," S-CUBED, La Jolla, CA., First Annual Report to AFOSR, SSS-R-82-5538, May 1982.

5. Hegemier, G. A., H. E. Read, H. Murakami, L. J. Hageman and R. G. Herrmann, "Development of Advanced Constitutive Model for Reinforced Concrete," S-CUBED, La Jolla, CA., Second Annual Report to AFOSR, SSS-R-83-6112, April 1983.

6. Hegemier, G. A., "Mixture Theories with Microstructure for Wave Propagation and Diffusion in Composite Materials," SM Archives, 3, 1978.

7. Hegemier, G. A., H. Murakami and A. Maewal, "On Construction of Mixture Theories for Composite Materials by the Method of Multivariable Asymptotic Expansions," Proceedings, Third International Symposium on Continuum Models of Discrete Systems, Freudenstadr, Germany, 1979.

8. Hegemier, G. A., G. A. Gurtman, "Finite-Amplitude Elastic-Plastic Wave Propagation in Fiber-Reinforced Composites," J. Appl. Phys., 45, 1974.

9. Murakami, H., G. A. Hegemier, and G. A. Gurtman, "A Nonlinear Mixture Theory for Quasi-One-Dimensional Heat Conduction in Fiber Reinforced Composites," Int. J. Solids Struct., 16, 1980.

10. Murakami, H., A. Maewal and G. A. Hegemier, "A Mixture Theory for Thermal Diffusion in Unidirectional Composites with Cylindrical Fibers of Arbitrary Cross-Section," Int. J. Solids Struct., 14, 1978.

11. Bazant, Z. P., and S. Kim, "Plastic-Fracturing Theory for Concrete," J. Engr. Mechs. Div., ASCE, Vol. 105 (1979), p. 407.

12. Prager, W., "Recent Developments in the Mathematical Theory of Plasticity," J. Appl. Phys., Vol. 20, No. 3 (1949), p. 235.

13. Read, H. E., Discussion of "Hysteretic Endochronic Theory for Sand" by Z. P. Bazant, R. J. Krizek and C.-L. Shieh, J. Engr. Mechs., Vol. 109 (4), August 1983, to appear.

14. Valanis, K. C., and H. E. Read, "A New Endochronic Plasticity Model for Soils," Chap. 14 in Soil Mechanics -- Transient and Cyclic Loads, Ed. by G. N. Pande and O. C. Zienkiewicz, John Wiley and Sons, Ltd. 1982.

15. Read, H. E., J. A. Trangenstein and K. C. Valanis, "A New Endochronic Constitutive Model for Soils," S-CUBED, La Jolla, CA., Final Report to EPRI, SSS-R-81-4926, November 1981.

16. Peyton, S., "The Failure Surfaces of Rocks, Soils and Concretes," S-CUBED, La Jolla, CA., Informal Report, January 1983.

17. Schreyer, H. L., "A Third-Invariant Plasticity Theory for Frictional Materials," J. of Structural Mechanics, Vol. 11(2) (1983) 177.

18. Wright, J. P., and I. Sandler, Weidlinger Associates, New York, Letter to Dr. Kent Goering, Defense Nuclear Agency, Washington, D.C., dated January 19, 1983.

19. Wright, J. P., and I. Sandler, Weidlinger Associates, New York, Letter to Dr. Kent Goering, Defense Nuclear Agency, Washington, D.C., dated July 21, 1983.

20. Nemat-Nasser, S., "On Finite Plastic Flow of Crystalline Solids and Geomaterials," J. Appl. Mechs., 50, December 1983.

21. Hageman, L. J., "A Mixture Theory with Microstructure Applied to the Debonding, Cracking and Hysteretic Response of Axially Reinforced Concrete," Ph.D. Dissertation, University of California, San Diego, 1983.

22. Mathey, R. G., and D. Watstein, "Investigation of Bond in Beam and Pull-out Specimens with High-Yield-Strength Deformed Bars," ACI Journal, March 1961.

23. Mirza, S. M., and J. Houde, "Study of Bond Stress-Slip Relationships in Reinforced Concrete," ACI Journal, January 1979.

24. Somayaji, S., "Composite Response, Bond Stress-Slip Relationships and Cracking in Ferrocement and Reinforced Concrete," Ph.D. Thesis, Univ. of Illinois at Chicago Circle, March 1979.

25. Hegemier, G. A., R. O. Nunn, and S. K. Arya, "Behavior of Concrete Masonry Under Biaxial Stresses," Proceedings of North American Masonry Conference, University of Colorado, Boulder, Colorado, August 1978.

26. Jimenez-Perez, R. P. Gergely, and R. White, "Shear Transfer Across Cracks in Reinforced Concrete," Report 78-4, Dept. Struct. Engr., Cornell University (NTIS: 780328), August 1978.

27. Paulay, T., R. Park, and M. H. Phillips, "Horizontal Construction Joints in Cast-in-Place Reinforced Concrete," ACI Special Publication, SP-42, Vol. 2, 1974.

28. Valanis, K. C., "On the Uniqueness of Solution of the Initial Value Problem in Strain Softening Materials," University of Cincinnati, Cincinnati, Ohio, submitted for possible publication to the Journal of Applied Mechanics (1984).

29. Pariseau, W. G., "A Finite Element Approach to Strain Softening and Size Effects in Rock Mechanics," Proc. Third Intl. Confr. on Num. Meths. in Geomechs., Aachen, Germany, April 2-6, 1979.

30. Hudson, J. A., E. T. Brown and C. Fairhurst, "Shape of the Complete Stress-Strain Curve for Rock," Proc., 13th Symp. Rock Mechs., University of Illinois, Urbana, Illinois, 1971.

31. Hallbauer, D. K., H. Wagner and N. G. W. Cook, "Some Observations concerning the Microscopic and Mechanical Behavior of Quartzite Specimens in Stiff, Triaxial Compression Tests," Intl. J. Rock Mech. Min. Sci., Vol. 10 (1973), 713.

32. Brady, B. T., W. I. Duvall and F. G. Horino, "An Experimental Determination of the True Uniaxial Stress-Strain Behavior of Brittle Rock," Rock Mechanics, Vol. 5 (1973), 107.

33. Horii, H., and S. Nemat-Nasser, "Compression-Induced Microcrack Growth in Brittle Soilds: Axial Splitting and Shear Failure," to appear in J. Geophys. Research.

34. Hettler, A., and I. Vardoulakis, "Behavior of Dry Sand Tested with a Large Triaxial Apparatus," submitted for publication, June 1983.

35. Deman, F., "Achsensymetrische Spannungs - und Verformungsfelder in trockenem Sand," Dissertation, University of Karlsruhe, 1975.

36. Hettler, A., "Verschiebungen starrer under elastischer Grundungskörper in Sand bei monotoner und zykilischer Belastung," Dissertation, University of Karlsruhe, 1981.

37. Vardoulakis, I., "Constitutive Properties of Dry Sand Observable in the Triaxial Test," Acta Mechanica, Vol. 38 (1981), 219.

38. Dresher, A., and I. Vardoulakis, "Geometric Softening in Triaxial Tests on Granular Material," Geotechnique, Vol. 32, No. 4 (1982), 291.

39. Dilger, W. H., R. Koch and R. Kowalczyk, "Ductility of PLain and Confined Concrete under Different Strain Rates," Journal of the Amer. Concrete Inst., Jan/Feb (1984), 73.

40. Hsu, T. T., F. O. Slate, G. M. Sturman and G. Winter, Micro-cracking of Plain Concrete and the Shape of the Stress-Strain Curve," Journal of the Amer. Concrete Inst., Vol. 60, No. 2 (1963), 209.

41. Shah, S. P., and F. O. Slate, "Internal Microcracking, Mortar-Aggregate Bond and the Stress-Strain Curve of Concrete," Proc. Intl. Confr. on the Structure of Concrete and Its Behavior under Load, London September 1965, published by Cement and Concrete Assn., London, 1968.

42. Maher, A., and D. Darwin, "Mortar Constituent of Concrete in Compression," Journal of the Amer. Concrete Inst., March-April 1982, 100.

43. Iyengar, K. T., P. Desayi and K. N. Reddy, "Stress-Strain Characteristics of Concrete Confined in Steel Binders," Magazine of Concrete Research, Vol. 22, No. 72 (1970).

44. Somes, N. F., "Compression Tests on Hoop-Reinforced Concrete," Proc., ASCE, Vol. 96, No. ST7 July 1970, 1495.

45. Sargin, M., Gosh, S. K., and V. K. Handa, "Effects of Lateral Reinforcement Upon the Strength and Deformation Properties of Concrete," Magazine of Concrete Research, Vol. 33, No. 75-76 (1971).

46. Wu, F. H., and L. B. Freund, "Deformation Trapping Due to Thermoplastic Instability in One-Dimensional Wave Propagation," Brown University, Providence, R. I., Report MRL-E-145, April 1983.

47. Lax, P. D., Comm. Pure Appl. Math., Vol. 11 (1958), 175.

48. Petrovsky, I. G., Lectures on Partial Differential Equations, Interscience, New York (1954).

49. Malvern, L. E., "The Propagation of Longitudinal Waves of Plastic Deformation in a Bar of Material Exhibiting a Strain-Rate Effect," J. Appl. Mechs., June 1951, 203.

50. Valanis, K. C., Private communication to H. E. Read, April 3, 1984.

51. Hegemier, G. A., and H. E. Read, "Some Comments on Strain Softening," Proceedings of Workshop on the Theoretical Foundations for Large-Scale Computations of Nonlinear Material Behavior, Northwestern University, October 24 - 26, 1983.

52. Nayak, G., and O. C. Zienkiewicz, "Elasto-plastic Stress Analysis. A Generalization of Various Constitutive Relations Including Strain Softening," Intl. J. Num. Meths. Engrg., Vol. 5 (1972) 113.

53. Prevost, J.-H., and K. Hoeg, "Soil Mechanics and Plasticity Analysis of Strain Softening," Geotechnique, Vol. 25 (1975), 279.

54. Lo, K. Y., and C. F. Lee, "Stress Analysis and Slope Stability in Strain Softening Materials," Geotechnique, Vol. 23 (1973) 1.

55. Pietruszczak, S., and Z. Mroz, "Finite Element Analysis of Deformation of Strain-Softening Materials," Intl. J. Num. Meths. Engrg., Vol. 17 (1981) 327.

56. Ottosen, N. B., "Evaluation of Concrete Cylinder Tests Using Finite Elements," J. Engrg. Mechs., Vol. 110 (3) (1984) 465.